Correlation between multiple elves and storm dynamics at the Pierre Auger Observatory

Adriana Carolina Vásquez Ramírez

Dissertation submitted in partial fulfillment of the requirements
for the degree of Doctor of Philosophy in Physics

Universidad Industrial de Santander

Facultad de Ciencias

Escuela de Física
Bucaramanga, Colombia

Università degli Studi di Torino

Dipartimento di Fisica
Torino, Italia

2024

Correlation between multiple elves and storm dynamics at the Pierre Auger Observatory

M.Sc. Adriana Carolina Vásquez Ramírez[1]

Dissertation submitted in partial fulfillment of the requirements for the degree of Doctor of Philosophy in Physics

Director: Ph.D. Roberto Mussa[2]
Co-Directors: Ph.D. Luis A. Núñez[1] and Ph.D. Enrico Arnone[3]

[1] Escuela de Física, Universidad Industrial de Santander, Bucaramanga, Colombia.

[2] Istituto Nazionale di Fisica Nucleare, Sezione di Torino, Italia.

[3] Dipartimento di Fisica, Università degli Studi di Torino, Torino, Italia.

Universidad Industrial de Santander

Facultad de Ciencias
Escuela de Física

Università degli Studi di Torino

Dipartimento di Fisica

2024

Acknowledgements

The most challenging aspect of pursuing a PhD is knowing when you have gathered enough results to conclude and draw meaningful insights. However, the most rewarding part is finishing with a desire to continue studying the phenomena that have accompanied you for so many years.

I would like to extend my heartfelt gratitude to my supervisors for their constant dedication and support in the development of this work. To Roberto Mussa, for introducing me to the world of transient luminous events and the electro-atmospheric mechanisms behind their origins. His relentless curiosity inspired me to delve into the secrets these phenomena hold.

To Enrico Arnone, for his continuous suggestions in writing and defending this thesis, as well as his support and guidance in consolidating the dual degree agreement between our universities, enabling collaborative work. I also wish to thank the Universidad Industrial de Santander and the University of Turin for facilitating this agreement and providing ongoing financial support for my participation in international conferences where I could discuss our results.

To Luis A. Núñez, my dear mentor since my undergraduate studies, for trusting in my hard and soft skills to tackle any interesting problem presented to me. Working with Luis allowed me to engage in the organization and follow-up of our research group's activities, creating master classes and mentoring undergraduate students, conducting

science outreach and women in STEM activities, which are vital for our society. These experiences made me a well-rounded scientist.

I am deeply grateful to my partner, Ricardo Choy, for his endless support, patience, and love. I also want to thank my parents and siblings, Orlando, María, Rhony, Ana Bell and Lindys, my colleague Rocio Mojica, and Tatiana Siabatto for being my continuous support network. Their belief in me has been the cornerstone of my journey, and I could not have accomplished this without them.

Thank you all!

Contents

List of Figures

List of Tables

Abstract

Elves are transient luminous events occurring above intense electrical storms. The light, emitted in the form of a rapidly expanding ring at the base of the ionosphere, is generated by the electromagnetic pulse of extreme lightning that propagates as a spherical wave from the lightning channel. Multi-elves are events consisting of two and up to four concentric rings of light expanding in succession with a time difference of tens of microseconds. The Fluorescence Detector (FD) at the Pierre Auger Observatory has been detecting elves with a dedicated trigger since 2013. The observatory was developed to detect cosmic rays but proved to be an extraordinary advancement in the observation of elves as compared to commonly adopted ground cameras. The FD's high temporal resolution of 100 ns allows for detailed event trace recording, therefore, leading to a full description of both the spatial and temporal evolution of the events. We enhanced trace processing by developing a new code as the previous algorithm primarily focused on analyzing single elves. This code identifies the most prominent peaks in the signal, performs Gaussian fitting to obtain the mean time of each peak, and calculates the temporal difference between them. Thanks to this new approach, we can now identify and report both double and triple elves at a rate never observed before. During the period 2014-2020, 6737 elves were detected by Auger, 27% of which are multi-elves. The origin of multi-elves is as yet not fully understood, with proposed production mechanisms including the reflection to the ground of the lightning's electromagnetic pulse and the rise and fall times of lightning's waveforms. Thanks to the Auger large sample, we present an unprecedented number of 63 double and 30 triple elves across

four different storms of the Cordoba region, Argentina, to test the currently proposed mechanisms. We studied the base times of the lightning waveforms (provided by Earth Networks) correlated with the elves detected at the FD, and we observed that those correlated to single elves are shorter than those correlated to multi-elves. Moreover, we found a linear relationship between the base time and the time gap of multi-elves, i.e., as the pulse widens, the rings of these events become more separated. Furthermore, our observations show that the time difference between rings does not vary with increasing the arc distance between the emission point in the ionosphere and the lightning location. This is in contrast with the electromagnetic pulse bouncing mechanism, which therefore appears to be ruled out for our sample. Eventually, we observed that elves detected at the Auger observatory were induced by lightning occurring in the most active regions of the storm and with the highest cloud tops, as evinced by GOES-16 satellite images, with no clear differences between single and multi-elves.

Keywords: Transient luminous events, ELVES, multi-elves origin, high temporal resolution, lightning's waveforms.

Resumen

Los ELVES son eventos luminosos transitorios (TLEs) que ocurren encima de tormentas eléctricas intensas. La luz, emitida en forma de un anillo que se expande rápidamente en la base de la ionosfera, es generada por el pulso electromagnético de un rayo que se propaga como una onda esférica desde el canal del rayo. Los multi-elves son eventos que consisten en dos y hasta cuatro anillos concéntricos de luz que se expanden sucesivamente con una diferencia temporal de decenas de microsegundos. El Detector de Fluorescencia (FD) del Observatorio Pierre Auger ha estado detectando elves desde 2013. El observatorio fue desarrollado para detectar rayos cósmicos, pero el FD resultó ser un detector extraordinario en la observación de elves en comparación con las cámaras comunes de TLEs. La alta resolución temporal de 100 ns del FD permite un registro detallado de los eventos, proporcionando una descripción completa de la evolución espacial y temporal de los mismos. En esta investigación, mejoramos el procesamiento de las trazas de los elves desarrollando un nuevo código. El algoritmo anterior se centraba principalmente en analizar elves simples, mientras que el nuevo código identifica los picos más prominentes en la señal, realiza un ajuste gaussiano para obtener el tiempo promedio de cada pico y calcula la diferencia temporal entre ellos. Gracias a este nuevo enfoque, ahora podemos identificar y reportar elves dobles y triples a una tasa nunca observada antes. Durante el periodo 2014-2020, se detectaron 6737 elves en Auger, de los cuales el 27% son multi-elves. El origen de los multi-elves aún no se comprende completamente, y los mecanismos de producción propuestos incluyen la reflexión en el suelo del pulso electromagnético del rayo y los tiempos de subida y

de bajada de los pulsos de las formas de onda del rayo. Gracias a la gran cantidad de datos de Auger, presentamos un número sin precedentes de 63 elves dobles y 30 elves triples en cuatro tormentas distintas en la región de Córdoba, Argentina, para probar los mecanismos propuestos actualmente. Estudiamos los tiempos base de las formas de onda de los rayos (proporcionados por la red Earth Networks) correlacionados con los elves detectados en el FD, y observamos que aquellos correlacionados con elves simples son más cortos que los correlacionados con multi-elves. Además, encontramos una relación lineal entre el tiempo base y la separación temporal de los multi-elves; es decir, a medida que el pulso se ensancha, los anillos de estos eventos se separan más. Además, nuestras observaciones muestran que la diferencia de tiempo entre los anillos no varía al aumentar la distancia de arco entre el punto de emisión en la ionosfera y la ubicación del rayo. Esto contrasta con el mecanismo de rebote del pulso electromagnético, que parece quedar descartado para nuestra muestra. Finalmente, observamos que los elves detectados en el observatorio Auger fueron inducidos por rayos que ocurrieron en las regiones más activas de la tormenta y con las nubes más altas, como se evidenció en las imágenes del satélite GOES-16, sin diferencias claras entre elves simples y multi-elves.

Palabras clave: Eventos luminosos transitorios, ELVES, origen de los multi-elves, alta resolución temporal, forma de onda de los rayos.

Chapter 1

Introduction

Transient luminous events (TLEs) refer to a group of electrical phenomena that occur due to the movement of charge between the Earth's surface and its atmosphere. This electromagnetic activity occurs within the so-called global atmospheric electric circuit, which maintains a continuous and significant electrical current in the atmosphere. Atmospheric electricity also includes the electrification of air, which happens due to ionisation by cosmic rays and the Earth's natural radioactivity. The atmospheric current varies daily due to electric storms that have a maximum in the local afternoon, and the overall global effect is the pattern known as the Carnegie curve (Harrison, 2013).

A variety of atmospheric electrical phenomena occur at various altitudes between thunderstorm tops and the ionosphere, induced by in-cloud (IC) or cloud-to-ground (CG) lightning strokes, or directly by charge redistribution processes. Blue jets and gigantic jets are types of upper-atmospheric lightning that propagate upward in the atmosphere and are observed from the top of storm clouds (Füllekrug et al., 2006). Red sprites take place between the stratosphere and mesosphere, and they appear in the form of jellyfish or clusters of carrots, exhibiting tendrils of reddish and blue plasma streamers, generally topped by patches of diffuse emission (Franz et al., 1990; Rodger, 1999). They are often accompanied by reddish halos with a diameter of tens km, but they can also occur independently (Füllekrug et al., 2006). Both sprites and halos are caused by the

quasi-static electric field induced by a typically positive cloud-to-ground stroke in the storm below.

ELVES, which stands for Emission of Light and Very Low-Frequency perturbations due to Electromagnetic pulse Sources, are observed at the base of the ionosphere. The electromagnetic pulse from lightning transfers energy to the free electrons in the ionosphere, exciting their molecules that, upon relaxation, release this energy in the form of light (Taranenko et al., 1993). The interaction of the pulse wave with the ionosphere results in rapidly expanding rings, which can attain a diameter of several hundred kilometres, but with a weak brightness due to a diffused and short-lived illumination, lasting on the order of several hundreds of microseconds only (or around 1 ms only) (Füllekrug et al., 2006).

At the top of thunderstorm clouds, satellites have observed bursts of gamma rays with energies up to 40 MeV. This phenomenon is called terrestrial gamma-ray flashes (TGFs) and was discovered in 1994 in the Compton Gamma-Ray Observatory (Fishman et al., 1994).The mechanisms responsible for the presence of these highly energetic particles in storms are not yet clear. However, it is believed that TGFs are produced by the intense electric fields near the tops of thunderstorms. Under favourable conditions, these fields become strong enough to trigger an upward avalanche of electrons. These high-energy electrons, moving at relativistic speeds, emit gamma rays as they deflect off air molecules.

TLEs and TGFs serve as indicators of particle acceleration within thunderstorms. Although numerous questions persist regarding particle acceleration mechanisms in the cosmos, thunderstorms' dynamic and complex environment offers a unique opportunity to examine some of these processes closely.

Transient luminous events are so fleeting and faint that observations in the sky were not reported until 1989 (Füllekrug et al., 2006). Since then, various dedicated scientific space missions, balloons, aircraft, and ground-based instruments have been developed to

detect TLEs. These devices can detect light, radio, or acoustic signals emitted by TLEs. Together with ground-based lightning monitoring networks, we have combined resources to study the relationship between TLEs, TGFs, lightning, atmospheric chemistry and climate. This collective effort has facilitated a global monitoring system for electrical storms, enhancing meteorological predictions on a planetary scale. In addition, studying the characteristics of storms, TLEs, and TGFs allows an advance in the design of communication and navigation system technologies that could be affected by these phenomena.

Studying our Earth's atmosphere can also provide information about atmospheres and environmental conditions in other planetary environments. For example, bright flashes have been observed in Jupiter's atmosphere that may be upper atmospheric responses to underlying thunderstorms, similar to what is observed in Earth's upper atmosphere. According to Giles et al. (2020), sprites, halos, and elves are prime candidates for these observations because of the altitude at which they occur and their duration.

As mentioned above, elves are rings of light propagating in the ionosphere above the source beam, which is the vertical lightning channel through which a current pulse travels. Several authors have reported events that present two concentric rings with such a small temporal separation that they must have originated from the same source (Barrington-Leigh and Inan, 1999; Newsome and Inan, 2010; Klimov et al., 2019; Aab et al., 2020; Romoli, 2023). Even elves of four rings can be produced, their number depending on the characteristics of the lightning that produced it. So far, two main models describe the origin of these multiple rings in elves. One relates the separation between the rings to the pulse duration of the current density pulse of the generating lightning (Marshall, 2012). While the other relates the time delay to the height of the beam (Marshall et al., 2015; Liu et al., 2017).

Our research focuses on studying the relationship between multi-elves and thunderstorm characteristics, analysing events detected at the Fluorescence Detector (FD) of the

Pierre Auger Observatory. This study examines the time gap between the various rings of multi-elves. Our objective is to compare our observations with the two models mentioned. Additionally, we investigate the relationship between our events and the characteristics of the lightning source, such as the current's polarity and peak value, the lightning's type and height, and its waveforms.

To observe the multiple rings of elves, we need detectors that can separate the pulses in the traces and have time resolutions on the order of microseconds. Fortunately, the Auger FD which has an unprecedented resolution of 100 ns (Abraham et al., 2010) with imaging capability, is very sensitive to elves, making it an excellent instrument for studying multi-elves, especially compared to other detectors which are typically either at very low time resolution (e.g., cameras) or with no imaging capability (e.g., photometers). The Observatory has been detecting elves since 2014 using a special trigger, and it can detect thousands of elves per year, including hundreds of multi-elves. In addition, the field of view of the Auger Fluorescence Detector includes the Córdoba region of Argentina, which is known for its severe thunderstorms (Witze, 2018) and high-energy lightning strikes known as super bolts (Holzworth et al., 2019).

In the forthcoming chapter, we explore notable characteristics of lightning and storms within the Auger FD's field of view. Additionally, we offer an overview of current knowledge regarding thundercloud charge distribution, lightning stroke processes, transient luminous events, and global detection of multi-elves. Lastly, we present the models detailing the origin of multi-elves.

We detail the Auger Fluorescence Detector capabilities and how it allows us to obtain high-resolution traces of the elves in chapter 3. Additionally, we discuss events detected between 2014 and 2020 and the seasonal distribution of elves and multi-elves.

In chapter 4, we analysed the lightning waveforms correlated with single, double, and triple elves detected at the Auger FD. Chapter 5 presents the study of the time delay behaviour of multi-elves concerning the source beam height. To compute the time gaps

of multi-ELVES events, we introduced a new, more efficient code, which is detailed in this chapter.

We explore the correlations of our events with other lightning properties in chapter 6, such as type of lightning, peak current and polarity, provided by Earth Networks (Zhu et al., 2022); and storm characteristics given by GOES-16 satellite imagery (Schmit et al., 2017). We present our conclusions in chapter 7.

Additionally, the data and codes used for the obtained results are provided in appendices A.1 - A.6.

Chapter 2

Multi-elves: a type of transient luminous events

Elves are transient luminous events that occur at the base of the ionosphere above intense electrical storms. They manifest as rapidly expanding rings of light generated by the electromagnetic pulse (EMP) produced by intense lightning strikes.

Multi-elves are events characterised by multiple concentric rings temporally separated by intervals on the order of microseconds. Therefore, we need detectors with temporal resolutions in the microsecond range to observe events with two, three and four rings. So far, few observations have reported double elves (Barrington-Leigh and Inan, 1999; Newsome and Inan, 2010; Klimov et al., 2019; Aab et al., 2020; Romoli, 2023), but only the last two have reported triple-ring elves. Later, in chapter 3, we will show how the high temporal resolution of our Fluorescence Detector has enabled the detection of several double- and triple-elves.

Even with these observations, a complete understanding of the origin of multi-elves remains elusive. However, two hypotheses were proposed to explain their existence. One links the second ring to the reflection at the ground of a component of the EMP from an in-cloud lightning strike (Marshall et al., 2015). The other hypothesis associates

the time delay with combinations of the rise and fall time of the lightning current density pulse (Marshall, 2012). There are also some simulations performed by Liu et al. (2017), which indicate that energetic in-cloud pulses (EIPs) can generate two- and even four-ring elves, which can also co-occur with terrestrial gamma-ray flashes.

In this chapter, we describe the various phenomena occurring around thunderstorms. This includes the storm formation and propagation of lightning (section 2.1); transient luminous events and terrestrial gamma-ray flashes (section 2.2). In section 2.3, we present the global detection of multi-elves and the proposed mechanisms behind multi-elves origin in section 2.4.

2.1 Lightning theory essentials

Transient luminous events and terrestrial gamma-ray flashes are produced by and primarily influenced by storms, their morphology and the specific type of lightning generated. This section outlines the formation of these storms, presents a basic model for cloud charge distribution, discusses the various types of discharges, and outlines the steps involved in a lightning strike.

2.1.1 Thunderstorms

A convective thunderstorm system usually develops when warm, moist, and unstable air rises from the plains due to a lifting mechanism, such as a mountain range. As this air ascends into colder regions, it forms dense clouds with significant vertical extension, known as cumulonimbus clouds.

This meteorological phenomenon is characterised by lightning and is usually accompanied by strong winds and rain or sometimes by hail or snow. Lightning is a natural

geophysical event characterized by the sudden electrostatic discharge between two electrically charged regions in the cloud or the Earth's surface, resulting in a temporary equalization of their electrical potentials.

Lightning detection is commonly based on either the visible or radio wave range, leading to two main categories of monitoring instruments:

- Observations from space are based on optical detection of emissions from the heated lightning channel (most commonly radiation at 777 nm), extending to the near UV range for research instruments. Examples are NASA's Optical Transient Detector (OTD) and Lightning Imaging Sensor (LIS) (Christian, 1992) aboard the Earth Observing System (EOS) Tropical Rainfall Measuring Mission (TRMM) satellite, or the LIS (Blakeslee et al., 2014) and the Modular Multi-spectral Imaging Array (MMIA) (Chanrion et al., 2019) aboard the International Space Station (ISS), or the Geostationary Lightning Mapper (GLM) (Rudlosky et al., 2019) onboard the satellites GOES-16 and GOES-17, or ESA/EUMETSAT's Meteosat Third generation MTG-L1 (Palacios et al., 2023).

- Observations from the ground are generally based on the detection of radio wave emissions (sferics) generated by lightning in the very low frequency (VLF) and low-frequency (LF) bands, which allow reflection within the Earth-ionosphere waveguide and therefore detection at an very long distance via ground networks of sensors. Research instruments extend up to the Very High Frequency (VHF) range to gather information on the initial stages of lightning. Examples of networks are the National Lightning Detection Network (NLDN) (Orville, 2008) adopted at continental scales, the Lightning Mapping Array (LMA) (Thomas et al., 2004; Lang et al., 2020) which operates on a local scale yet provides three-dimensional capabilities (LMAs are placed at multiple locations worldwide), the European lightning location system (EUCLID) (Schulz et al., 2016), the World Wide Lightning Location Network (WWLLN) (Rodger et al., 2004) or the Earth

Figure 2.1: Gigantic thunderstorms, reaching approximately 18 kilometres into the atmosphere, are a common occurrence in central Argentina, surpassing the height of typical thunderstorms by 6 kilometres. Two major projects, RELAMPAGO and CACTI, aim to enhance our understanding of these powerful storms. RELAMPAGO focuses on studying air temperature, wind patterns, rainfall, and lightning strikes to improve our models of how descending air from the eastern side of the Andes triggers these mega-thunderstorms. Meanwhile, CACTI explores the influence of atmospheric particles like dust and haze on storm development (Witze, 2018).

Networks Total Lightning Networks (ENTLN) (Lapierre et al., 2019).

Thunderstorms are more common in regions near the Earth's equator and the occurrence decreases towards the poles. This distribution is associated with the constant availability of warm and humid unstable air within tropical regions, which maximises in the deep convection of the Intertropical Convergence Zone (ITCZ), and with the seasonally varying convection in the middle latitudes.

The annual flash rate as measured by the OTD is 44 fl s^{-1} (Christian et al., 2003), with average values ranging from 10 in the mid-latitudes up to over 70 in the "lightning

chimney" of central Africa. The list of the hotspot places in the world ranks the Lake of Maracaibo in Venezuela in the first position (Albrecht et al., 2016), where 233 fl km^{-2} yr^{-1} occur, and the Congo basin hotspot in Africa in second place with 205 fl km^{-2} yr^{-1}, both places with latitudes close to the equator.

Within the field of view of the Auger Fluorescence Detector is the region of Córdoba, Argentina, which is well-known for its gigantic thunderstorms that generate most of the elves we detect. Figure 2.1 shows an example of mega-storms reaching cloud top heights (CTH) approximately 18 km into the atmosphere (Witze, 2018), surpassing the height of thunderstorms in the region which typically reach around 12 km.

The monthly climatology of lightning flash rates in Subtropical South America indicates that lightning activity shifts to the southwest from November, reaching central Argentina near the *Sierras de Córdoba* range and the Andean foothills. Figure 2.2 shows this seasonal change in lightning activity as reported in (Rasmussen et al., 2014). We observe a high rate of lightning between November and March around the Auger FD located at 35.2°S and 69.4°W.

Two major projects aim to enhance our understanding of these powerful storms in Argentina (Nesbitt et al., 2021): the Remote sensing of Electrification, Lightning, And Mesoscale/microscale Processes with Adaptive Ground Observations (RELAMPAGO) and the Cloud, Aerosol, and Complex Terrain Interactions (CACTI).

RELAMPAGO focused on studying the meteorological conditions associated with storms and their evolution in detail, including measurements of e.g., air temperature, wind patterns, rainfall, and lightning strikes to improve our models of how descending air from the eastern side of the Andes triggers these mega-thunderstorms. The CACTI project explores the influence of atmospheric particles like dust and haze on storm development. In chapter 6, we will show the correlation of data from these projects with the elves detected in Auger.

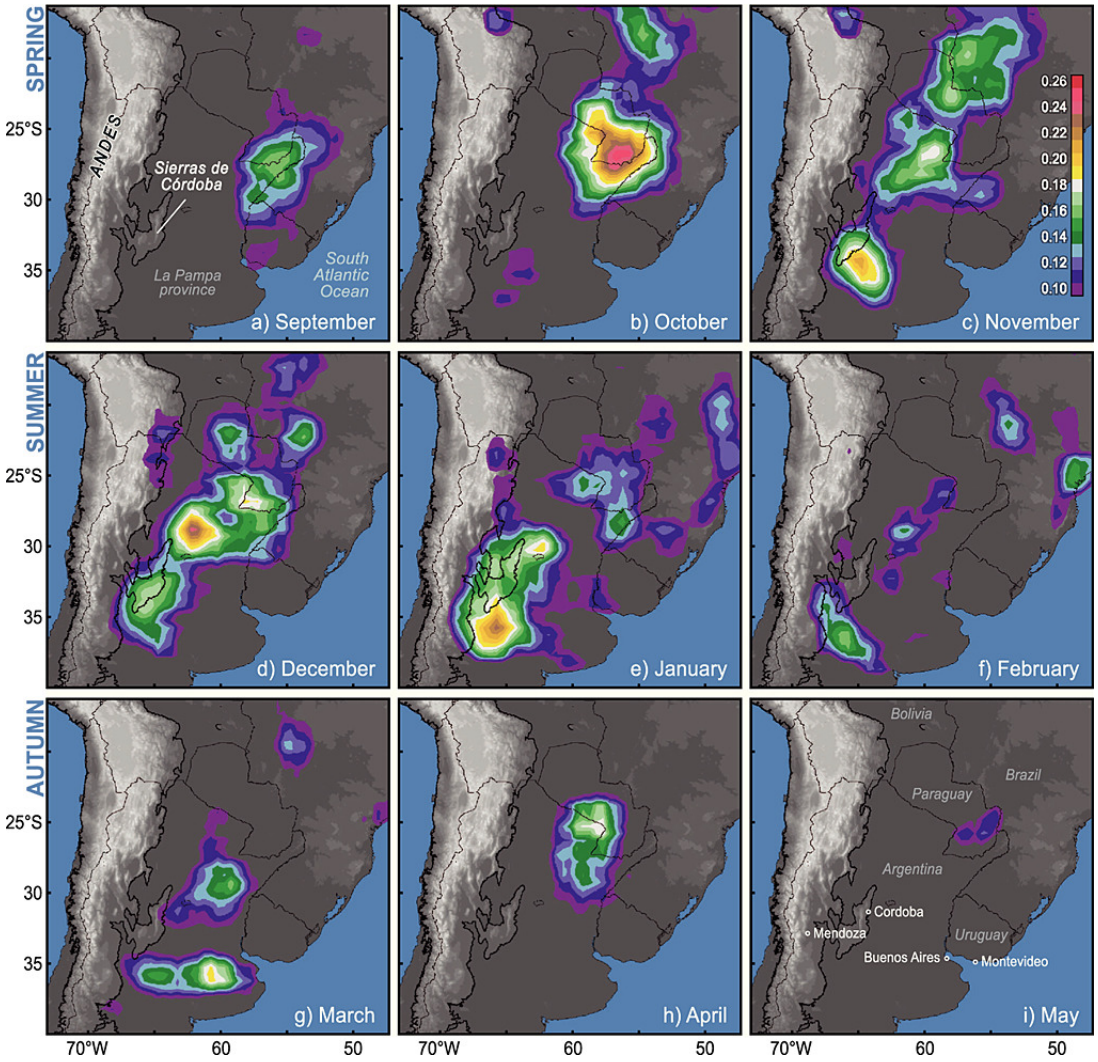

Figure 2.2: Monthly lightning climatology from the Lightning Imaging Sensor (LIS) and Optical Transient Detector (OTD) expressed as lightning rates (fl km^{-2} yr^{-1}) from September through May in Subtropical South America (Taken from (Rasmussen et al., 2014)). Starting in November, lightning activity shifts towards the southwest, reaching central Argentina near the Sierras de Córdoba range and the foothills of the Andes, intersecting the Auger Fluorescence Detector's field of view that is located around 35.2°S and 69.4°W.

After decades of devoted observation and research on lightning, our understanding of this natural event is still quite limited, with many questions underlying mechanisms yet to be completely understood, e.g, the initial breakdown process of lightning strokes within thunderclouds and the mechanisms that govern its propagation over extensive distances; the characterisation of the electrification process of convective thunderstorms and; the production mechanisms behind TLEs and TGFs. In the following sections, we present the mechanism of charge distribution in storms (section 2.1.2) and the processes involved in a lightning stroke as currently understood (section 2.1.3).

2.1.2 Thundercloud charge distribution

The mechanism for primary charge transfer in the cloud is the collisions between soft hail particles (graupel) and small ice crystals (Dwyer and Uman, 2014). The hail is heavy enough to fall or remain stationary in the storm's upward air currents, while the ice crystals are sufficiently light to be carried upwards, resulting in negative charging of graupel and positive charging of ice crystals. The standard tripole model gives the ideal charging structure of thunderstorms, where the cloud has a main middle negative, a main positive, and a lower positive charge zone (see figure 2.3). Often, a further screening layer, the fourth region of a significant negative charge, appears at the top of the cloud.

After the charged layers are formed, a quasi-static electric field will surround the storm. The maximum electric field in thunderclouds measured by balloons and aircraft is between 0.1 and 0.3 MV/m (Dwyer and Uman, 2014). These values are far below the breakdown threshold of dry air at sea level of 2.6 MV/m and a 6 km altitude of 1.6 MV/m, which would in principle be needed to cause lightning.

The hydrometeor-initiated positive streamer system is the most popular process to provide the additional energy necessary to bridge the gap between the breakdown threshold

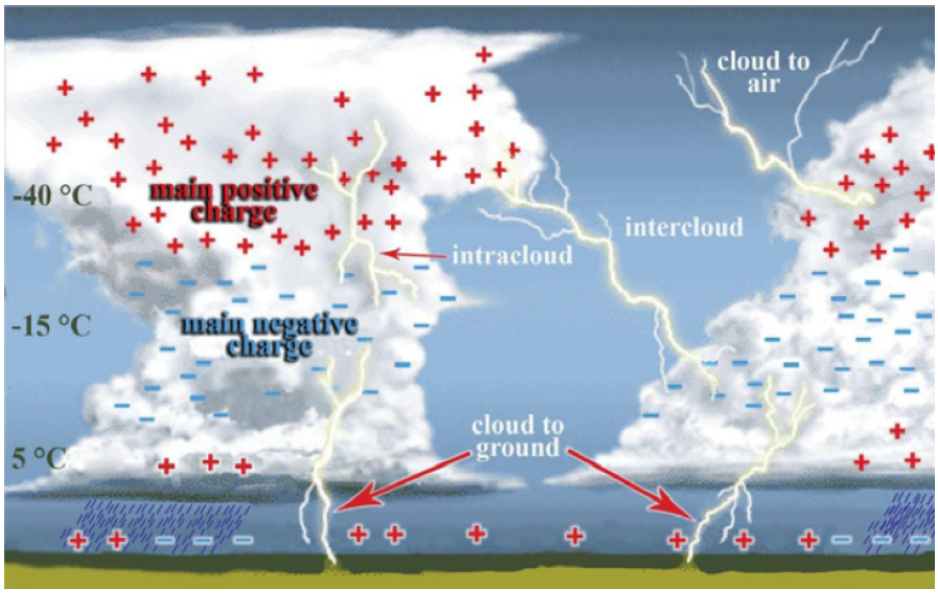

Figure 2.3: Charging structure of two adjacent storms. According to the three-pole model, the upper part of the cloud is dominated by the main positive charge, followed by the main negative layer and a small layer of positive charge in the lower part. The main types of lightning are shown: within the cloud (IC), between two clouds (CC), from cloud to ground (CG) and even from cloud to air (CA). Taken from (Dwyer and Uman, 2014).

of air and the maximum electric field in thunderclouds. It is also believed that cosmic rays may be involved in producing local enhancements of the electric field, but the studies in this are not sufficient to justify the physical mechanisms proposed to describe the link between cosmic rays, lightning and climate (Kumar et al., 2018).

2.1.3 Process in a lightning stroke

Lightning can be defined as a long electric spark that occurs once an initial breakdown happens in the cloud. Normally, lightning lasts around 300 ms and has an average length of 5 to 10 kilometers (Dwyer and Uman, 2014). However, rare cases of extremely long lightning flashes have been reported. The world's greatest extent single lightning flash was reported by the World Meteorological Organization (WMO) on 29 April 2020. It was observed between Texas and Mississippi with an extension of 768 km (Peterson

et al., 2022). The WMO also reported the longest-duration for a single lightning flash of 17.102 s, which occurred between Argentina and Uruguay on 18 June 2020.

The development of a lightning stroke occurs through several physical processes. As an example, figure 2.4 shows stages in the development of a cloud-to-ground discharge which is described below (Rakov and Uman, 2003):

- The initial breakdown process initiates the stepped leader's movement by redistributing local charges, creating strong current variations and EMPs. This occurs in fast pulses separated by tens of microseconds, as shown at t = 1.00 ms.
- The stepped leader is responsible for transporting charges from one layer to an oppositely charged layer, which is located several kilometres away. This process is shown at t = 1.10 ms. Most of the charges accumulate at the leader tip instead of along the trailing channel. The path to the opposite layer is determined by local air density and temperature, which results in steps at potential bifurcations along the way (t = 19.00 ms). Typically, stepped leaders propagate over tens of ms.
- When the charges in the leader tip come into contact with a charged layer or another leader tip of opposite charge polarity, the attachment process takes place, as shown at t = 20.00 ms. The duration of the attachment is estimated to be only a few microseconds, and its exact mechanism is not yet fully understood.
- Approximately 10 μs after the attachment process, the first return stroke occurs. The charges deposited along the channel flow at speeds close to the speed of light and reach peak current values as high as 300 kA for positive CG lightning in less than 30 μs. These highly energetic events can be measured across a wide range of electromagnetic frequencies.
- At t = 40.00 ms, the K- and J- processes initiate the motion of charges down the lightning channel by readjusting charge within the cloud.

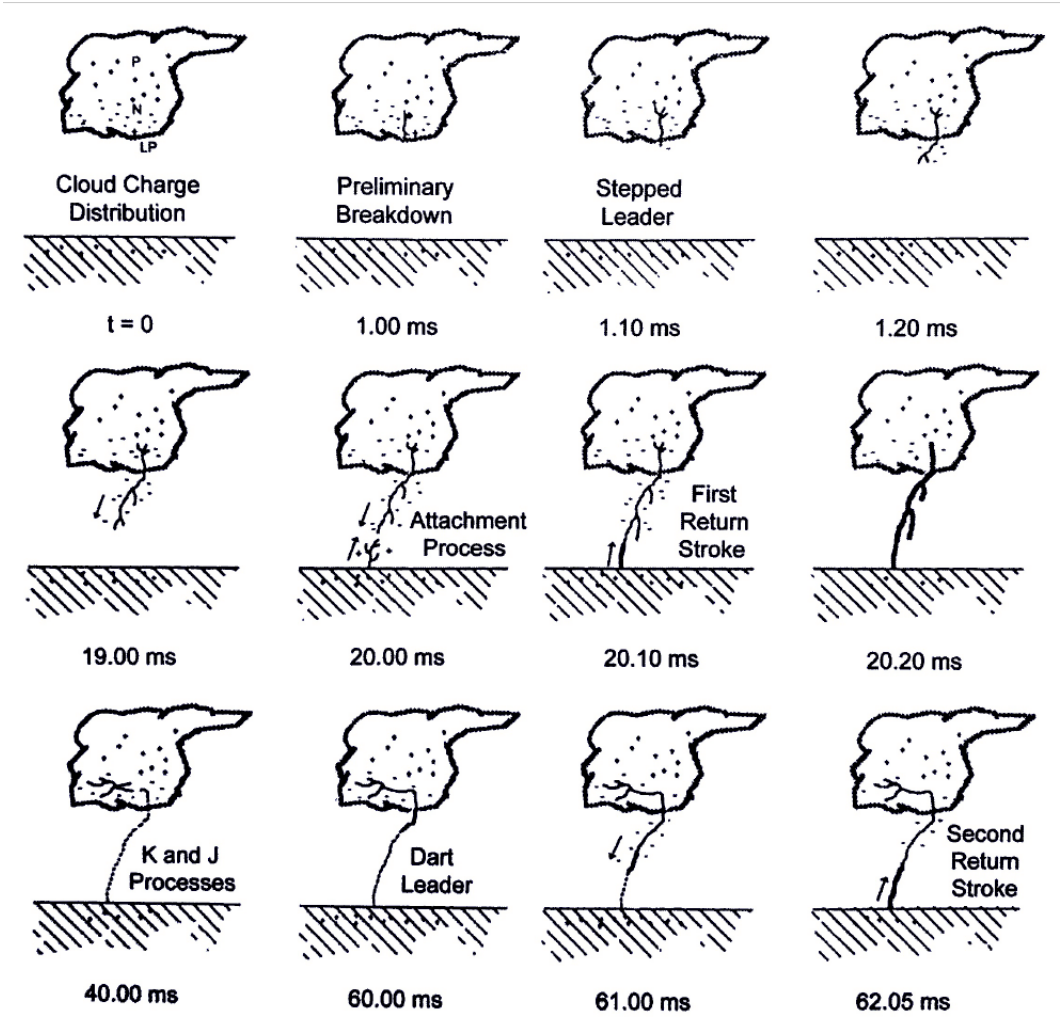

Figure 2.4: The sequence of events in a cloud-to-ground lightning stroke process. Enough charge builds up in the convective thunderstorm to allow for possible discharges. The 60 ms long process to the second return stroke consists of many energetic events that could create EMPs. Taken from (Rakov and Uman, 2003).

- Then the dart leader occurs, transporting a large amount of charge from the origin of the discharge to the opposite layer via the path of least resistance (the main channel of the stepped leader). Subsequently, a secondary return stroke may occur, characterized by currents significantly lower than those of the initial discharge.

Lightning flashes can occur in the cloud (IC), between clouds (CC), from cloud to ground (CG), or even from cloud to air (CA), as shown in figure 2.3. Depending on the charges that travel through the lightning channel, four types of charge transfer exist: downward negative, downward positive, upward negative and upward positive. Downward negative flashes account for more than 90% of global CG lightning, and the remaining discharges are downward positive (Dwyer and Uman, 2014). Some lightning leaders are initiated from tall objects (100 m) and move from the ground to clouds.

These lightning strokes may induce light emissions in the atmosphere called transient luminous events, or even gamma emissions known as terrestrial gamma-ray flashes. The following section is dedicated to the description of these phenomena and how they have been detected over the years.

2.2 Elves and transient luminous events

Transient luminous events are short light emissions that occur in the upper layers of the atmosphere, i.e. in the stratosphere and mesosphere, up to the lower edge of the ionosphere (Rodger, 1999; Neubert, 2003; Neubert et al., 2005; Füllekrug et al., 2006; Pasko et al., 2012; Dwyer and Uman, 2014). These events originate above thunderstorms from IC or CG lightning or emerge from the thunderstorm top directly initiated by charge imbalances in the upper layers of the cloud. The family of TLEs consists of sprites, blue starters or blue glimpses, blue jets, gigantic jets, elves and halos. Figure 2.5 shows the different phenomena in the upper atmosphere produced by thunderstorms, including

TLEs and TGFs.

Elves are a class of TLEs occurring at the base of the ionosphere above intense electrical storms. The light, emitted as a rapidly expanding ring, is generated by extreme lightning's electromagnetic pulse that propagates as a spherical wave from the lightning channel (Füllekrug et al., 2006). As predicted by Inan (1990) and Inan et al. (1997) the upward passage of short and intense electromagnetic pulses (5–20 V/m at 100 km distance) from natural lightning heats ionospheric electrons, inducing transitions upon collision with atmospheric molecules. After reverting to lower-energy states, these molecules emit light over a broad spectrum through fluorescence. Taranenko et al. (1993) described elves as a very brief (less than 1 ms) intense brightness produced at the base of the ionosphere.

Table 2.1 summarises the main characteristics of elves, sprites, blue jets and halos, comparing their length, altitude, photon flux, time length and global rate. These phenomena have been sporadically reported since as early as 130 years ago when MacKenzie (1886) described what would become known as a "gigantic jet". Wilson (1925) proposed that electrical breakdown could occur tens of km high above active thunderstorms.

Decades later, the first image of a sprite was captured when Winckler and his students were testing a Low-Light Television camera (LLTV) for an upcoming research rocket flight in 1990 (Franz et al., 1990), so a lightning mapping program with LLTV-like cameras with a time resolution of approximately 17 ms was set up on the Space Shuttle. The videos revealed a widening transient glow that was the first reported elve (Boeck et al., 1992) and more than a dozen upward lightning strikes over a storm.

In 1993, NASA began funding ground and airborne research in this field (Sentman and Wescott, 1993). In that period, the same Winclker LLTV was installed at the Yucca Ridge Field Station (YRFS), where about 250 events were detected several hours above a storm (Lyons, 1994a,b). Besides, these events were found to produce signals in the VLF band (Füllekrug et al., 2006). The following year, the first colour images of sprites

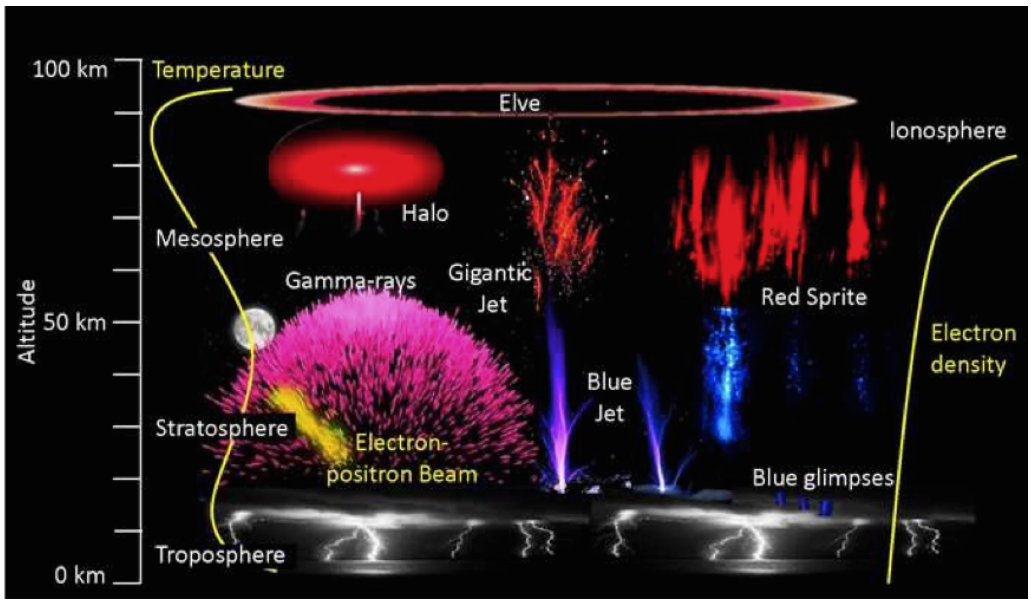

Figure 2.5: Upper atmospheric phenomena generated by thunderstorms, including Terrestrial Gamma Ray Flashes and Transient Luminous Events. This figure shows the typical dimensions and altitudes at which these phenomena occur. (Taken from (Gaskill, 2018)).

Table 2.1: Summary of the main characteristics of the transient luminous events (Füllekrug et al., 2006; Dwyer and Uman, 2014; Chen et al., 2008)

Event	**Sprites**	**Blue jets**	**ELVES**	**Halos**
Description	Reddish plasma with blue branches down	Upward lightning coming out of the cloud top	Rapid expansion red light toroidal disc	Diffuse red light emission in the form of a disc
Trigger	+CG lightning	Electrical breakdown between the main and the screening layer	EMP from a CG or IC lightning ($I > 80$ kA)	-CG lightning +CG lightning with sprites
Length	$\sim$ 40 km	40 - 70 km	$\sim$ 300 km diameter	$\sim$ 25 km diameter
Altitude	70 - 75 km	Cloud top	80 - 100 km	65 - 80 km
Photon flux	$\sim$ 1 MR	$>$ 1 MR	$\sim$ 1 MR	0.50 - 1 MR
Time length	1-10 ms	$\sim$ 300 ms	$\sim$ 1 ms	$\sim$ 1 ms
Global rate	1 min^{-1}	0.01 min^{-1}	35 min^{-1}	1 min^{-1}

were registered, and the blue jets appeared (Sentman et al., 1995). From the YRFS observations made between 1994 and 1995, the correlation between sprites and positive cloud-to-ground lightning (+CG) became evident (Barrington-Leigh et al., 1999).

In 1995, Fukunishi et al. (1996) reported new measurements at the YRFS of diffuse optical flashes that extended horizontally for about 100-300 km and lasted less than 1 ms. These flashes occurred at altitudes of 75-105 km in the lower ionosphere, just after cloud-to-ground lightning discharges. This confirmed the theoretical predictions of elves from several authors (Inan, 1990; Inan et al., 1997; Taranenko et al., 1993). Later, these phenomena were studied from linear arrays of photometers, with a resolution time enhanced to 40 μs (Inan et al., 1997) producing the first measurements of the rapid lateral expansion of the optical luminosity of elves.

For a more detailed study of the spatial and temporal structure of the TLEs, a variety of photometric sensors, radio measurements, high-speed cameras, high-resolution cameras, and high-speed telescopic images were used (Füllekrug et al., 2006). The optical programs of the YRFS and the New Mexico Tech's Langmuir Lab revealed that the first observations thought to be elves were the halo that preceded some sprites (Füllekrug et al., 2006).

Detecting TLEs using satellites is more efficient compared to ground-based detection methods. For instance, the data recorded by ISUAL (Imager of Sprites and Upper Atmospheric Lightning on board of FORMOSAT-2 satellite) (Chen et al., 2008) revealed a significantly greater prevalence of elves relative to other TLEs in ground-based observations (Sato and Fukunishi, 2003), primarily due to the challenges associated with detecting these events from ground-based camera systems. Chen et al. (2008) showed that elves are the most frequently occurring TLE, with an overall rate of 35 events min^{-1} outnumbering both sprites and halos (1 min^{-1}) and gigantic jets (0.01 min^{-1}). They also conclude that elves occur more frequently over the oceans than over the land, and their rate increases when the sea surface temperature exceeds 26°C.

Another example is the observations conducted by the Atmosphere-Space Interactions Monitor (ASIM) (Neubert et al., 2019) onboard the ISS, which comprises the first space mission with a complete set of instruments designed to measure lightning, TLEs and terrestrial gamma-ray flashes. The capabilities of the Modular Multispectral Imaging Array of ASIM allowed the detection of thunderstorm coronas referred to as Blue Luminous Events (BLUEs) (Soler et al., 2021), presenting their first nighttime climatology, including the global geographical and seasonal distribution. Such observations may suggest a more substantial impact of the TLEs family on the atmosphere and climate than previously assumed.

The climatology of TLEs in Europe reveals significant activity during the summer over continental regions and in late autumn over coastal zones and the sea (Arnone et al., 2020). This analysis was conducted based on optical observations from the Eurosprites campaigns of several research groups worldwide, covering extensive regions of Europe and coastal territories. Between 2009 and 2013, a total of 8319 TLEs were observed above 1018 thunderstorm systems, which were utilized for the investigation of their distribution and seasonal variation over Europe and portions of the Mediterranean Sea.

The analysis of the altitude fluctuation of elves performed by van der Velde and Montanyà (2016) is an example of the large statistics of elves in Europe. They reported altitude variations in elves emissions ranging from 80 to 96 km from 389 events recorded by ground-based low-light cameras in northeastern Spain. The authors suggested that those variations are more likely linked to the solar cycle and geomagnetic disturbances which modulate the altitude of the base of the ionosphere. They also reported that night-to-night changes of 1-3 km in elves heights are possibly influenced by long-period neutral density and temperature changes, such as gravity waves and tides, or variations in meteoric dust particles and chemical factors affecting the electron density gradient.

Besides, intense bursts of gamma rays that originate from the Earth's atmosphere were observed at the top of the clouds (Fishman et al., 1994; Smith et al., 2005; Marisaldi

et al., 2010; Roberts et al., 2018; Neubert et al., 2019). Terrestrial gamma-ray flashes were discovered in 1994 by the Burst and Transient Source Experiment (BATSE) on-board the Compton Gamma-Ray Observatory (CGRO) (Fishman et al., 1994), and then measured by several spacecraft, including the Reuven Ramaty High Energy Solar Spectroscopic Imager (RHESSI) (Smith et al., 2005), Fermi (Roberts et al., 2018) and the Astro-rivelatore Gamma a Immagini Leggero (AGILE) (Marisaldi et al., 2010).

The energy spectra of TGFs extend to tens of MeV, so the only viable mechanism to produce them is through bremsstrahlung interactions of energetic electrons and positrons with air atoms (Dwyer et al., 2012). The runaway electron mechanism (Wilson, 1925) explains how electrons may obtain large energies in thunderstorms. Dwyer (2008) showed two theories that could explain the origin of TGFs: the cold runaway seeding of Relativistic Runaway Electron Avalanches and the Relativistic Feedback Discharge mechanism (Dwyer, 2012; Liu and Dwyer, 2013).

Liu et al. (2017) demonstrated that elves and multi-elves may accompany TGFs when originate from a specific category of IC discharge referred to as energetic in-cloud pulses. ASIM has already reported its first elve accompanying a TGF (Neubert et al., 2019), and subsequently, Bjørge-Engeland et al. (2022) presented a global distribution map featuring 17 of these events, associated with high peak current lightning, ranging from 76 to 486 kA. Detecting these phenomena will facilitate the understanding of the inter-relations of TLEs, TGFs, and lightning.

2.3 Global detection of multi-elves

As we investigate elves with multiple rings, we will review various observations of multi-elves in this section. The global detection of multi-ring elves is relatively scarce due to the requirement for exceptionally high temporal resolutions of detectors.

Table 2.2: Non-exhaustive list of past, present, and future experiments that may detect elves or are specifically made to detect them. Updated from (Merenda, 2020).

Experiment		**Location**	**Time Resolution**	**Wavelenght**	**DAQ period**
Discovery Shuttle		Space	17 ms	360 - 720 nm	10/1990
Fly's Eye		Ground - USA	16 μs	185-800 nm	
Fukunishi	2 CCD	Ground - USA	17 ms	400 - 800 nm	06/1996 - 08/1996
	PMT		15 μs		
ISUAL	Imager	Space	14 ms	623 - 750 nm	05/2004 - 08/2016
	SP		100 μs	337 nm / 391.4 nm	
	AP		500 - 5 μs	370 - 450 nm / 530 - 650 nm	
Eurosprite		Ground - Europe		Optical	2009 - 2013
Watec 902H2 CCD camera		Ground - Spain	20 ms	400-1000 nm	06/2008 - 02/2016
PIPER		Ground - USA	40 μs	300 - 450 nm	
JEM - GLIMS		Space			11/2012 - 08/2015
Auger FD		Ground Argentina	100 ns	300 - 420 nm	03/2013 Present
TUS		Space	0.8 μs		08/2016 - 11/2016
Mini - EUSO		Space	2.5 μs	300 - 400 nm	08/2018 -
ASIM	2 CCDs	Space	65 ms	337, 391, 650-740, 762, ... nm	2018 -
	3 PMTs		100 kHz	337, 391, 650-740, 237, ... nm	

Only a few authors have reported cases where two of these elves' pulses appear close together in time (Barrington-Leigh and Inan, 1999; Newsome and Inan, 2010; Klimov et al., 2019; Aab et al., 2020; Romoli, 2023), sometimes only tens or a few hundred microseconds apart. These pulses, often called elves doublets, are thought to be associated with the same event because they are too close to be related to different return strokes. Very few authors have been able to report triple-peaked elves (Aab et al., 2020; Romoli, 2023).

In table 2.2 a comparison of the location, temporal resolution, the wavelength at which they detect and the data acquisition period (DAQ) of several detectors of elves. Some of these detectors have reported multi-elves. The first one was an unusually bright event exhibiting a double-pulse structure in several photometers of the Fly's Eye detector (Barrington-Leigh and Inan, 1999), as shown in the left panel in figure 2.6.

The high resolution (40 μs) of the ground-based Photometric Imager of Precipitated Electron Radiation (PIPER) (Newsome and Inan, 2010), enabled the observation of

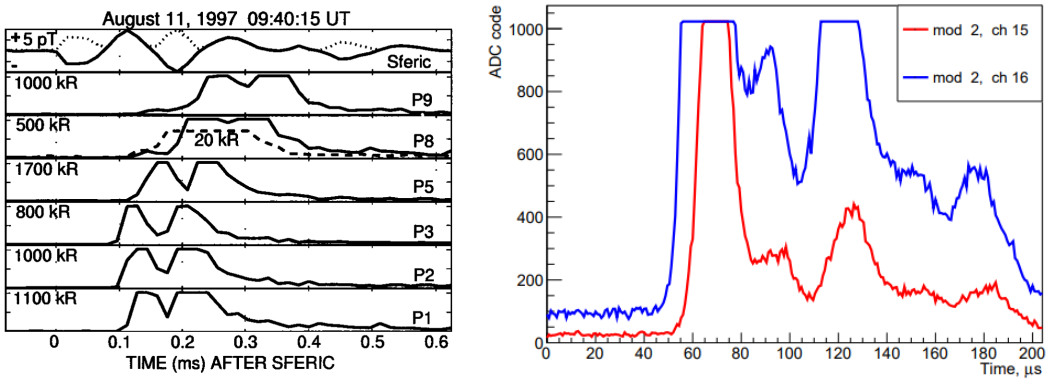

Figure 2.6: Left: sferic and photo-metric signals of an unusually bright event that exhibits a double-pulse structure in several pixels of the Fly's Eye (Barrington-Leigh and Inan, 1999). Right: multi-elve waveforms in pixels 15 and 16 of the TUS instrument, revealing two prominent peaks with some less bright pulses (Klimov et al., 2019).

40 double elves in four storms in New Mexico, USA, with an average time gap of 120 μs. An example is shown in the top panel of figure 2.7. In this study, they discuss the mechanisms that could be behind the origin of the multiple rings of elves without finding an explanation. Figure 2.8 shows the number of events detected per storm and the percentage of double elves and double elves occurring with halos (labelled as "halos" in the plot).

The Tracking Ultraviolet Setup experiment (TUS) (Klimov et al., 2019) reports an event with multiple peaks owing to its impressive 0.8 μs resolution. The brightest peaks in the traces of the multi-elve exhibit a temporal difference of approximately 60 μs, however, some of the pulses lack clarity (see figure 2.6).

More recently, the Multiwavelength Imaging New Instrument for the Extreme Universe Space Observatory (Mini-EUSO) reported an event with three peaks, featuring an inter-ring distance of 83 and 95 μs, along with some double and quadruple events (Romoli, 2023). Figure 2.7 shows two examples of such events.

In contrast, the Fluorescence Detector of the Pierre Auger Observatory has detected hundreds of double and triple elves, constituting around 27% of the total annual

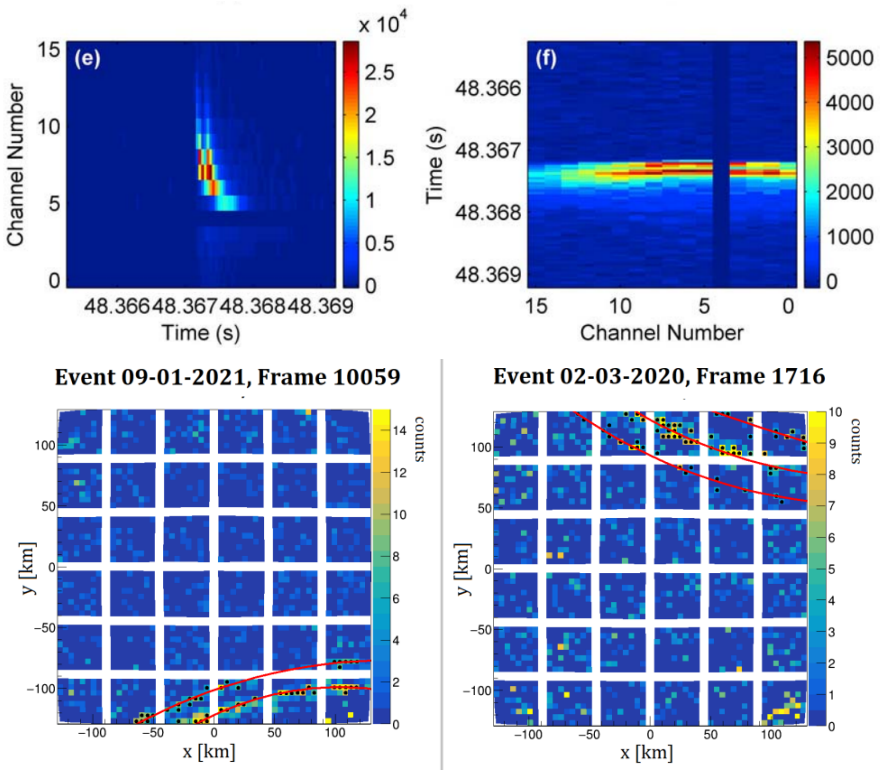

Figure 2.7: Top: An example of an elve doublet detected in PIPER, illustrating the vertical distribution of light in the field of view over time from left to right (left panel) and the horizontal distribution of light over time from top to bottom (right panel) (Newsome and Inan, 2010). Bottom: Multi-elves recorded by Mini-EUSO. Left: a double ring event with an inter-ring distance of 50 μs. Right: a multiple-ring event with 83 and 95 μs inter-ring distances. The red lines depict the result of an iterative circle-fitting algorithm applied to each frame (Romoli, 2023)

.

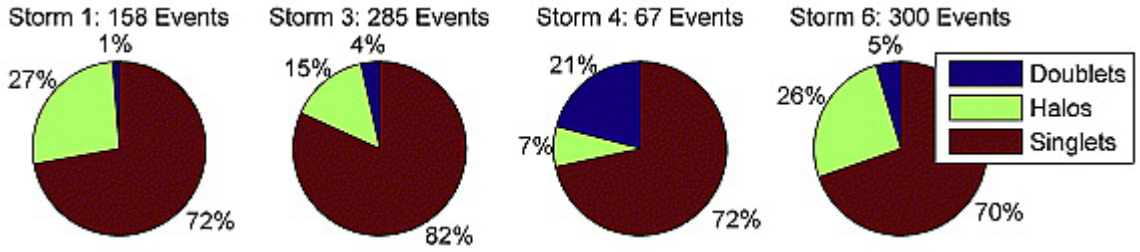

Figure 2.8: Distributions of counts of elves detected per storm in the PIPER (Newsome and Inan, 2010). "Doublets" are two-ringed elves, "Halos" refers to elves occurring with a halo, and "Singlets" are single elves without additional elves or halos.

events (Vásquez Ramírez et al., 2022). Leveraging an unprecedented temporal resolution of 100 ns, we observed the first elve with three distinct pulses in its traces on March 4, 2016, at 05:32:39 UTC (Aab et al., 2020) (see figure 3.4 (e)).

The Pierre Auger Observatory is the world's most extensive infrastructure for studying ultra-high energy cosmic rays, combining the facilities of a Surface Detector (SD) and a Fluorescence Detector (Abraham et al., 2010). Apart from its primary activity, the FD has been detecting elves over the Pacific and Atlantic oceans and Córdoba in Argentina (Aab et al., 2020). In chapter 3, we describe the operation of the Auger Observatory, which, considering its efficiency and duty cycle, can be currently considered the best ground-based instrument for observing elves in the near-ultraviolet band (Mussa et al., 2012).

2.4 Origin of the multi-elves

As previously mentioned, there are reports of multiple-peaked elves that occur in close succession, ranging from tens to a few hundred microseconds apart. The cause of these multiple peaks is not yet completely understood and may originate from competing mechanisms under different conditions. Based on early ground observations of elves by a photometer array, two main mechanisms were proposed and modelled.

In section 2.4.1, we introduce a model proposed by Marshall (2012) which suggests that double elves are caused by the rise and fall times of the lightning waveform pulse. Later, Marshall et al. (2015) discarded this model because unrealistic long rise times are necessary to produce the doublets detected in PIPER and proposed an alternative model. In this new approach, described in section 2.4.2, the second ring in an elve doublet is created by the electromagnetic pulse from compact intracloud lightning (CID) that bounces off the ground and reaches the ionosphere base with a time delay. Using this mechanism, Liu et al. (2017) conducted simulations of energetic in-cloud pulses of

varying durations that produced double and quadruple elves. The results are shown in section 2.4.4.

In the study of 40 double elves observed in PIPER with a time delay between 80 and 160 μs (Newsome and Inan, 2010) the EMP bouncing model was dismissed because would require an unrealistic source height. For example, for 120 μs the EMP source should be at 18 km above the ground, which is too high for CG or even IC lightning. They argued that these events are also unlikely to be caused by multiple return strokes since the interstroke period is around 60 ms.

To further investigate these mechanisms and improve the comparison with observations, the Auger Observatory's extensive sample of multi-elves can be utilized. Chapters 4 and 5 present the outcomes of the multi-elves analysis at the Pierre Auger Observatory, in comparison with these two models.

2.4.1 Double elves time delay related to the rise and fall time of lightning current density pulses

In the time-domain model of the lightning electromagnetic pulse interaction with the lower ionosphere proposed by Marshall (2012), double elves are an effect of the rise time, τ_r, and fall time, τ_f, of the lightning pulse waveform.

For the simulation of double elves, Marshall (2012) defines the lightning current waveform ($J_s(t)$) in equation 2.1, showing a linear rise to its maximum value in time τ_r, and an exponential decay back to zero with time constant τ_f.

$$J_s(t) = \begin{cases} J_0 t/\tau_r & t < \tau_r \\ J_0 e^{-(t-\tau_r)^2/\tau_f^2} & t \geq \tau_r \end{cases} \tag{2.1}$$

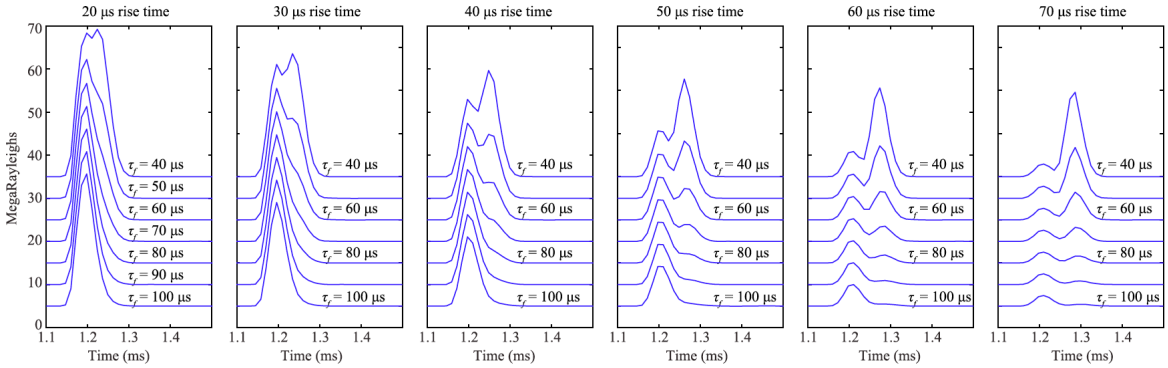

Figure 2.9: Results of the simulations of elves doublets for various rise and fall times values as measured in Channel 11 of the vertical PIPER array. Simulations performed by Marshall (2012) to explain the origin of the double elves.

Figure 2.9 shows the simulated brightness of the double-elves for various combinations of τ_r and τ_f as described in (Marshall, 2012). The simulations show how these events appear if detected by the PIPER photometer array instrument (channel 11), which can be considered as a high temporal resolution example of ground observation.

Under the mechanism proposed by this model, two important conclusions can be drawn:

- Every elve is a doublet, and the rising and falling edges of the current waveform trigger the emissions.
- A clear double elve implies similar rise and fall times of the current waveform, and both must be long enough to separate the two pulses in time.

Repeating these simulations but varying the distance between the camera observation point and the lightning source from 400 km to 500, 600, and 700 km, it was observed that the shape of the elves changes in the camera, but the main features of the temporal evolution of the simulated brightness does not change: the magnitudes of the two peaks are directly related to the rise and fall times, while the temporal difference between them is directly related to the rise time, as shown in figure 2.10.

According to Marshall (2012), these results align with PIPER observations reported

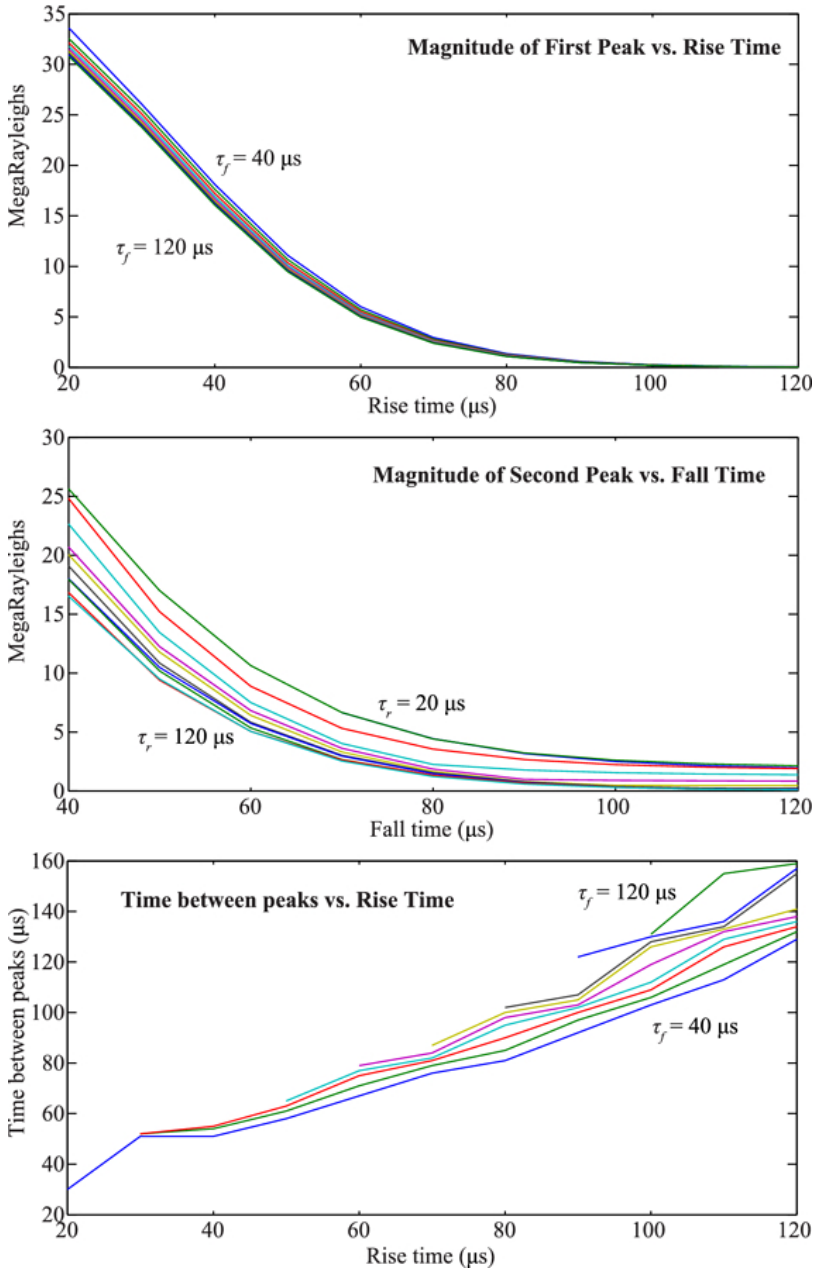

Figure 2.10: Magnitude of the first (top panel) and second (middle panel) peak of an elve doublet with varying τ_r and τ_f. (Bottom) Time difference between the two peaks as a function of the time constants. In some of the elves, one of the peaks is washed out by the other, more dominant peak, so a time difference cannot be established. Taken from (Marshall, 2012).

by Newsome and Inan (2010), where approximately 60 elves doublets show no preference for the distance from the discharge.

2.4.2 The electromagnetic pulse bounce mechanism from intracloud lightning producing multi-elves

This geometrical model proposed by Marshall et al. (2015) shows a direct correlation between the time gap of double elves rings and the source lightning height (h_s). As shown in figure 2.11, the first peak in the elve trace is created by the electromagnetic pulse taking a direct path from the lightning source to the base of the ionosphere, while the second peak is generated by the ground reflection of the EMP, which reaches the ionosphere with a time delay (ΔT). Moreover, the relative brightness of the first and second peaks of the elve might be associated with the orientation angle (α) of the source relative to the vertical.

The relationship between ΔT and h_s may be described by equations 2.2 and 2.3.

$$d_{2,1}^2 = (R_E \pm h_s)^2 + (R_E + h_{iono})^2 - 2\,(R_E \pm h_s)\,(R_E + h_{iono}) \cos\left(\frac{\mathrm{ArcR}}{R_E + h_{iono}}\right), \quad (2.2)$$

$$\Delta T = \frac{d_2 - d_1}{c}. \quad (2.3)$$

In these equations, d_2 and d_1 represent the distances travelled by the EMP in the direct-to-source and ground reflection paths, respectively. Additional parameters include R_E, which represents the Earth's radius, h_{iono}, denoting the height of the base of the ionosphere, and ArcR, defining the arc distance between the lightning position and the emission point P in the ionosphere (located at $\mathrm{Lat_{pix}}$, $\mathrm{Lon_{pix}}$). The location of the lightning bolt is defined by $\mathrm{Lat_s}$ and $\mathrm{Lon_s}$. The schematic illustrating these locations can be found in figure 2.11.

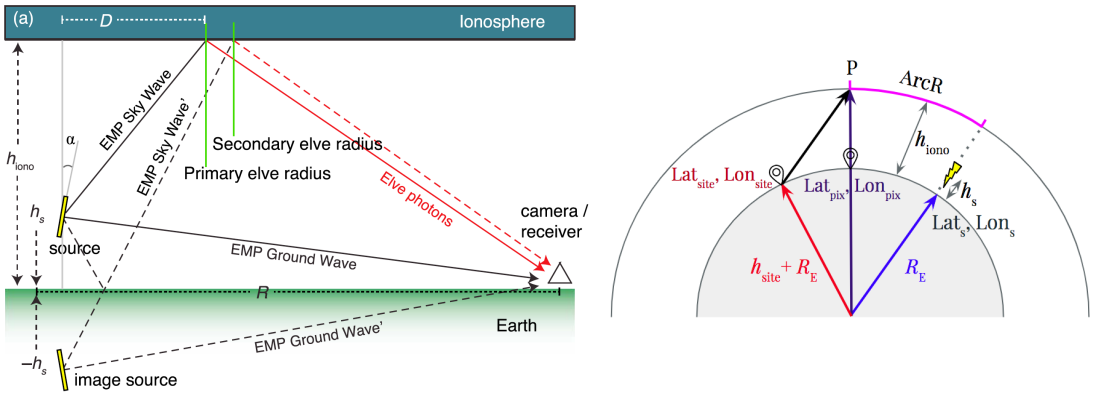

Figure 2.11: Left: schematic of the bounce mechanism of the electromagnetic pulse of an IC lightning occurring at a height h_s (Marshall et al., 2015). The first ring of the elve occurs due to the electromagnetic pulse with a direct path to the sky. In contrast, the second one originates from the pulse component that "bounces" off the ground and arrives in the ionosphere with a time delay. Right: schematic of the arc distance (ArcR) between the lightning source ($\mathrm{Lat_s}$, $\mathrm{Lon_s}$) and the emission point at the ionosphere P ($\mathrm{Lat_{pix}}$, $\mathrm{Lon_{pix}}$).

A calculation of the ΔT for different heights, h_s, at the same emission altitude in the ionosphere ($h_{\mathrm{iono}} = 92$ km) is shown in figure 2.12. Note that the time gap decreases as the arc distance to the lightning increases. This behaviour is independent of both the lightning's and the ionosphere's height, as varying the ionosphere slightly changes the curve. The values of h_s in these plots are typical values reported for IC lightning. For example, lightning occurring at h_s =14 km within gigantic storms in Argentina (CTH≈18 km) could originate double elves with a maximum value of $\Delta T = 100\,\mu$s.

This model has a constraint linked to the height of the stroke since observations of double elves with $\Delta T > 120\,\mu$s would result in unrealistic high values of h_s and therefore, the origin of such multi-elves could not be explained with this model.

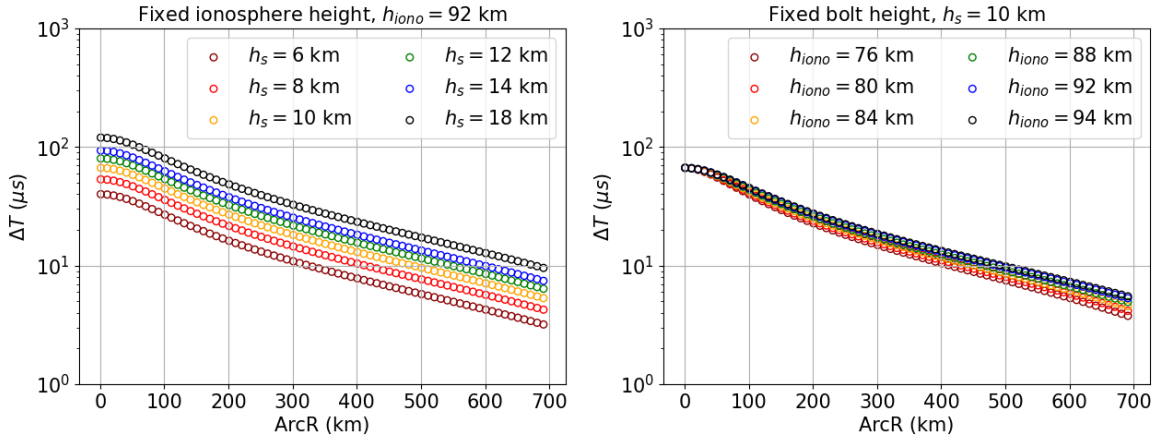

Figure 2.12: Left: time delay between two peaks of an elve, given by the equations 2.2 and 2.3, with the ionosphere height fixed at $h_{\text{iono}} = 92$ km and various values of lightning height (h_{s}). Right: varying the ionosphere height does not change the decreasing functionality of the curves of ΔT with distance ArcR; they slightly shift upwards or downwards along the y-axis (fixing h_{s} to 10 km).

2.4.3 IC lightning: the narrow bipolar events and the energetic in-cloud pulses

The proposed mechanism for EMP bounce in multi-elves depends on the altitude of the source, and two types of IC lightning that produce highly energetic radio frequency emissions, namely narrow bipolar events (NBEs) and energetic in-cloud pulses, were suggested to be related to multi-elves.

Lightning NBEs, or compact intracloud discharges (CIDs), were reported as the most powerful natural emitter of VHF radio waves on Earth with very short pulse duration (10-20 μs) (Le Vine, 1980; Smith et al., 1999). Studies suggest that NBEs are the initial breakdown process or the lightning precursors of thunderstorms' electrical discharges (Rison et al., 2016).

CIDs occur between the main positive charge layer and the screening layer, as shown in the right panel of figure 2.13. NBEs are created by Fast Positive Breakdown (Rison et al., 2016), consistent with the theory of positive streamers initiating lightning. Liu

et al. (2019) indicates that a system of 10^7-10^8 streamers can reproduce the current moment, charge transfer and radio spectrum of NBEs.

Additional studies show that dielectric breakdown can also begin with negative polarity discharges (Tilles et al., 2019), called Fast Negative Breakdown. They have similar spatial extent, peak current, charge moment change, VHF power rise time and VHF peak power but different speeds concerning Fast Positive Breakdown. NBEs produced by the Fast Negative Breakdown process are less common than those created by Fast Positive Breakdown (Tilles et al., 2019).

EIPs were first reported by Lyu et al. (2015) as very high peak-current IC lightning events (I_{pk} >200 kA) with LF radio emissions different from the NBEs. The measured source altitudes indicated that EIPs are typically generated between 10 and 13 km, placing them between the main negative and upper positive charge layers as shown in figure 2.13. From the analysis performed in (Lyu et al., 2015), clear IC pulses were seen within a few milliseconds before and after EIPs, and +EIPs often follow a lower altitude +NBE, suggesting that EIPs occur after the initiation and during the propagation of a negative leader.

Elves doublets were observationally confirmed to correlate with high altitude CIDs (Marshall et al., 2015). The authors calculated the lighting height using the maximum value of the ΔT detected among the vertical and horizontal channels of the PIPER (Marshall et al., 2008). They also suggest that many single elves labelled as CG-lightning generated are produced by CIDs. However, the temporal resolution of the PIPER (40 μs) was shown to be not sufficient to separate the peaks of these elves.

Liu et al. (2017) showed through simulations that EIPs can generate elve doublets and even quadruplets, depending on the duration of the EIP. These results suggest that different proposed mechanisms and EMP sources such as CG, CIDs or EIPs may produce a diversity of elves and multi-elves. This diversity depends on the properties of the discharge that produced the EMP, mainly the type of source, its altitude and

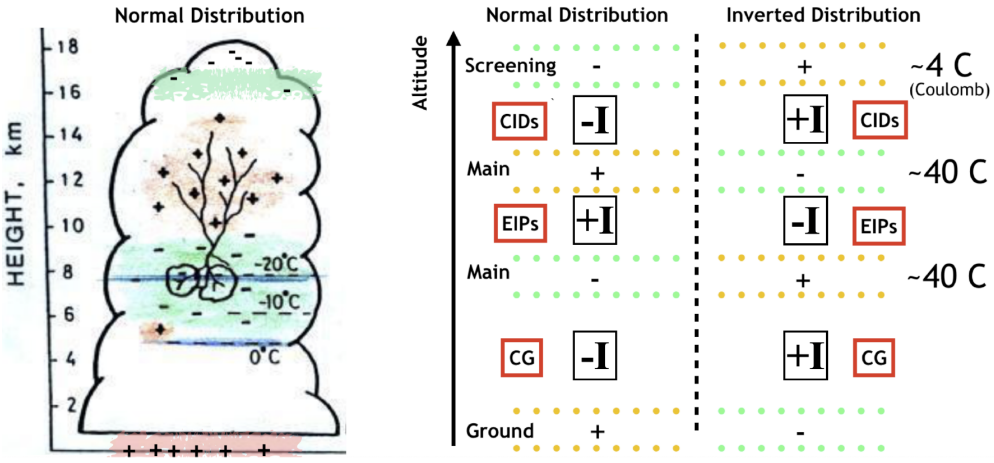

Figure 2.13: Left: Scheme of the normal charge distribution in a thunderstorm, with the height interval where discharges typically occur within the cloud (IC). Centre: CIDs can occur between the main positive layer and the negative screening layer, while EIPs can occur between the main positive and negative layers within a normal charge distribution. Right: In an inverse charge distribution of the storm, CIDs, EIPs, and CG with currents of polarity opposite to those of a normal distribution can occur. Taken from (Merenda, 2020).

duration. For example, elve doublets induced by EIPs are less separated in space and time than elves induced by CIDs.

Liu et al. (2017) showed a further interesting consequence of the EIP source, which is the simultaneous production of elves and TGFs from the same source. A summary of these results is shown below.

2.4.4 Energetic in-cloud pulses, multi-elves and terrestrial gamma-ray flashes

Based on the electromagnetic pulse bounce mechanism, Liu et al. (2017) simulated the link between elves and terrestrial gamma-ray flashes associated with energetic in-cloud pulses. They employed a cylindrical source at an altitude of 12 km, with a length of 1 km and a radius of 500 m from which both an elves-producing EMP and a TGF arise. The source was simulated with pulses of different duration, ranging from a short one

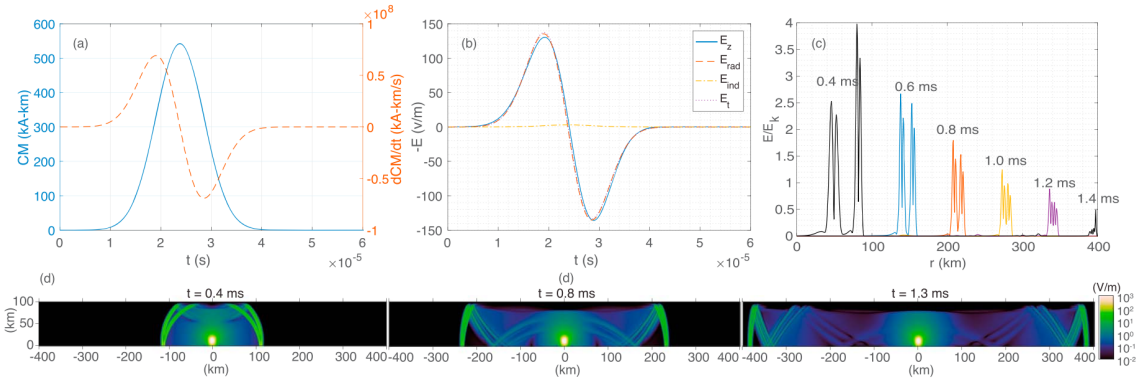

Figure 2.14: The source current of an EIP of 11.2 μs duration and its electric field. (a) The current moment waveform and its time derivative. (b) The electric field on ground at a distance of 100 km. The solid line shows the field from the simulation, the dashed and dash-dotted lines are analytical solutions of the radiation and induction components, and the dotted line is the sum of those two components. (c) The time evolution of the electric field profile at an altitude of 89.5 km, at which the vertical profile of the normalised electric field at r = 100 km, has the maximum peak during the entire simulation. (d) Cross-sectional views of the electric field distribution at 0.4, 0.8, and 1.3 ms (Liu et al., 2017).

of 11.2 μs, similar to the TGFs reported by Fermi, and a longer one with a 100 μs duration.

Figure 2.14 (a) shows the current moment waveform of a short EIP and its time derivative, (b) the electric field on the ground at a distance of 100 km, (c) the time evolution of the electric field profile at 89.5 km altitude and (d) the cross-sectional views of the electric field distributions at different times.

In panel (c), the magnitude of the electric field shows four peaks at different times: the main pair corresponds to the two extremes of the temporal derivative of the current moment waveform, while the lagging pair is the reflection of the leading pair off the ground. Each colour represents a set of pairs at a given time. Note that as one moves away from the source, the main and lagging pairs approach each other, as expected by the EMP bounce mechanism. However, the distance between the two peaks of the leading pair, associated with the temporal derivative of the current moment waveform, remains more or less constant at each indicated time in the figure.

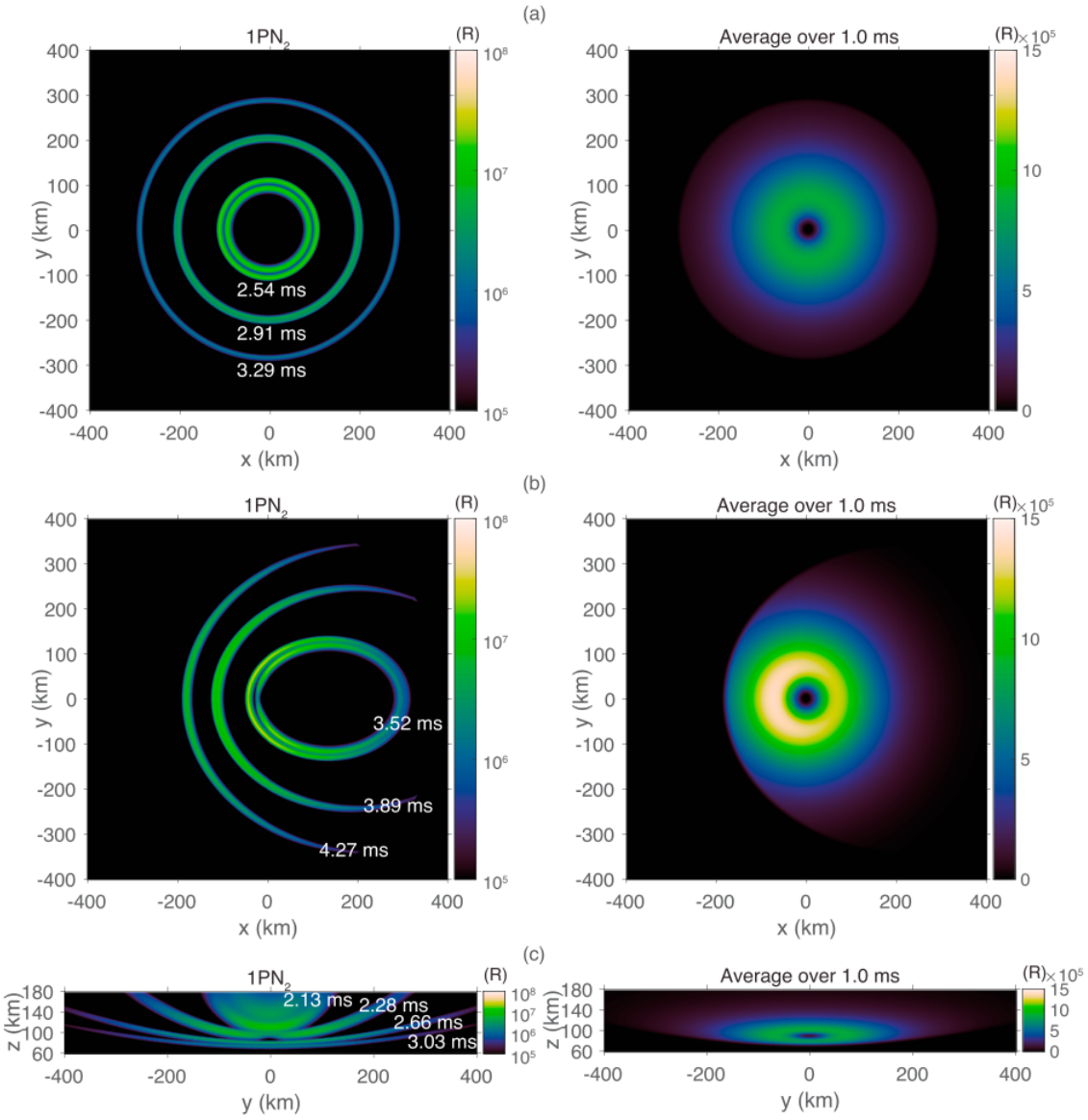

Figure 2.15: Simulation of the emission light from the elve projected at 90 km altitude when viewed from a spacecraft at 700 km altitude (a) right above the centre and (b) with a horizontal displacement of 700 km from the centre. (c) The elve projected on the yz plane is viewed from a point at x = 600 km. The left panels show the instantaneous intensity in rayleighs at selected moments, and the right panels show the intensity averaged over one ms (Liu et al., 2017).

The emissions corresponding to the elve are shown in figure 2.15, viewed under three representative geometries. The first is viewed directly over the centre, while the second viewpoint has a horizontal offset of 700 km from the centre. The third panel shows how elves would appear from the Earth's surface, projected onto a YZ plane 600 km from the centre. In the left panel of that figure, the temporal evolution of the elve ring pair is depicted, where they are distinguishable at 2.54 ms until they overlap, as observed at 3.29 ms. The figures on the right show the intensity averaged over 1 ms of the elve.

These simulations were repeated with a pulse of 33.6 μs, resulting in an elve quadruplet. The four rings correspond to the rise and fall time of the waveform and their reflections. From these simulations, Liu et al. (2017) conclude that elves produced by EIPs of around 10 μs are doublets, and for EIPs of longer durations (30-40 μs), elves multiplets greater than two can be produced. Also, bright and short TGFs are more likely to have accompanying elves because their source current moment waveforms vary more rapidly and radiate stronger electromagnetic pulses.

On October 10, 2018, a TGF was detected in conjunction with an elve at the east of Sulawesi island in Indonesia at 13:01:33.100080 UTC (Neubert et al., 2019). The TGF was captured by the low-energy X-ray detector (LED) and high-energy detector (HED) of the ASIM. Figure 2.16 displays the signals of the LED, HED, and three ASIM photometers. The 777.4 nm emissions are from the current in a lightning leader channel, and the 337 nm emissions are mainly from the lightning discharge in the cloud (leader and streamers). The UV emissions are the signature of an elve.

The TGF event exhibits a relatively short duration (about 30-40 μs) compared to past observations (Neubert et al., 2019). The authors proposed the scenario shown in the bottom panel of figure 2.16, involving an intra-cloud lightning flash of positive polarity, where the electric field ahead of the leader contributes to the generation of the TGF. The UV elve is detected with a delay corresponding to the travel times of the EMP to the ionosphere and of UV photons from the ionosphere to the instruments. The

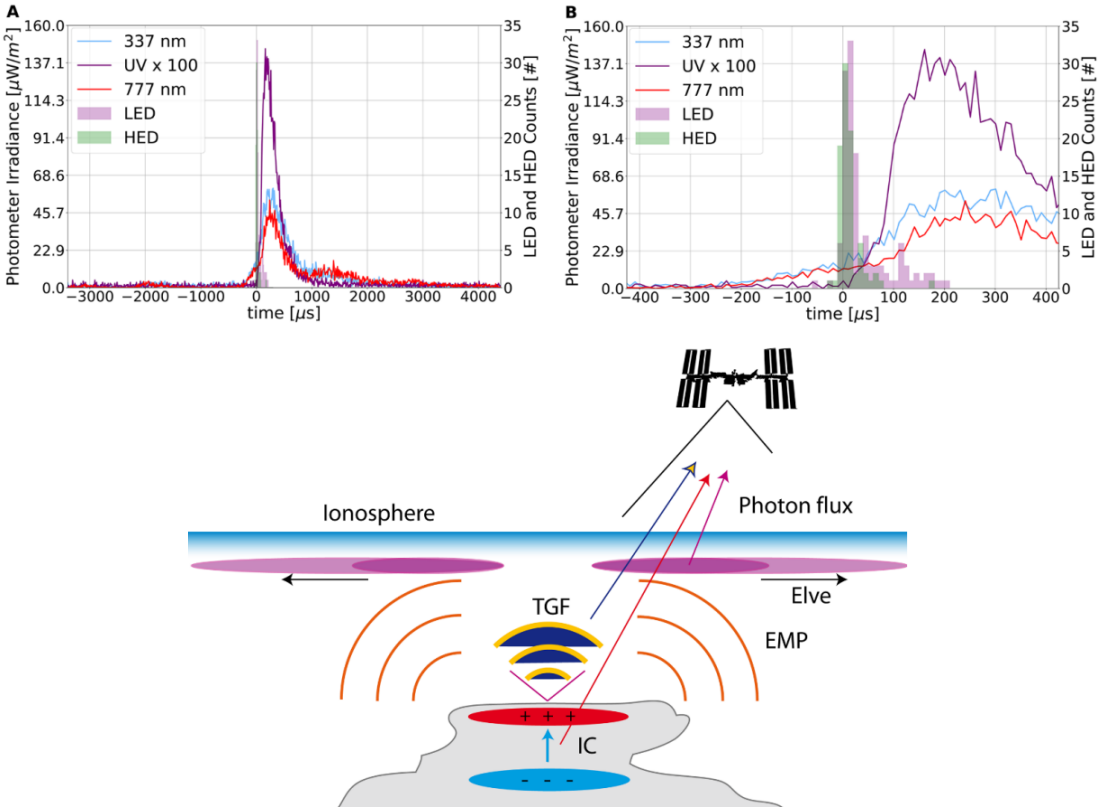

Figure 2.16: Light curves of the event. The gamma-flash trigger time is at t = 0, corresponding to 13:01:33.100080 UTC. (A) Photometer (left axis), X-ray and gamma-ray (right axis) measurements around the time of the event. LED is the low-energy X-ray detector (50-350 keV), and HED is the high-energy detector (300 keV-30 MeV). The UV photometer measures 180-235 nm multiplied by 100 to show the same scale as the optical photometers. All three photometers sample at 100 kHz. (B) The same data shown zoomed in further at the time of the TGF. Bottom: The proposed scenario of an intra-cloud lightning generating a TGF and electromagnetic pulse (EMP). The EMP excites expanding waves of UV emission in the lower ionosphere (elve). TGF and UV emissions are observed by ASIM on the ISS (arrows) (Neubert et al., 2019).

initiation of the UV pulse aligns with the current pulse, commencing 10 μs after the onset of the TGF.

Years later, were reported additional events of TGFs with accompanying elves detected in ASIM (Bjørge-Engeland et al., 2022), showing that TGFs with shorter duration tend to be linked to higher peak currents compared to those with longer term, and it is likely that these events were associated with energetic in-cloud pulses.

Chapter 3

Multi-elves at the Pierre Auger Observatory

The Pierre Auger Observatory, located in Malargüe, Argentina, is the world's most extensive infrastructure for studying ultra-high energy cosmic rays that detects the properties of the most energetic particles in the universe and aims to discover their sources. These high-energy subatomic particles interact with the Earth's atmosphere, creating extended air showers. The observatory combines the facilities of a surface array (SD) of 1,600 water-Cherenkov detectors and a Fluorescence Detector (FD) to measure air showers over 3,000 km^2 (Abraham et al., 2010).

The detection of elves in the Auger FD was a serendipitous discovery in 2005, reported as UV light emissions in the form of semicircles or *smiling faces* (Mussa et al., 2012). Upon recognising them as transient luminous events, a dedicated trigger for elves detection was implemented in 2013.

The Fluorescence Detector has an observation footprint for elves covering 3×10^6 km^2 (Aab et al., 2020), including the Córdoba region where large thunderstorms occur. Furthermore, the FD boasts an exceptionally high temporal resolution compared to other detectors. This combination of features allows us to compile a database compris-

ing hundreds, and even thousands, of elves per year.

In this chapter, we summarise the characteristics of the FD related to elves detection in section 3.1, along with the number of events detected annually from 2014 to 2020. In section 3.2 we show the capabilities of the HEAT to detect events occurring close to the observatory. Additionally, we demonstrate that elves exhibit a seasonal distribution, highlighting the months in which multi-elves are most commonly detected (see section 3.3).

3.1 The Fluorescence Detector

The Fluorescence Detector (Abraham et al., 2010) at the Pierre Auger Observatory consists of four sites located at the top of small hills (Los Leones (LL), Los Morados (LM), Loma Amarilla (LA) and Coihueco (CO)), at the limits of the SD array (see left panel of figure 3.1). The four FD buildings contain six independent telescopes (top panel of figure 3.2), each with a 30° field of view in azimuth × 30° elevation. Combining the six telescopes covers 180° in azimuth.

Each telescope has a shutter and a UV filter. The light passes through the filter to a segmented spherical mirror that focuses it on the camera. The telescope elements are shown at the bottom left of the figure 3.2. The telescope cameras comprise 440 hexagonal photomultiplier tubes (PMT) in a 22-row by 20-column matrix arrangement as shown in figure c of 3.2. These PMTs represent the pixels of the camera and are positioned on a spherical surface in steps of 1.5° (Abraham et al., 2010) (see figure a and b of 3.2).

The UV optical filters and photomultiplier tube cameras limit red and infrared light detection for all TLEs. The FD can detect elves because the parameter of its PMTs is optimised to detect faint light in the 300-420 nm band. The light pulses are digitised

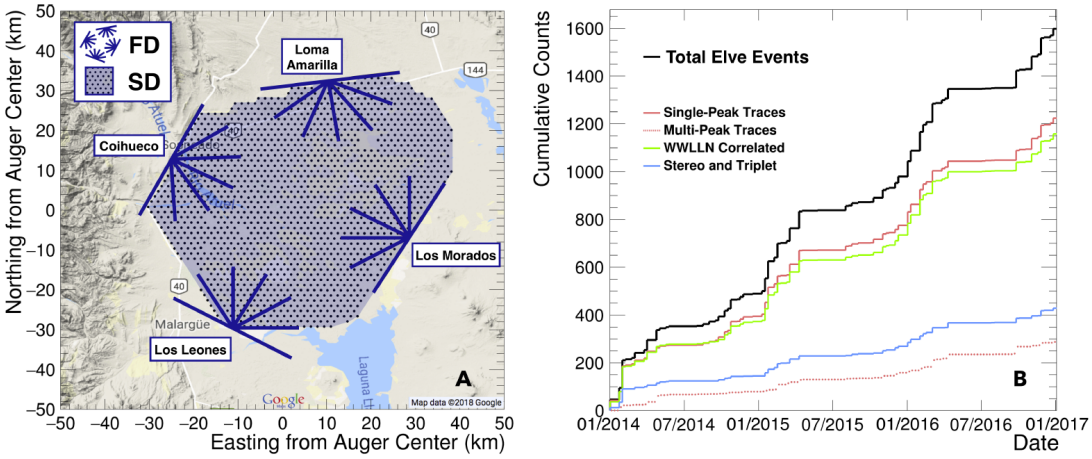

Figure 3.1: Left panel: distribution of the Surface and Fluorescence Detectors of the Pierre Auger Observatory. The blue dots are water-Cherenkov stations of the SD, while the blue lines show the field of view of the 24 FD telescopes. The telescopes are located in the perimeter of the SD in four buildings: Los Leones, Los Morados, Loma Amarilla and Coihueco. Right panel: the cumulative elves data acquired by the Auger FD reached 1,598 counts in the 2014–2016 acquisition period. The count of elves with one peak in the traces contrasts the count of multi-peak elves. The number of Auger elves correlated to a WWLLN event within 5 ms is displayed in green. Taken from (Aab et al., 2020).

every 100 ns and then the signal is rebinned to 2 μs. In the online selection of events, the data of each PMT is processed through a three-stage triggering system (Mussa et al., 2012).

Although the viewing distances range from 3 to 30 km for CRs, the Auger FD has detected elves at 250-1,000 km (details in figure 3.3). The FD is operational during locally clear nights with low background light and clear local conditions. This is about two weeks every moon cycle, from the last quarter to the first quarter, accumulating about 1,200 hours of on-time over 12 months, equivalent to a 15% duty cycle. In addition, the observatory employs lasers, lidars, and infrared cloud cameras to measure the optical transparency of the atmosphere over the array.

The traces of a cosmic ray event last about 1 μs, while the signal of an elve will be bright well after 200 μs (Merenda, 2020). In figure 3.3, a CR recorded on the camera can be seen as a line of activated pixels, and the elve is a wavefront with a radial evolution.

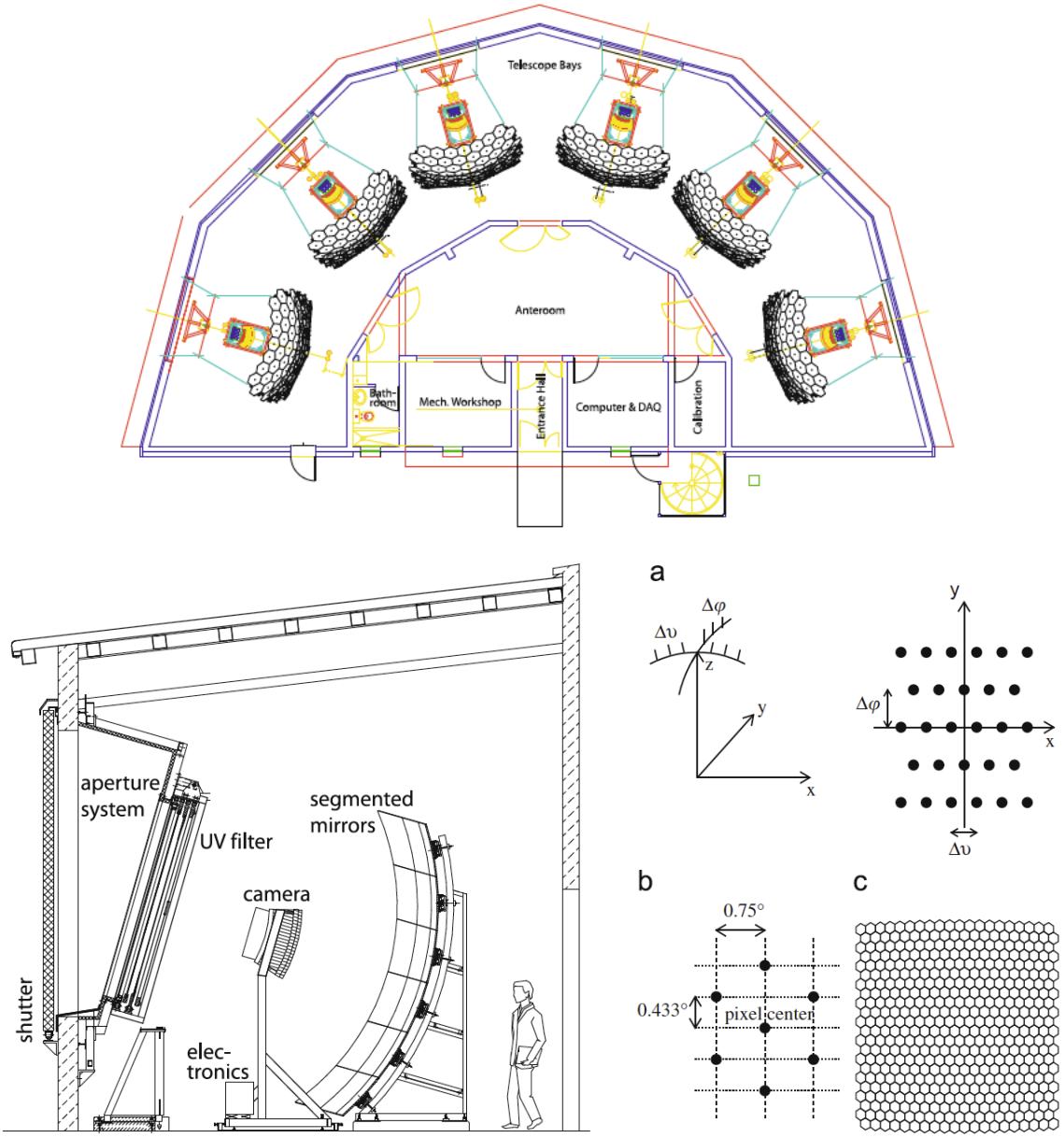

Figure 3.2: Top panel: structure of the FD buildings with six independent fluorescence telescopes. Each has a field of view of 30° × 30° in azimuth and elevation, which in total covers 180° in azimuth. The bottom panel left: structure and components of the telescopes of each FD; right: geometric construction of the FD's cameras: a) the centres of the pixels are located on a spherical surface in steps of 1.5°, (b) positioning of the pixel vertices relative to their centres, and (c) arrangement of the 440 camera pixels in a 22×20 matrix. Taken from (Abraham et al., 2010).

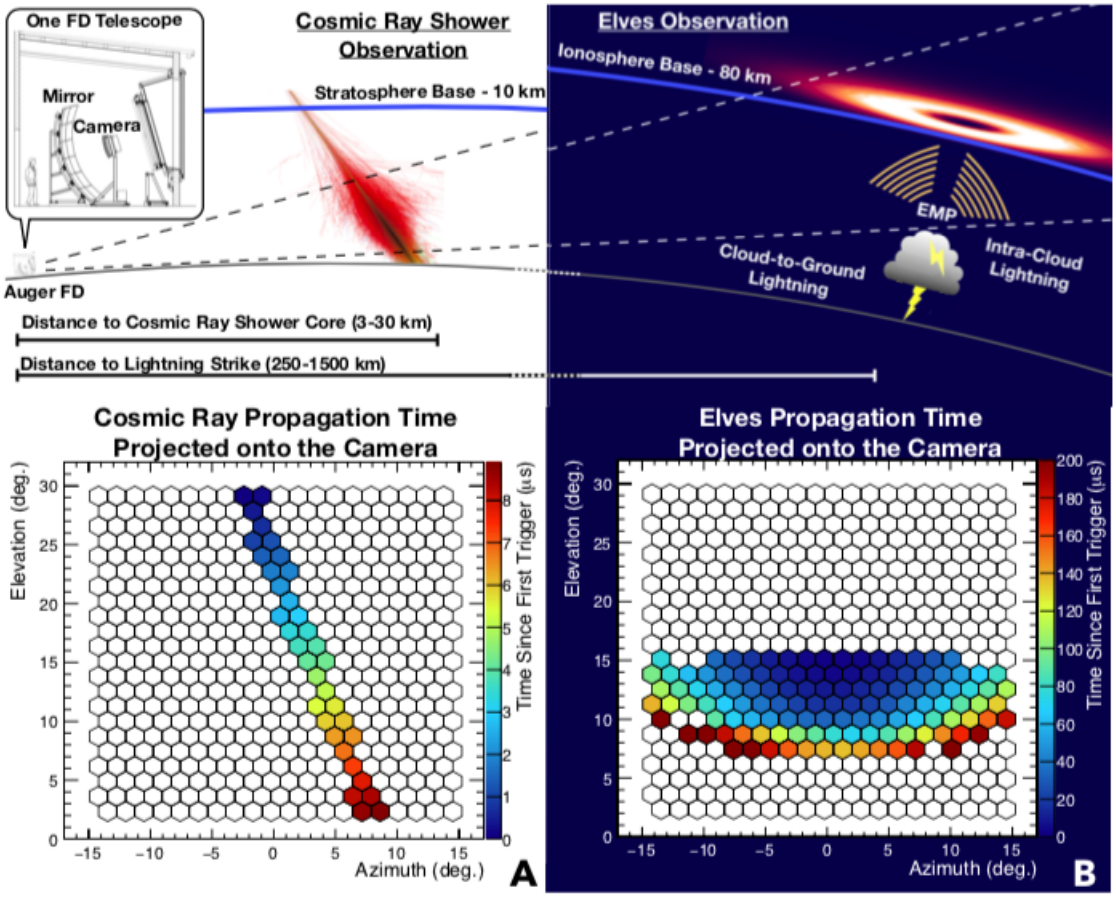

Figure 3.3: Observation of cosmic rays and elves on an FD telescope. Time of propagation projected on the camera of A) a CR and B) an elve. The time is measured from the system's first shot, with the blue pixels being the first to be activated and the red ones the last. It can be seen that the cosmic ray activates a line of pixels with a precise time sequence and that the elve is seen as a wavefront with a radial evolution. Taken from (Aab et al., 2020).

To illustrate the typical signals in the camera pixels, we show in figure 3.4 a single (A and B), a double (C and D), and a triple elve (E and F). In the left panel of the figure, the traces of each event are observed in different pixels: in (C), two peaks are visible in each trace, while in (E), three peaks are observed. The right panel displays the photon counts integrated over 10 μs to observe the typical arc shape of elves in the FD.

Since 2013, the Pierre Auger Observatory has taken data with this triggering system for the elves study. During the first year, it was observed that the standard 100 μ long FD traces did not allow us to see the light emitted from the ionosphere region located vertically on the source beam (Mussa, 2019). Therefore, the FD reading scheme (Extended Readout) was modified to acquire three consecutive pages in these cases.

This change allows studying the angular distribution of the light emission above the beam. Elves data from 2014 to 2016 were taken with a maximum trace length of 300 μs. From 2017, this trace was extended to 900 μs to fully observe the high light intensity region for most of the events (Mussa, 2019).

In the right panel of figure 3.1, the cumulative elves data acquired by the FD during the 2014-2016 period. This plot represents one of the initial reports Aab et al. (2020), capturing both single- and multi-peak elves and their correlation with the World Wide Lightning Location Network. The authors also showed that the Auger FD observed the first elve with three peaks. In section 3.3, we present data analysis spanning seven years, covering the period from 2014 to 2020.

3.2 The High Elevation Auger Telescopes detecting closer elves

Near the Coihueco FD site, the observatory has another fluorescence detector, the High Elevation Auger Telescopes (HEAT) (Abraham et al., 2010) comprising three telescopes

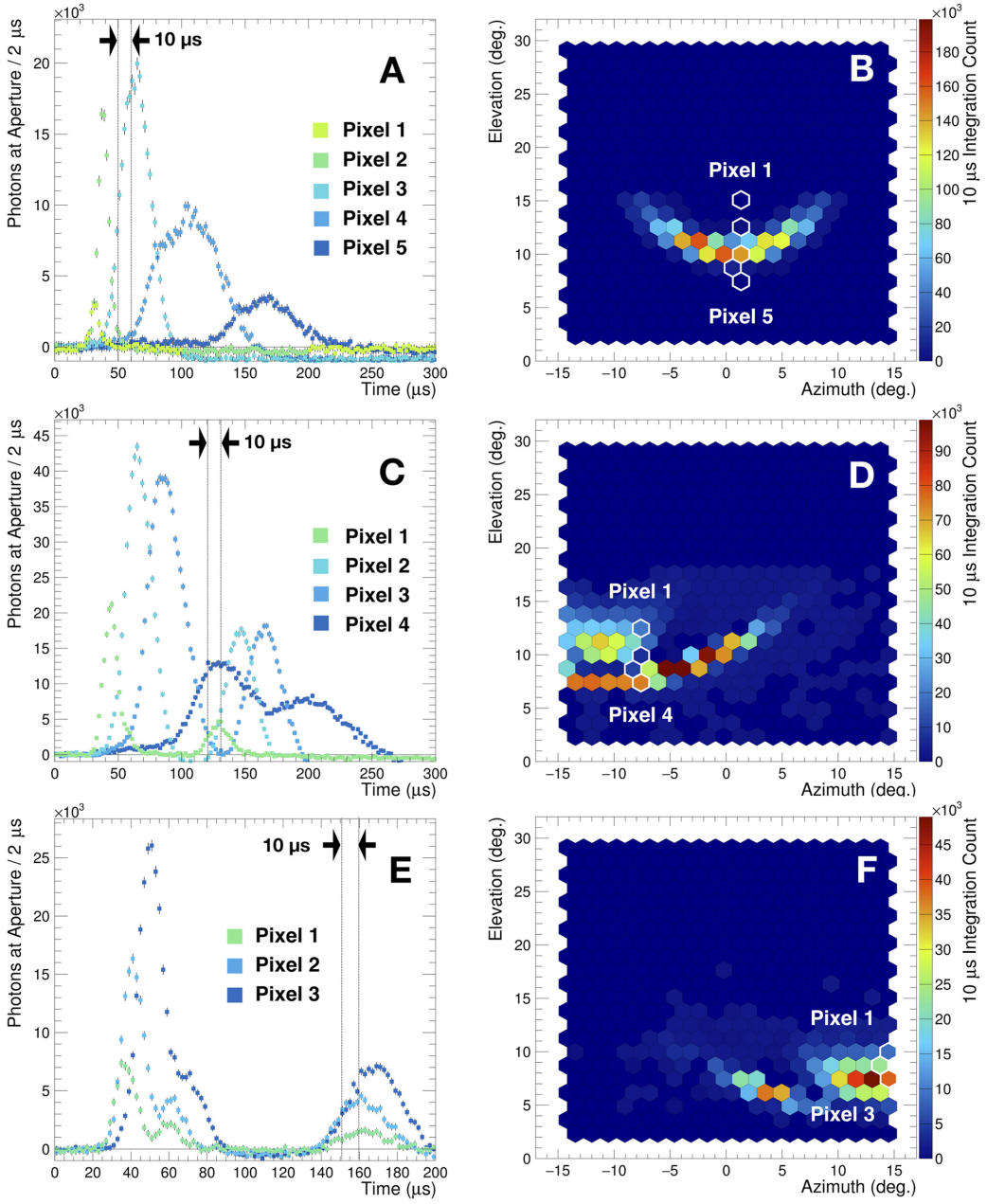

Figure 3.4: (A) Some 300-μ-long traces of typical single-peaked elve observed in the FD at Los Leones, on 2 February 2014 at 05:12:22 UTC. (B) We selected 10 μs of the signal captured by the camera to show the arc shape of the elve. (C, D) Selected traces and a 10-μs snapshot of a double-peaked event seen in Coihueco on 17 January 2016 at 04:52:31 UTC. (E, F) 200-μ-long traces and a 10-μs snapshot of a multipeaked event seen in Los Leones, on 4 March 2016 at 05:32:39 UTC (Aab et al., 2020).

with the same size and aperture as the other 24 FD telescopes. These telescopes have the unique feature of allowing the optical axis of their mirrors to be tilted to an elevation angle of 45 degrees, as opposed to the standard 16.5 degrees.

The HEAT expands the dynamic range of the Observatory by detecting cosmic ray showers with lower energy. This can also observe elves, enabling the detection of events originating from storms closer to the observatory within a range of approximately 150 to 250 km. The tilted entrance window prevents direct light from the lightning bolt, enabling optimal observation of the area with the maximum light emission (Abdul Halim et al., 2023).

In figure 3.5, the HEAT is depicted, along with the field of view of its three telescopes in operational mode (HEAT up, red pixels in figure) and calibration mode (HEAT down, green pixels). The pixels of its three telescopes coincide with the FoV of the Coihueco telescopes enabling cross-calibration of the observed events.

The HEAT electronics operate at twice the speed of the standard FDs, with each trace consisting of 2000 bins to cover the same time window as the FD traces (100 μs). The elves trigger is configured to capture a maximum of three consecutive pages, resulting in a total trace length of 300 μs. In contrast, elves traces in the standard FDs can extend up to 900 μs. Due to the tilted geometry, HEAT can only observe a partial view of the complete elve. Consequently, only a few events trigger the HEAT and standard FD telescopes simultaneously (Abdul Halim et al., 2023).

In January 2021, we implemented the elves detection trigger in the HEAT (Abdul Halim et al., 2023), resulting in fascinating nearby events available for analysis. On February 15, 2021, at 01:15:14 UTC, a double elve phenomenon was observed using a HEAT camera. The light from the first ring of the elve is visible in panel (A) of figure 3.6. After 12 μs, in panel (B), the light of the second ring emerged within it. In panel (C), another 12 μs later, the light from both rings of the elve was observable. Note that the light shown in these figures is the light detected in the microsecond after the time

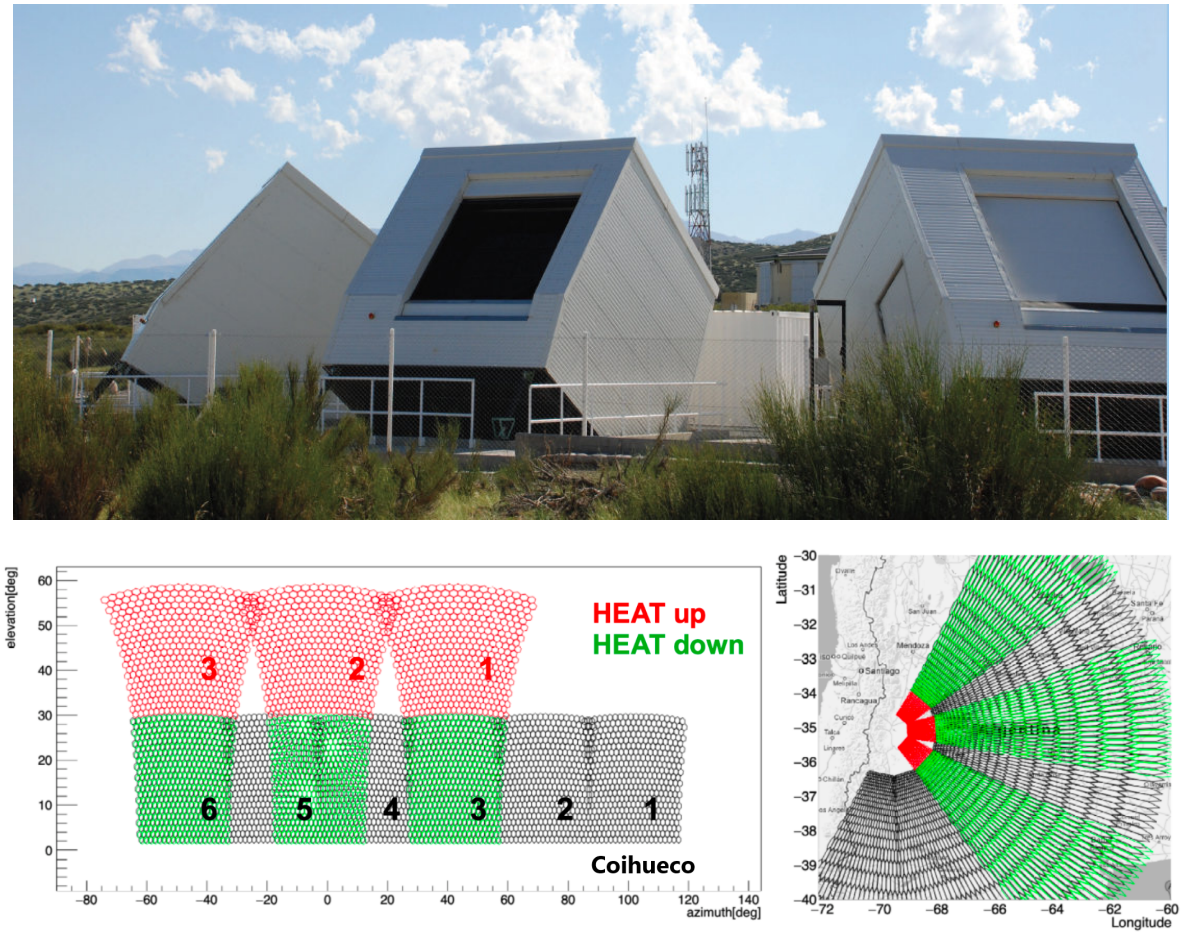

Figure 3.5: Top: the three telescopes of the High Elevation Auger Telescopes (HEAT) are designed to detect cosmic ray showers with lower energy and are also capable of observing elves. Bottom: the field of view of the HEAT telescopes in operation mode (red) and calibration mode (green), compared to the Coihueco telescopes. HEAT-up allows the detection of elves originating from storms closer to the observatory (Abdul Halim et al., 2023).

indicated above, e.g. in the first frame is 943362 μs after 01:15:14 UTC and 943374 μs after in the second frame. It is not the integral of light in those time ranges.

This event serves as evidence of the efficiency of HEAT in detecting the rings of the multi-elves compared to those observed with the FD (for instance, the elves depicted in figure 3.4).

3.3 Seasonal distribution of multi-elves

Previously, we mentioned that the Fluorescence Detector has been monitoring elves with a dedicated trigger since 2013. According to a data analysis conducted between 2014 and 2016, a total of 1598 events were reported by Aab et al. (2020). The analysis also revealed that the majority of the events detected in the Auger FD happened during the southern summer, while production was minimal between June and August (see the right panel of figure 3.1).

We have successfully reconstructed 6737 events from 2014 to 2020 and can confirm the seasonal occurrence of elves. The critical event counts between May and August are evident in table 3.1, where the number of elves per month for each year is presented. The left panel in figure 3.7 shows the average number of elves per month during this period, indicating that between November and April, hundreds of elves are detected each month, while from May to August, there is a drop to less than 25 events per month, nearly zero in June and July.

As depicted in figure 2.2, lightning activity starts to shift southwestward in November, extending into the field of view of our elves detector located around 35.2°S and 69.4°W. This explains the high frequencies that we observed in the number of elves detected between November and April. The same figure shows the dissipation of lightning in May in agreement with the critical number of elves that we detected between May and

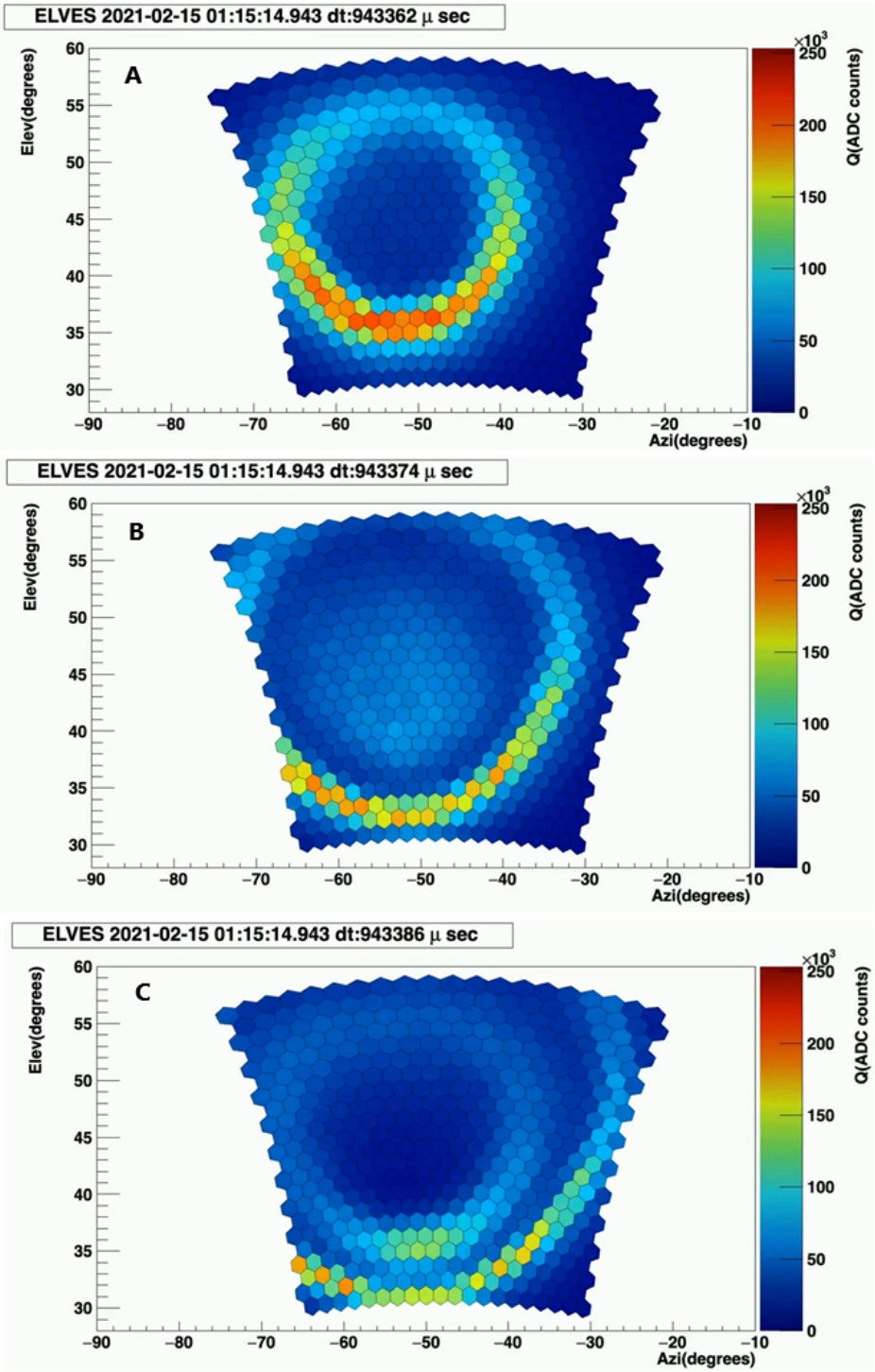

Figure 3.6: On February 15, 2021, at 01:15:14 UTC, a double elve event was detected in a HEAT camera. In panel (a), the light from the first ring of the elve. Panel (b) shows the light of the first ring 12 μs later, and inside it, the light from the second ring appears. After another 12 μs (panel c), the light from both the first and second rings of the elve is visible. A complete video of this event available in double_heat.mp4.

Table 3.1: Number of elves detected in the FD each month from 2014-2020. Between May and August, the number of events decreases critically.

Year	Jan	Feb	Mar	Apr	May	Jun	Jul	Aug	Sep	Oct	Nov	Dec
2014	95	136	27	87	14	5	0	10	31	75	23	5
2015	284	87	81	75	1	0	0	29	4	20	42	50
2016	135	151	95	49	0	0	3	0	31	56	97	78
2017	297	119	454	80	14	0	3	7	9	5	52	100
2018	128	199	24	81	41	2	2	0	73	8	236	81
2019	239	135	460	16	46	2	1	5	74	62	161	488
2020	125	96	16	351	1	10	2	41	1	276	212	26

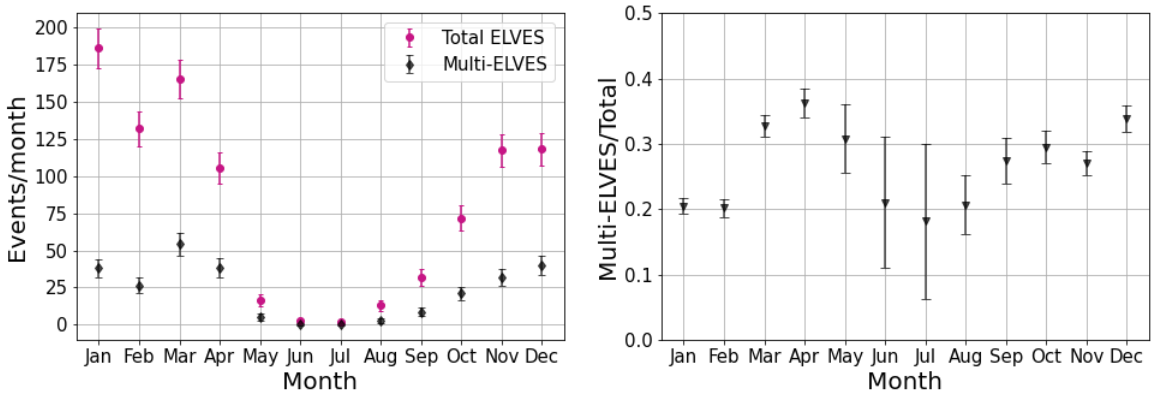

Figure 3.7: Left panel: monthly distribution of total events and multi-elves during 2014-20. Right panel: monthly ratio of multi-elves to the total number of elves. The highest ratio occurs in April, followed by December and March.

August.

We also identified the multi-elves detected each month over these 7 years. The left panel in figure 3.7 displays the average number of multi-elves per month, with a peak value of above 50 events per month in March. In the right panel of the figure, the annual fluctuation of the ratio of multi-elves relative to the total events is depicted. The highest value was in April, with a ratio of 0.36, followed by December and March, with ratios of 0.34 and 0.33, respectively. Results between May and August show large error bars due to limited data statistics during those months.

Additionally, we analyzed the variation in the number of events per year during the period 2014-2020. The table 3.2 summarises the total number of events, the total

Table 3.2: The total number of events and multi-elves detected by the FD in 2014-20. The number of events increased from 2017 onwards, but the ratio of multi-elves to the total remains roughly constant(Vásquez Ramírez et al., 2022).

Trace length (μs)	**Year**	**Total events**	**Total ME**	**Ratio** (ME/Total)
300	2014	508	115	0.226
300	2015	673	201	0.299
300	2016	695	190	0.273
900	2017	1140	323	0.283
900	2018	875	233	0.266
900	2019	1689	500	0.296
900	2020	1157	311	0.269

number of multi-elves, and the ratio (ME/total). From 2017 onwards, the number of detected events increased compared to 2014-16. This is due to the improved trigger implemented in 2017 (Mussa, 2019).

With the extension of the readout system that year, from 300 μs to 900 μs trace length, we could expect an increase in the number of detected multi-elves to the total number of events, since a longer trace allows us to observe events with two peaks farther apart from each other. However, the annual ratio of multi-elves to total events (ME/Total in table 3.2) remains more or less constant, and over the period 2014-20, it is around 0.273 ± 0.023 per year.

Using the GPS label of events, we can group elves by year and day; in figures 3.8 and 3.9, the annual distribution of events per day is presented: the colour bars represent the total number of elves per day, while the black bars in each histogram represent the number of multi-elves per day. The grey bands denote periods of inactivity of the Auger Fluorescence Detector since it operates during nights with clear local conditions.

The 2014, 2015, and 2016 histograms exhibit fewer events per day compared to those of 2017-2020, where some days surpass 200 elves. For each year, we have highlighted the day with the highest number of multi-elves: April 29th for 2014, January 18th for 2015, and March 8th for 2016. In 2017-2020, notable days include April 2nd, 2017; November 10th, 2018; March 4th, 2019; and April 28th, 2020. Note that these dates

consistently fall within March, April, November and December, as expected by the seasonal distribution of elves and multi-elves that we reported.

Some of these days were selected for a more detailed analysis of multi-elves traces and the correlation of these events with lightning strikes detected by Earth Networks and storms mapped by GOES-16. Subsequently, in chapters 4, 5, and 6, the main findings of this research regarding the investigation into the origin of multi-elves associated with the characteristics of lightning in storms are presented.

The processing of the data for the reported seasonal distribution and the histograms of elves per day is available in the repository of appendix A.2. This code allows a preliminary identification of multi-elves. Later, we implemented a more efficient code (details in appendix A.4) for analyzing the traces of events from four storms, which resulted in the identification of additional multi-elve events.

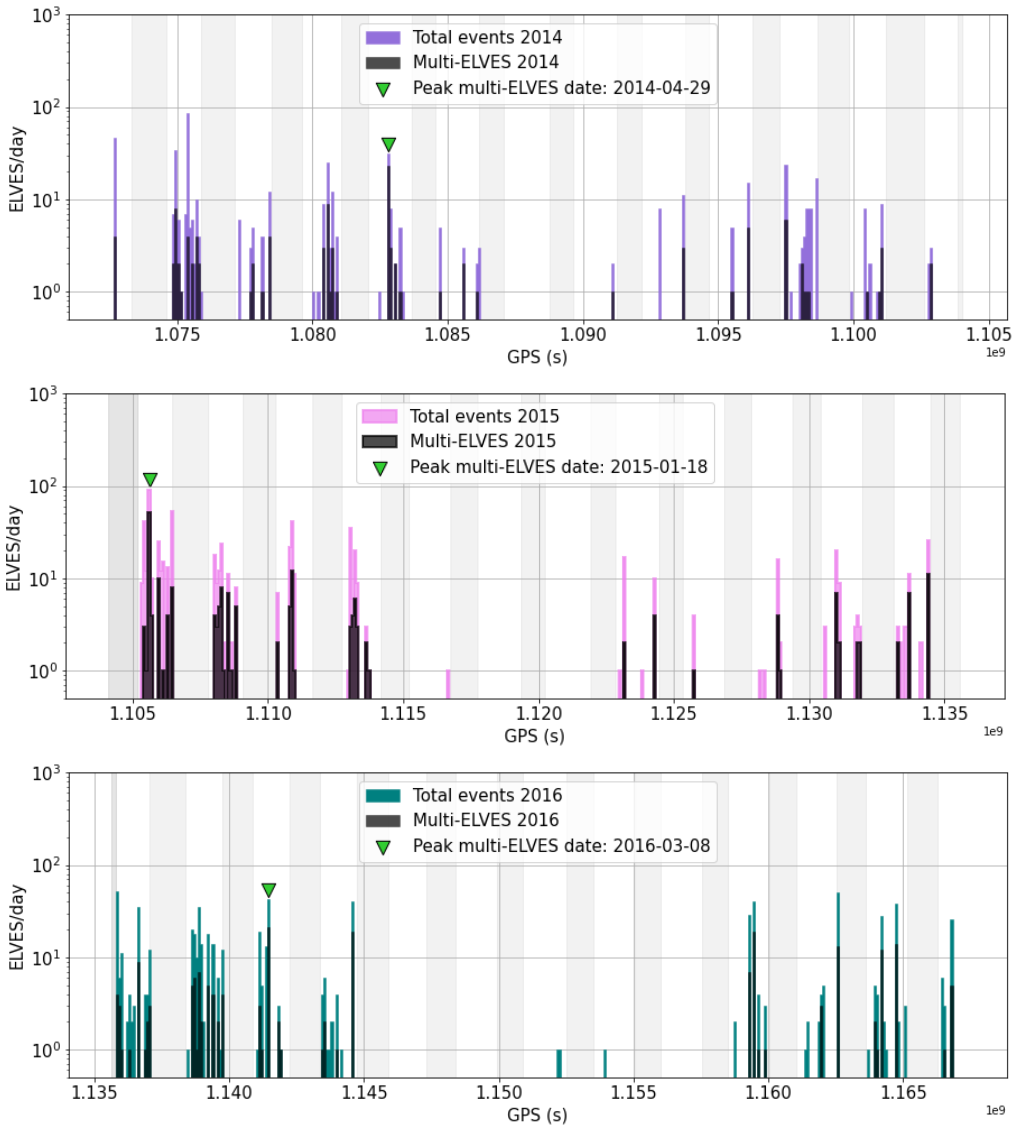

Figure 3.8: Total number of elves per day (colour histograms) and multi-elves per day (black histograms) for the years 2014 (top), 2015 (middle), and 2016 (bottom). The grey bands represent days of inactivity of the Auger Fluorescence Detector. During 2014-2016, elves data were collected with a trace length of 300 μs. The green triangles for each year indicate the day with the most multi-elves.

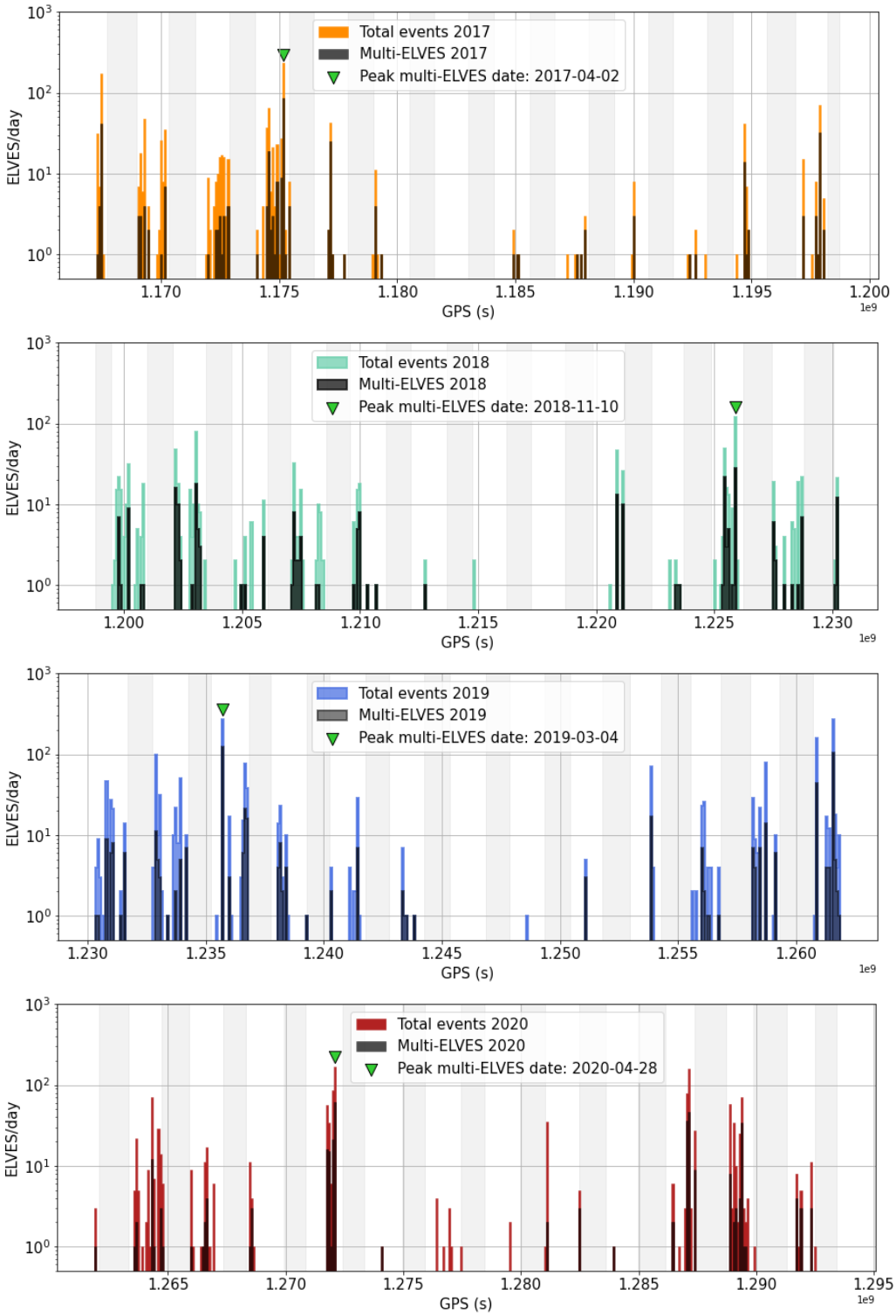

Figure 3.9: Total number of elves per day (colour histograms) and multi-elves per day (black histograms) for the years 2017 (top), 2018, 2019 (middle), and 2020 (bottom). The grey bands represent days of inactivity of the Auger Fluorescence Detector. Since 2017, the trace length for elves data acquisition was extended to 900 μs. The green triangles for each year indicate the day with the most multi-elves.

Chapter 4

Origin of multi-elves in lightning waveforms

This chapter presents the correlation results between elves detected by the Fluorescence Detector and the lightning waveforms provided by Earth Networks. The aim is to investigate whether the origin of multi-elves is related to the shape of the current pulse of the lightning that produces them.

According to the model proposed by Marshall (2012), each elve event is a doublet, and the edges of the current waveform trigger the emissions. However, the rise and fall times of the pulse must be long enough to produce clear elves with well-separated peaks.

In section 4.1 we present the configuration of the ENTLN sensor network deployed within our research area in Argentina, along with an examination of various components comprising lightning waveforms. In section 4.2, we compare the current pulses of lightning correlated with single, double, and triple elves. Section 4.3 delves into the methodology employed for determining the base time of these waveforms.

4.1 Lightning waveforms from Earth Networks

The Earth Networks Total Lightning Network is a global coverage ground-based network comprising 1800 broadband electric sensors that detect both IC and CG flashes, providing timing, geolocation, classification and peak current of the event. On average, the ENTLN reports about 50 lightning events per second worldwide (Zhu et al., 2022).

The ENTLN sensors record raw electric field waveforms, which are used to calculate real-time lightning geolocation through the time-of-arrival technique. In the vicinity of the Auger Fluorescence Detector's field of view, numerous sensors are positioned, providing the lightning waveforms correlated with our elves' events. The left panel of figure 4.1 displays the map featuring ENTLN sensors (red markers) surrounding the FD's FoV, marked by four stars on the same map.

To correlate our elves with ENTLN lightning, we first reconstruct the location and time of the lightning source (t_0), as described in appendix A.1. The time (in nanoseconds) allows us to locate a unique lightning strike within an area bounded by the latitude and longitude reconstructed for the lightning. Most events typically exhibit a single correlation, and rarely there is a need to choose between two lightning events. Ultimately, the one with the smaller temporal difference from t_0 is selected.

In the right panel of figure 4.1, the waveforms detected by various sensors during an event on April 28, 2020, at 08:34:53 UTC are presented. Note that in the top panel, each sensor's detection time is shown without correction for the distance between the event and each antenna. The black arrow represents the time of occurrence of the lightning reconstructed by the Auger FD (labelled as t_0 in the figure), which in this example is approximately 268.80 ms after the time indicated above.

In the bottom panel, it is observed that after correcting for the distances between the sensors and the lightning, these waveforms align considerably with t_0. This is just an

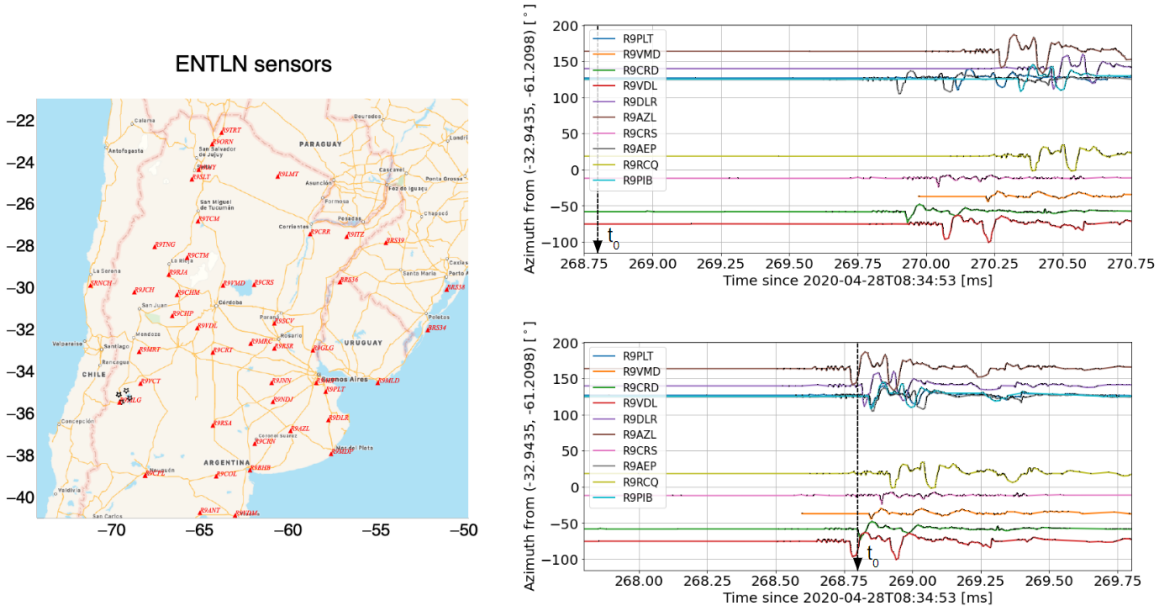

Figure 4.1: Left: array of Earth Networks (ENTLN) sensors around our area of interest. The Auger FD eyes' locations are marked on the map as four stars. Right: waveform of lightning occurring on April 28, 2020, at 08:34:53 UTC, as seen from different sensors of ENTLN. The top panel displays the signals with their arrival times at each antenna. The bottom panel shows the signals corrected for the transit time between the antenna location and the lightning strike location as calculated by the Auger reconstruction algorithm (t_0).

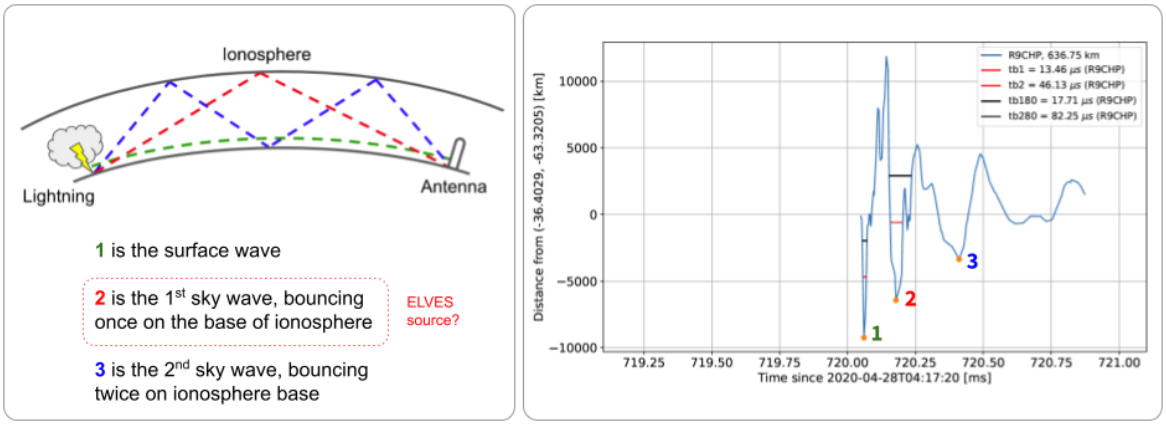

Figure 4.2: Left: scheme of the waveform components detected by an antenna. The first corresponds to the direct wave from the lightning to the antenna (green curve), the second bounces once in the ionosphere before reaching the antenna (red), and the third bounces twice in the ionosphere before being detected (blue). The second component is the most likely to produce elves. Right: example of identifying the three principal components of a waveform detected at antenna R9CHP, 636.75 km from where the lightning occurred.

example of what typically happens when aligning the waveforms of an event to the calculated t_0, demonstrating the efficiency of our lightning location algorithm. Furthermore, in chapter 6, a detailed analysis shows that the mean difference between the time of the lightning reconstructed from Auger and ENTLN is about tens of microseconds.

After correlating and obtaining the waveform associated with the elve, it is essential to consider its main components. The first component travels directly from the source lightning to the antenna (surface wave in figure 4.2). The second component bounces once in the ionosphere before being detected at the antenna (1st sky wave in figure 4.2). This component is the most likely to produce the elves observed in the FD, as it excites the molecules in the ionosphere, forming the observed light emissions. We selected the second component of the waveforms to study the lightning current density pulse and its association with single or multiple elves.

There are other components with multiple bounces between the ionosphere and the Earth's surface, such as the second sky wave that bounces twice before reaching the antenna. The right panel in figure 4.2 shows an example of the waveform detected

on April 28, 2020, at 04:17:20 UTC in the R9CHP sensor, located at a distance of 636.75 km from the lightning source. The three most prominent peaks of the signal are indicated, representing the amplitude of each component. After 720.50 ms a fourth component can be observed but significantly attenuated.

4.2 Lightning waveforms correlated with single and multiple elves

When studying the second component of the ENTLN waveforms correlated with elves from the Pierre Auger Observatory, we observed that pulses correlated with single elves tend to be narrower than those correlated with multiple elves. These events correspond to the night of April 27-28, 2020, where we observed the highest proportion of multi-elves in the period 2014-2020: 76 single, 32 double, and 31 triple elves (totalling 139 events).

The panel (a) in figure 4.3 shows the definition of the base time of the second component of the lightning waveform (t_{b2}) at 95% of its amplitude, which we used in this analysis. Panel (b) illustrates an example of the second component of a waveform pulse corresponding to a lightning strike correlated with a single elve event (in red), a double elve (in black), and a triple elve (in green), with t_{b2} of 56, 130, and 148 μs, respectively.

In panel (d) of the same figure, a histogram of the average base time of events correlated with single elves (red bars), double elves (black bars), and triple elves (green bars) is presented. Additionally, the base time of the pulse's first component (t_{b1}), commonly used in ENTLN for calculating the lightning source height, is shown for comparison (panel (c)). It is noteworthy that, unlike the first component (which mean values are $\bar{t}_{b1} = (30 \pm 13)\mu s$, $(35 \pm 13)\mu s$ and $(36 \pm 11)\mu s$ for singles, doubles and triples, respectively), the base time of the second component is relatively distinguishable between

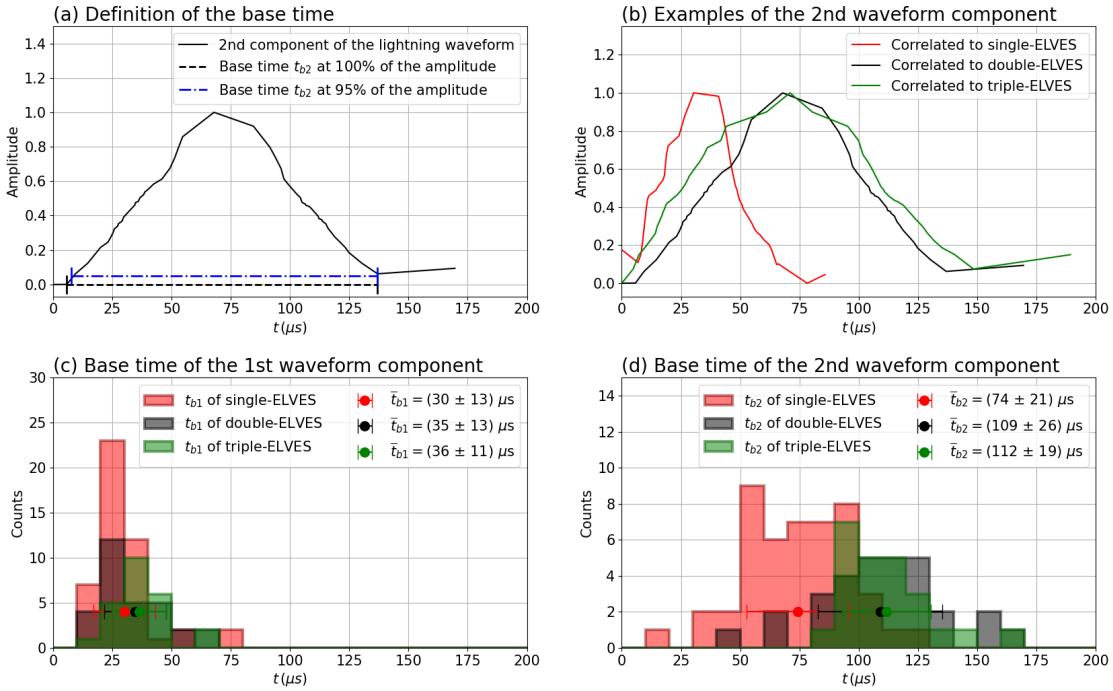

Figure 4.3: (a) Definition of the base time of the lightning waveform pulse given by Earth Networks. (b) Examples of typical lightning waveform pulses correlated with single (red), double (black) and triple elves (green). Histogram of the base time of the (c) first component and (d) second component of the waveform pulses correlated with the elves detected on April 27-28, 2020. The mean value $\bar{t}_{b2}$ of the single elves histogram is $(74 \pm 21)\mu s$, which is shorter than mean values from double and triple elves histograms, $(109 \pm 26)\mu s$ and $(112 \pm 19)\mu s$ respectively.

events correlated with single elves and multi-elves. The single elves histogram has a mean value of $\bar{t}_{b2} = (74 \pm 21)\mu s$, which is shorter than mean values from double and triple elves histograms, $(109 \pm 26)\mu s$ and $(112 \pm 19)\mu s$ respectively.

More interestingly, we found some events that did not follow this rule, i.e., single elves events related to very wide waveforms, as shown in the top-left panel of figure 4.4. Upon closer examination of the traces of the elve occurring on April 28, 2020, 02:30:53 UTC, we noticed a second peak but with a very low amplitude relative to the threshold we used to identify a multi-elve event. By adjusting this threshold, we could calculate the time difference of this double elve mislabeled as a single event (details of the algorithm for determining ΔT in chapter 5). In the top-right panel of figure 4.4, the time difference between the rings of this multi-elve is depicted, and within this plot, there is an example

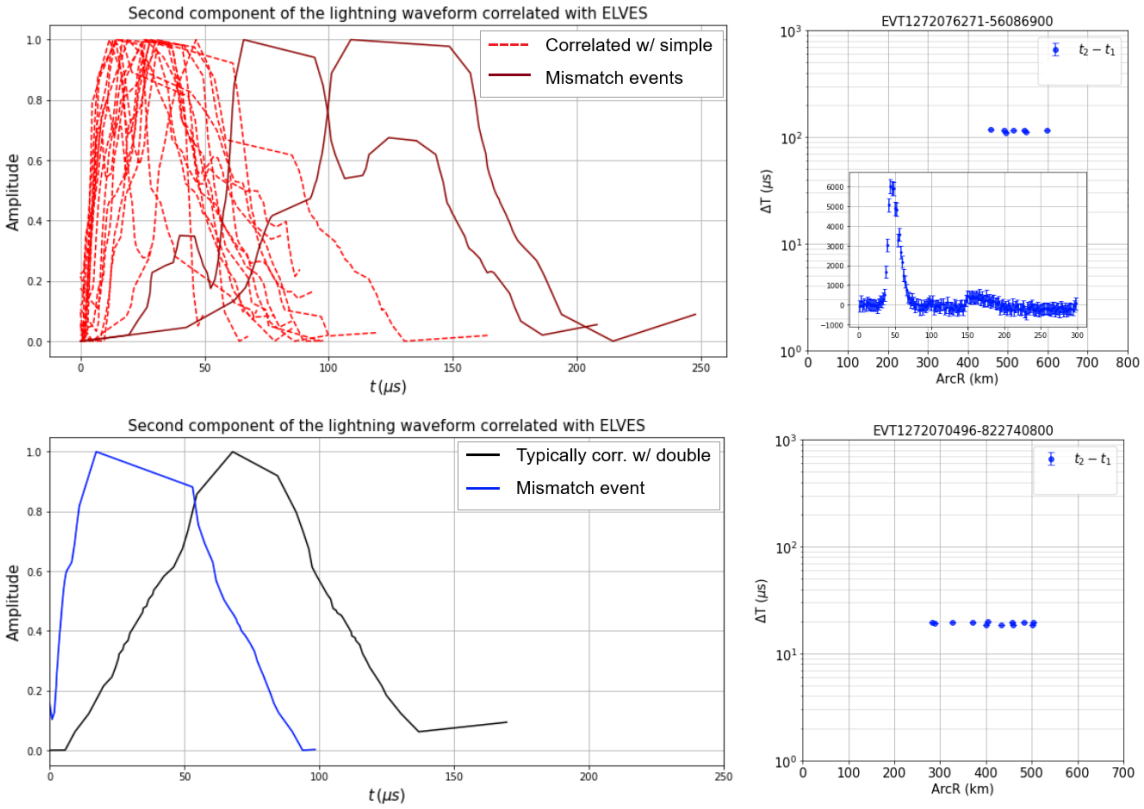

Figure 4.4: Top: waveform initially correlated with a single elve, where the base time is much greater than that of the single elves group (left). Analysing the traces of the elve, we observed that some of them have a second peak with a very low amplitude compared to the first peak. After tuning the code parameters, we obtained the corresponding ΔT of this misidentified double elve. Bottom: example of a waveform correlated with a double elve (blue) with a base time similar to those waveforms correlated with a single elve (left). Upon inspecting the time between the peaks of the elve, we noticed that this event has a ΔT of about 20 μs (right).

trace showing two peaks.

We also found double elves events related to waveforms that did not seem to follow this rule. For example, the bottom-left panel in figure 4.4 shows the second component of a waveform with the typical width of those correlated with multiple elves and a narrower pulse correlated with a double elve. However, as shown in the bottom-right panel in the figure, this double elve has a slight time difference of about 20 μs compared to other events with more than 100 μs. That is, the smaller base time corresponds to the smaller time gap between the rings.

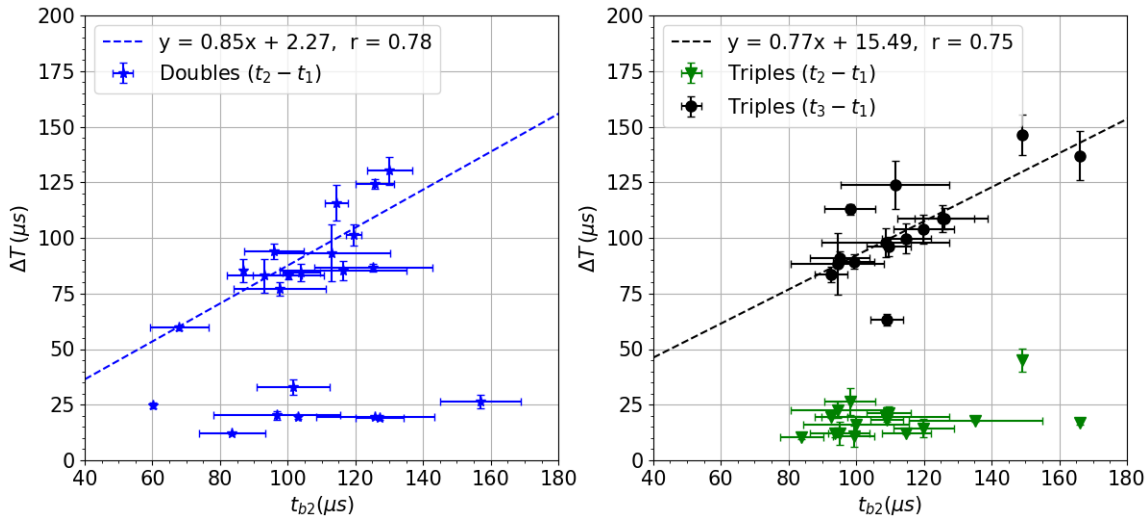

Figure 4.5: Base time of the second component of waveforms (t_{b2}) correlated with double elves (left) and triple elves (right). In both cases, it can be observed that, beyond 50 μs of peak separation time for multi-elves (ΔT), there is a high correlation with t_b: $r = 0.78$ in the fitting of doubles (blue dashed line) and, $r = 0.75$ in the triple events (black dashed line). With an increased base time of the waveform, the temporal gap between the peaks of multi-elves also increases.

The relationship between the base time of the second component of the waveform and the time gap between the rings of multi-elves is shown in figure 4.5. In this plot, we noticed that above 50 μs of ΔT, it increases with the base time (t_{b2}) of the pulse for both double and triple elves events. In the same figure, the corresponding fittings for each case are displayed, with a correlation coefficient of $r = 0.78$ for double elves and $r = 0.75$ for triples.

Additionally, the slopes of these fittings are similar, with values of 0.85 for doubles and 0.77 for triples. The error of ΔT for each event is determined from its standard deviation (see details in the following chapter), and similarly, the error of t_{b2} represents the standard deviation calculated from signals recorded by several antennas situated at a similar distance from the lightning strike (see details in the next section).

From these results, we show that the origin of the multiple rings of elves with $\Delta T \geq 50\,\mu$s depends on the duration of the current density pulse of the lightning that produce them. As Liu et al. (2017) showed short EIPs of 20 μs tend to produce double elves,

while longer EIPs of 30 to 40 μs can better separate the rings, visualising quadruplet elve events. Note that these times refer to the first component of the waveforms while we analyse the second component, which is usually much longer.

Results below 50 μs do not show a clear relationship. We recall that varying combinations of rise time and fall time can produce different ΔT values. In this case, employing the base time which is a combination of both, can result in these two subgroups in the graphs or maybe they originate from two different mechanisms. In the next chapter, we analyse these events with the model of the bounce mechanism of the electromagnetic pulse of a IC-lightning, which could explain such short ΔT values.

4.3 Base time calculation and data set

For the study of the rise (τ_r) and fall time (τ_f) of lightning waveforms on the night of April 27-28, 2020, we chose those correlated with single, double and triple elves.

Many of these signals showed saturation even though the distance between the lightning strike and the antenna was greater than 500 km. Therefore, we decided to conduct the study with the pulse base time (t_{b2}) instead of the separate rise and fall times because it is impossible to determine where the τ_r ends and where the τ_f begins. Additionally, according to the model revised in section 2.4.1, τ_r and τ_f should be large enough to separate the peaks of the elve, meaning that with a longer t_{b2}, we should have a greater temporal difference (ΔT) between those peaks.

In the study of waveforms, the base time of pulses is usually measured at a certain percentage of their amplitude to avoid overestimation. In this case, we found optimal values of the base time for 95% of their amplitude in 101 events out of the 131 correlated with ENTLN. In figure 4.6, the calculation of the base time of the first (t_{b1}) and the second component (t_{b2}) of the waveform at 95% of the amplitude from four sensors is

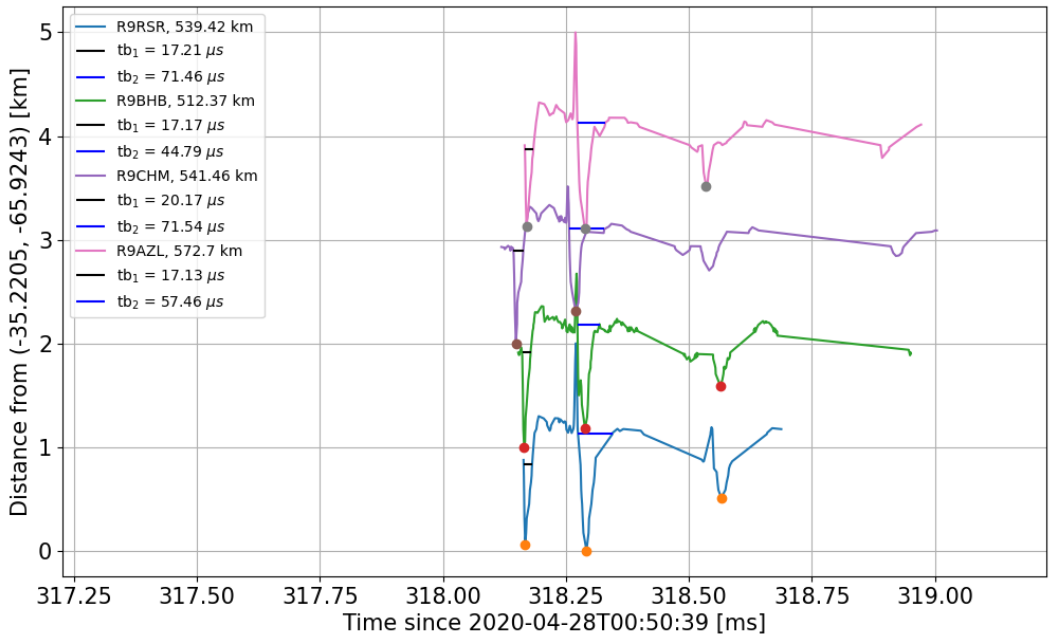

Figure 4.6: Example of the calculation of the base time of the first (t_{b1}) and second (t_{b2}) components of the lightning waveform correlated with a single elve. The legend displays the sensor ID, the distance from the sensor to the lightning strike, and the corresponding base times obtained for each sensor.

presented.

Of the remaining 30 events, 15 showed an incorrect calculation of their base time at 95% of the pulse amplitude, 13 events had poor waveforms, and 2 were waveforms of double pulses in the same component, where it is difficult to make a correct calculation. Appendix A.3 shows the algorithm for base time calculation and some examples of these cases in figure A.3.

Having the signal of the same lightning on several sensors, we calculated the average value of the base time of the second component of those signals at 95% of its amplitude, as defined in panel (a) of figure 4.3. We also obtained the standard deviation of these data. Note that in figure 4.5, some events do not show this deviation because the beam signal was reported at only one antenna in the distance range we chose (sensors located between 500 and 600 km away from the lightning).

The large standard deviations observed in some of these events may stem from the fact that the pulse measured at one antenna, located at a certain distance from the lightning strike, may arrive attenuated at another antenna situated farther away. For example, in figure 4.6, we obtained $t_{b2} = 57.46\mu$s at a distance of 572.70 km in sensor R9AZL, and 44.79 at a distance of 512.37 km in sensor R9HBH. Nonetheless, it was necessary to consider this wide range between 500 and 600 km for conducting a global analysis of the storm, as the majority of events exhibited some signal within this range.

Chapter 5

Multi-elves observations challenging the electromagnetic pulse bounce mechanism

Through the pre-processing phase of multi-elves traces detected at the Pierre Auger Observatory from 2014 to 2020, we observed that the temporal difference between their peaks remains relatively constant. The behaviour persisted across multi-elves events of four distinct storms occurring at varying distances from the observatory. This is in contrast to what was expected based on the electromagnetic pulse bounce model, which predicts a decrease in time delay with increasing arc distance to the lightning source.

In this chapter, we present the detailed data from the four storms used for our analysis (see section 5.1). In section 5.2, we present the analysis of the time gap behaviour of multi-elves. To accomplish this, we developed a specialised code for analysing multi-elves traces, enabling more efficient results than the previous code for single elves analysis (see section 5.4).

Interestingly, we found some events with a time gap not exhibiting constant behaviour. However, upon closer examination, we observed that these could be attributed to other

Table 5.1: Total number of singles, doubles, and triples elves detected in four storms at different dates and distances from the Auger FD. The percentage of multi-elves about the total (% ME) varies for each storm, and the total number of multi-elves detected for the four storms represents 25%.

Storm date	**Total events**	**Singles**	**Doubles**	**Triples**	**% ME**
November 10, 2018 (01:26:46 - 07:49:03) UTC	117	96	9	12	18%
December 20, 2019 (01:56:40 - 06:14:18) UTC	158	133	16	9	16%
April 27-28, 2020 (23:36:58 - 09:36:05) UTC	139	75	33	31	46%
March 14, 2021 (00:51:03 - 06:34:07) UTC	62	53	8	1	15%
Total events analysed	**476**	**357**	**66**	**53**	**25%**

transient luminous events. These events are discussed in the section 5.5.

5.1 Data set

As we mentioned before, the night with the largest fraction of multi-elves in 2014-20 is between April 27 and 28, 2020 (see figure 3.9). Therefore, we have chosen this and two other thunderstorms that occurred on the morning of November 10, 2018, and December 20, 2019. Additionally, we selected the storm detected in the HEAT on March 14, 2021, to examine events occurring closer to the observatory.

The number of single and multi-elves (doubles and triples) within different storms displays notable variability, as shown in the table 5.1. In the November and December storms, the occurrence of multi-elves of the total events (%ME) is about 18% and 16%, respectively, whereas, in April, this proportion significantly escalates to 46%. Within the HEAT observations conducted in March, the percentage of multi-elves is 15%.

Among the 476 events analysed, a remarkable 25% consisted of 66 double and 53 triple events combined. This number of events surpasses the highest number of doubles de-

tected by the PIPER (40 events) in four storms in New Mexico, USA (Newsome and Inan, 2010). In addition, we report 53 triples while the PIPER's temporal resolution only allows it to detect doubles with ΔT ranging from 60 to 180 μs. These findings highlight the prevalence of multi-elves phenomena within the analysed data, indicating that they often appear during the storms we investigated.

5.2 Time delay of double and triple elves

This section shows the results of calculating the time difference among the pixels triggered by the multi-elves from four storms detected in the FD. We observed that ΔT of double and triple elves are usually constant; therefore, we can calculate the mean value of ΔT.

In figure 5.1, we show the resulting histogram of each storm analysed and the time delay histogram of all events. Each storm exhibits a distinct distribution of ΔT, and it is evident that the storm of April 27-28, 2020, presents the highest occurrence of multi-elves.

The high temporal resolution of the FD allows us to report unprecedented events with ΔT as short as 7 μs. However, most events fall within the range of 10 μs to 40 μs, as shown in the last histogram in the same figure. There is a gap in the ΔT distribution between 40 μs and 60 μs, followed by a subsequent increase between 60 μs and 120 μs.

Furthermore, we have observed events with time delay exceeding 200 μs and, in some cases, around 450 μs. These longer ΔT events involve elves in conjunction with other TLEs, such as halos (see section 5.5 for further details). In figure 5.2, we present the percentage of single, double and triple elves, together with the percentage of single and double elves occurring with halos (labelled as "Halos" in the plots). Note that the April storm has the highest percentage of double and triple elves.

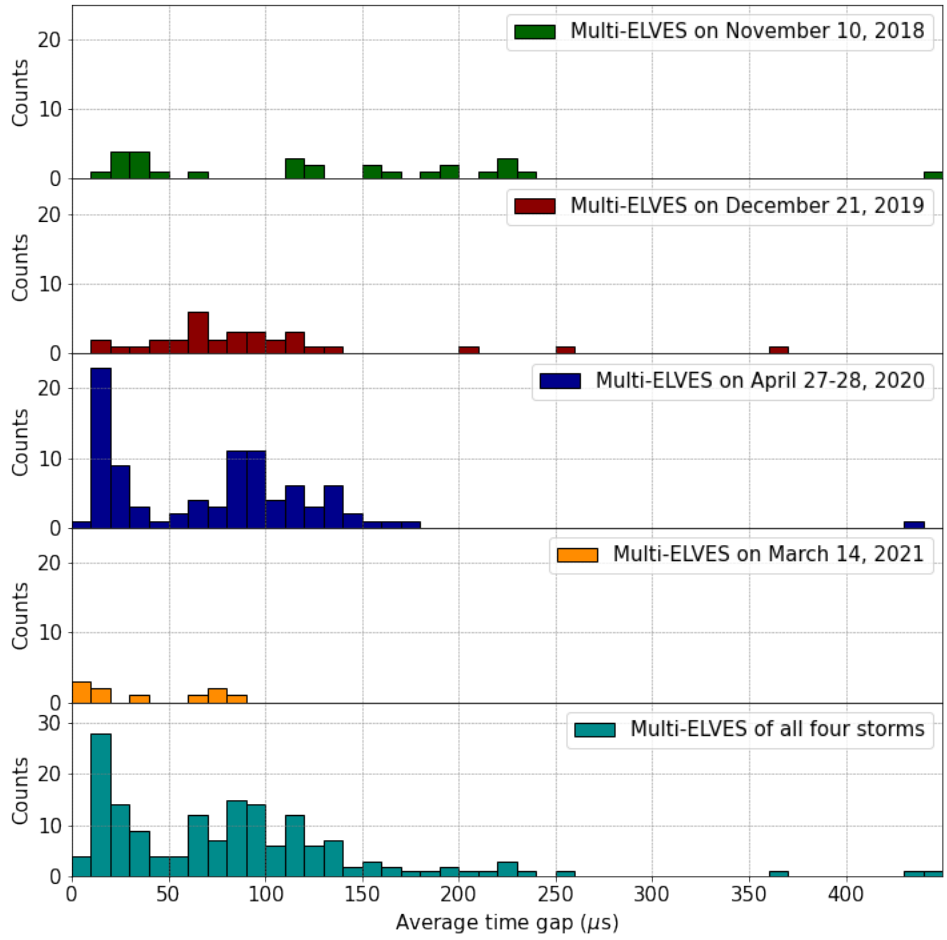

Figure 5.1: Distribution of the average time gap of the multi-elves detected in the FD of four storms. Each storm has a different distribution, with the April storm having the most events. The FD's high temporal resolution allows reporting events with ΔT below 10 μs. The last histogram shows that most events fall within the 10 to 40 μs range. There is a decrease in event frequency between 40 and 60 μs, followed by an increase between 60 and 120 μs. Additionally, some events have ΔT exceeding 200 μs and, in rare cases, around 450 μs.

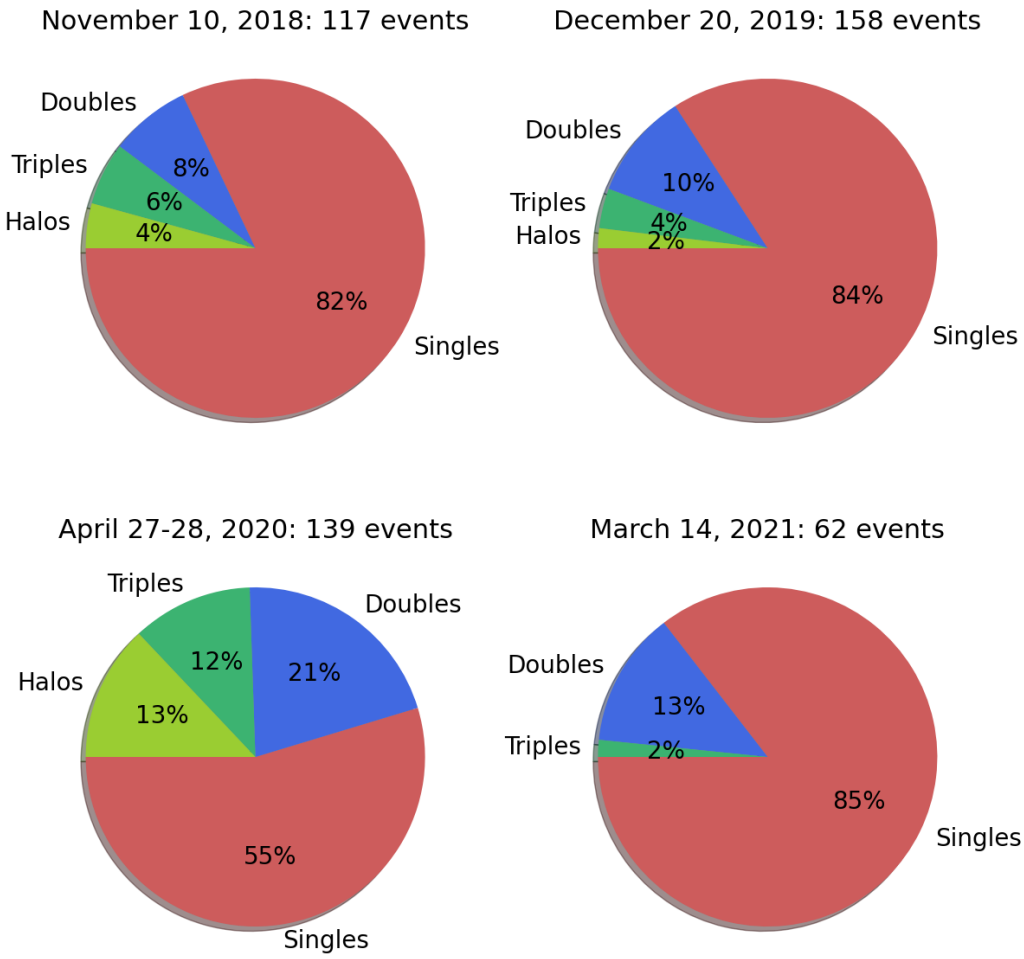

Figure 5.2: Percentages of single, double, and triple elves, along with the percentages of single and double elves occurring in conjunction with halos (denoted as "Halos"). These events were detected during four different storms within the field of view of the Auger fluorescence detector. Notably, the April storm exhibits the highest percentage of double and triple elves.

Compared to the events from the four storms reported by Newsome and Inan (2010) as shown in figure 2.8, we have a higher percentage of double events. Additionally, we report an unprecedented number of 30 triple-ring events. Our ratio of doubles and triples concerning elves + halo events is lower than that reported by Newsome and Inan (2010). This discrepancy may be attributed to the PIPER detection window being on the order of milliseconds, whereas the Auger FD detection window is 900 microseconds. This difference enables the PIPER to detect halos occurring around a few milliseconds apart from the detection of elves.

In the next section, we analyse the behaviour of the time difference between the rings of the multi-elves based on the bouncing of the electromagnetic pulse model originated by an IC lighting.

5.3 Behaviour of the time between multi-elves rings challenging the EMP bounce mechanism

To analyse the behaviour of the time delay of the multi-elves with the distance to the lightning source, we recall the model proposed by Marshall et al. (2015). From equations 2.2 and 2.3, we determine how ΔT varies with ArcR distance from the geometry of our FD cameras (figure 2.12). Each camera has 440 pixels that individually collect a part of the elve light ring.

As shown in the scheme of right panel of figure 2.11, we obtain the position of point P ($\mathrm{Lat_{pix}}$, $\mathrm{Lon_{pix}}$) by projecting the pointing direction of one camera pixel onto the base of the ionosphere, along with the corresponding site ($\mathrm{Lat_{site}}$, $\mathrm{Lon_{site}}$). As mentioned earlier, we reconstruct the location of the lightning ($\mathrm{Lat_s}$, $\mathrm{Lon_s}$) from the measured light-time distributions of the recorded elve.

The time gap ΔT between the two pulses emitted from the base of the ionosphere in a

multi-elve event should follow a dependence from the arc distance ArcR, given by the equations 2.2 and 2.3, if it is due to the EMP bounce mechanism. However, we have not found double elves events with this characteristic behaviour as the ΔT tends to be constant. We observe the same tendency in ΔT values of triple elves. Some events exhibit mixed behaviour, with most of the data staying relatively constant, while a few points show a decrease or no clear trend.

In figure 5.3 we show an example of each case for reference: (A) is a double elve with quasi-constant ΔT which is labelled as "double flat" and (B) is a "double mixed" elve which has few points not following the constant behaviour. In the case of triple elves, we have the example of a "triple flat" in figure (C), one with mixed behaviour in (D) and the only multi-elves event that seems to follow the bounce model curves (empty markers in the plot) for a lightning strike at a height of 5 km in (E). However, this event shows some outliers highlighted in blue that do not follow the model.

In figure 5.4, we show that out of the 63 double elves detected in the four storms mentioned earlier, 65% display a quasi-constant time gap while 35% exhibit mixed behaviour. Among the 30 triples, 80% show quasi-constant ΔT and 17% are mixed. Figure 5.5 illustrates the temporal difference between double and triple elves from the storm with the most multi-elves, and figure 5.6 from the other three storms, indicating that this result is independent of the unique characteristics of each storm.

Our observations challenge the current understanding of the mechanism responsible for generating multi-elves with in-cloud lightning sources since ΔT of these events do not follow the curves of the model (empty marker functions in figure 5.5 and 5.6). The following section outlines the methodology used to calculate the time gap between multi-elves peaks.

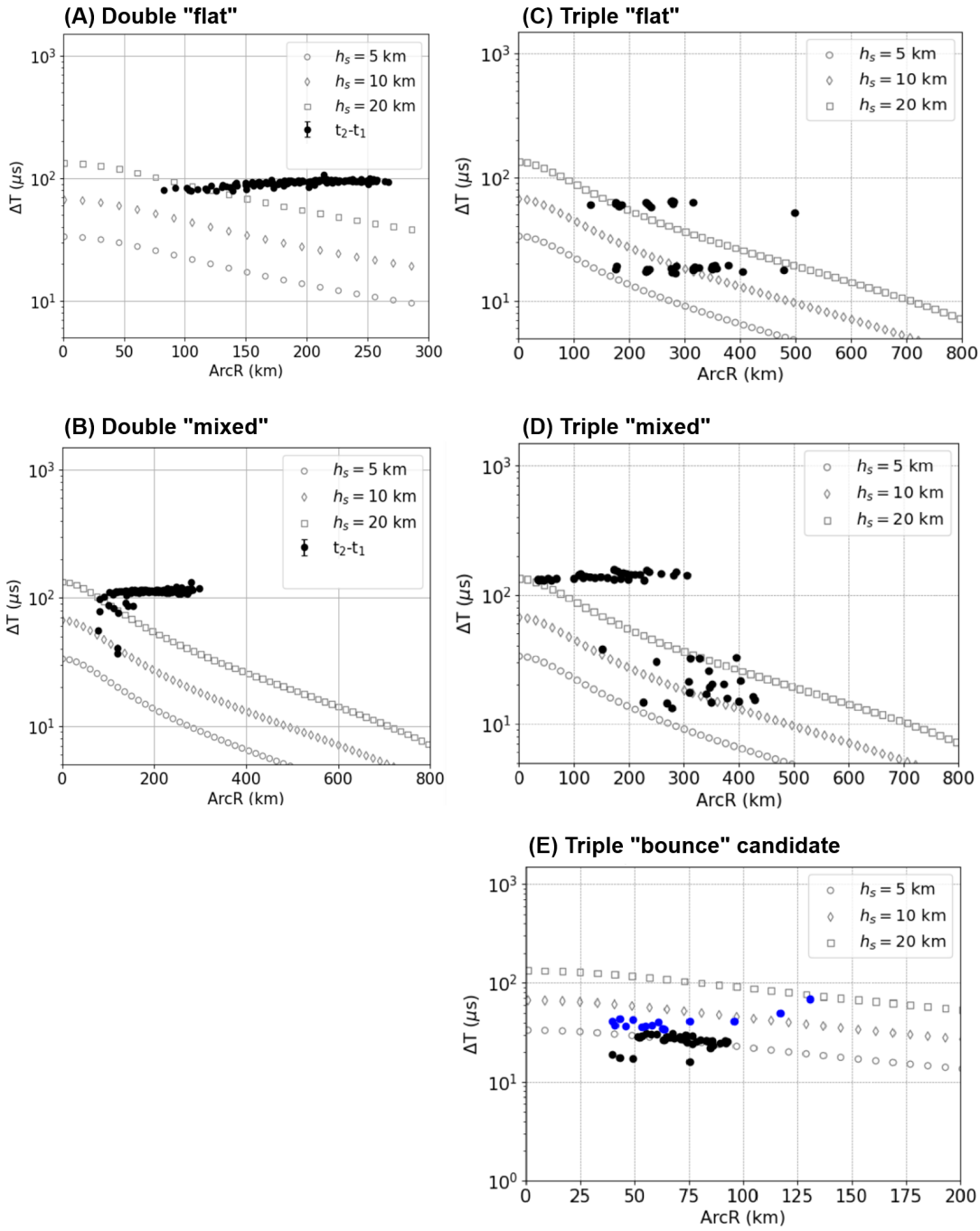

Figure 5.3: Examples of the classification of double and triple elves according to the behaviour of their time gap (ΔT). The "flat" events (A and C) have a quasi-constant ΔT while in the mixed events (B and D) this tendency prevails with some points that decrease with ArcR distance or do not follow a clear behaviour (as shown in panel D). Panel (E) shows a candidate of the electromagnetic pulse bouncing mechanism, being unique among a total of 93 multi-elves from four storms.

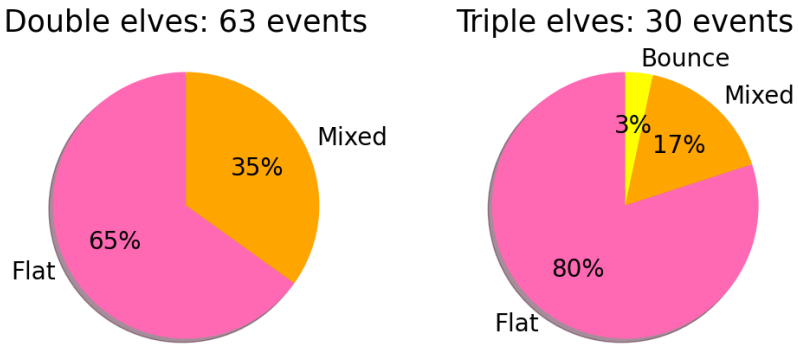

Figure 5.4: Percentage of doubles and triples following quasi-constant ("flat") and mixed behaviour for the 63 doubles and 30 triples detected in total in the four selected storms.

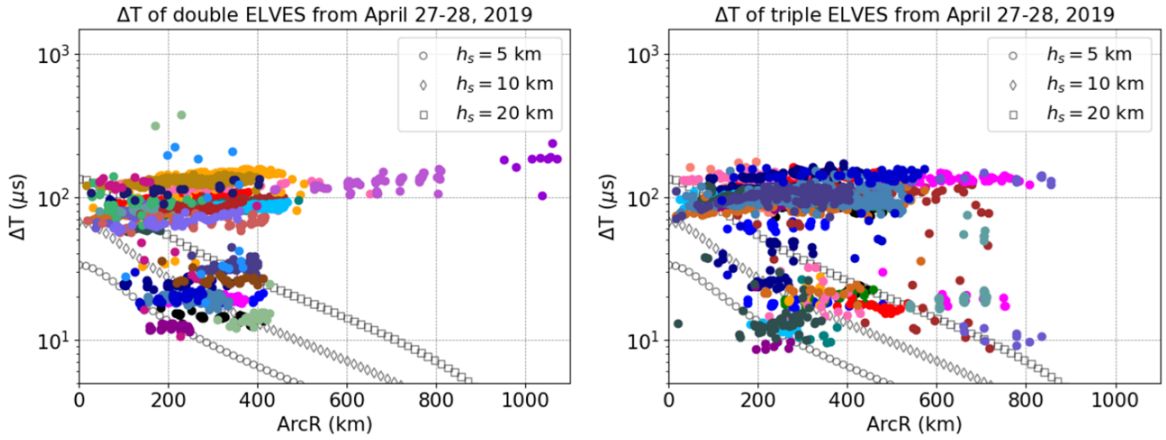

Figure 5.5: Left panel: quasi-constant double elves type time difference in the April 27-28 storm, 2020. The empty markers functions show different curves that the time delay ΔT would follow if the second peak of the elve was originated by the bouncing of the electromagnetic pulse of an in-cloud lightning at a height h_s. Right panel: quasi-constant time difference between the second and first peak and between the third and first peak of triple elves. Even triple elves have this ΔT behaviour with the arc distance.

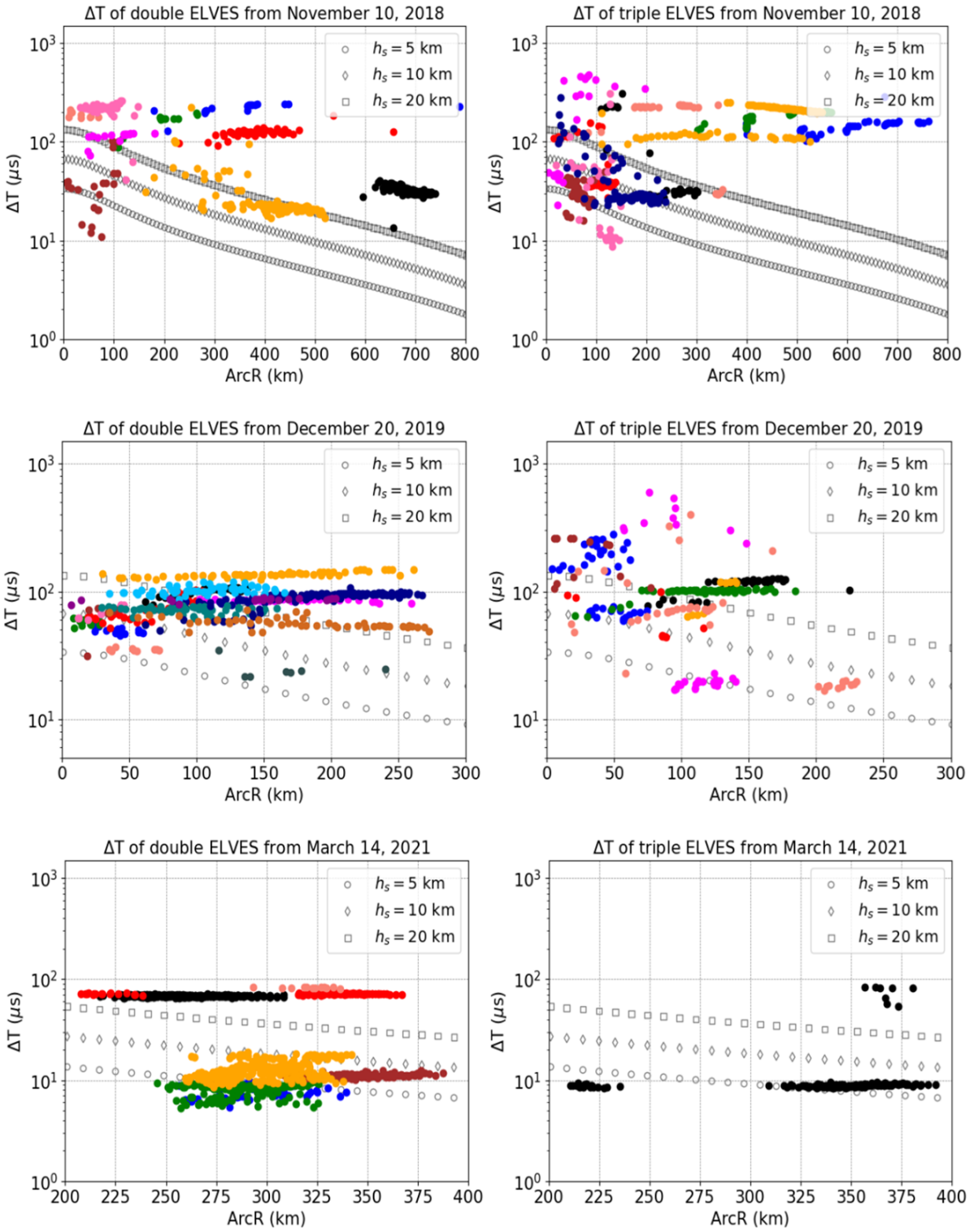

Figure 5.6: Left panel: quasi-constant double elves type time difference frequently detected in the Auger FD. The empty markers functions show different curves that the time delay ΔT would follow if intracloud lightning originated at a height h_s. Right panel: quasi-constant time difference between the second and first peak and between the third and first peak of triple elves. The March storm shows that even in the events closest to the observatory, between 200 and 400 km, a constant ΔT trend prevails.

5.4 Multi-elves traces analysis

To analyse the traces of the multi-elves, we developed an algorithm that fits a multiple Gaussian function $f(t)$ to the signal of each pixel triggered in the FD cameras. The fitting process starts with the initial parameters, which include the time values t_1, t_2, and t_3, obtained using the "`find_peaks()`" Python function from `SciPy` library. This function is designed to locate the most prominent peaks in the signal and requires customisation through three parameters: threshold, peak width, and prominence (details on how the code works in appendix A.4).

The middle panel of figure 5.7 provides an example of the determination of t_1 and t_2 for a double peak event (left), and t_1, t_2, and t_3 for a triple peak event (right). In both cases, the characteristic parabolic shapes of elves can be observed for a specific row of the camera.

It is important to emphasise that not all pixels of a double event will exhibit two distinct peaks. In some cases, the peaks may overlap completely, forming a single pulse, while in others, the peaks may be too close to each other for the algorithm to find them separately. For example, the same figure shows that in the triple elve event (EVT1272097126-621594500), columns 5 and 14 have only the first peak, columns 1-4 and 15-16 have the first and second peaks, while columns 6 and 8-13 have all three peaks. However, this event is labelled triple because at least five triggered pixels had three peaks.

After finding the peaks, we perform the corresponding Gaussian fitting (single, double, or triple) using t_1, t_2 and t_3 as the initial parameters. Then, as shown in the bottom panel of figure 5.7, we choose the fit that minimises the error according to the signal data (using the "`Minuit`" Python function from `iminuit` library). From this we obtain the values of times (t_1, t_2 and t_3), amplitudes (a_1, a_2 and a_3) and peaks width (σ_1, σ_2 and σ_3) of the pulses as the example of a double elve shown in figure 5.8. Finally, we

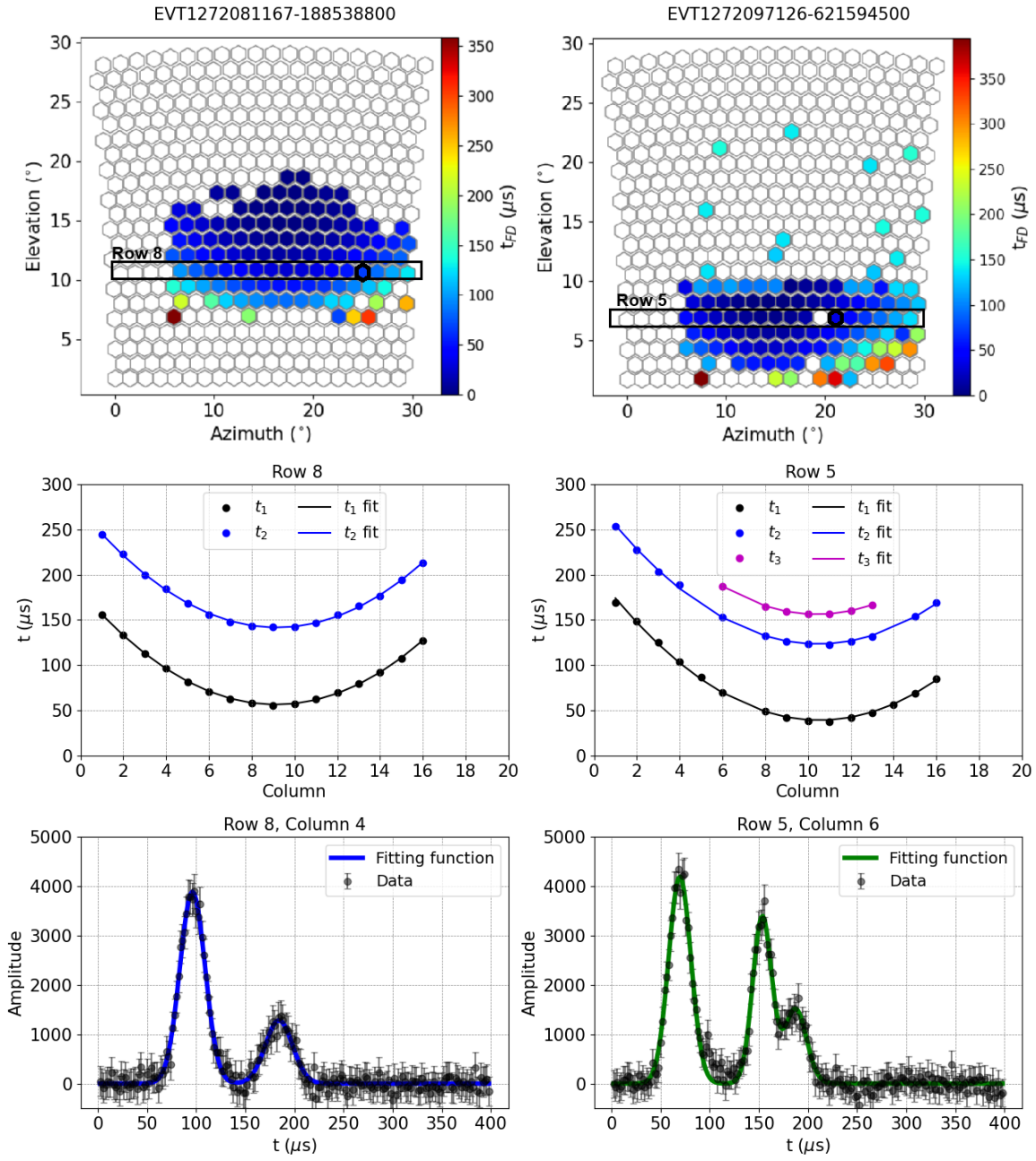

Figure 5.7: Top panel: arrival time of light from a double (left) and triple (right) elve, detected in FD cameras on April 28, 2020, at 03:52:29 UTC and 08:18:28 UTC respectively, where a particular row and pixel are marked to illustrate an example of the multiple peaks in the traces of these events. Middle panel: examples of the most prominent peaks t_1 and t_2 in row 8 of the double elve (left) and t_1, t_2 and t_3 in row 5 of the triple elve (right). The distinct parabolic patterns of the elve emission can be observed in both cases. Bottom panel: examples of the fitting with multiple Gaussian functions of the signal corresponding to row 8 and column 4 of the double elve (left), as well as the signal of row 5 and column 6 of the triple elve (right).

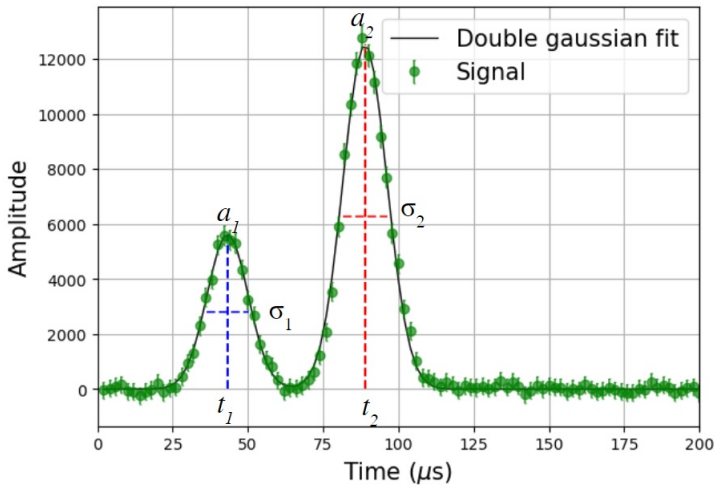

Figure 5.8: Example of the fit with a multiple Gaussian function for a double elve photo-trace, that calculates the times (t_1 and t_2), amplitudes (a_1 and a_2) and peaks width (σ_1 and σ_2) to obtain the time difference ΔT.

can determine the time difference ΔT_d between the peaks of double elves and, for triple elves, we have ΔT_d and ΔT_t.

$$\Delta T_d = |t_2 - t_1| \tag{5.1}$$

$$\Delta T_t = |t_3 - t_1| \tag{5.2}$$

As each event is unique, the parameters of "`find_peaks()`" cannot be fixed; instead, we must choose the combination of values that yields the best result (default values of threshold, peak width, and prominence in the appendix A.4). However, the values used for the multi-elves at the four FD sites are generally similar, but higher thresholds are necessary for the HEAT. This is due to the larger amplitudes of the signals recorded by the HEAT, as the observed elves are closer to the detector than those observed from LL, LM, LA, and CO.

This new Python code's efficiency outperforms the previous one used for processing single elves signals[1], where the second peak was associated with the residual of a simple

[1]The **FdProcessElves.cc** is the core class for elves reconstruction developed by Roberto Mussa.

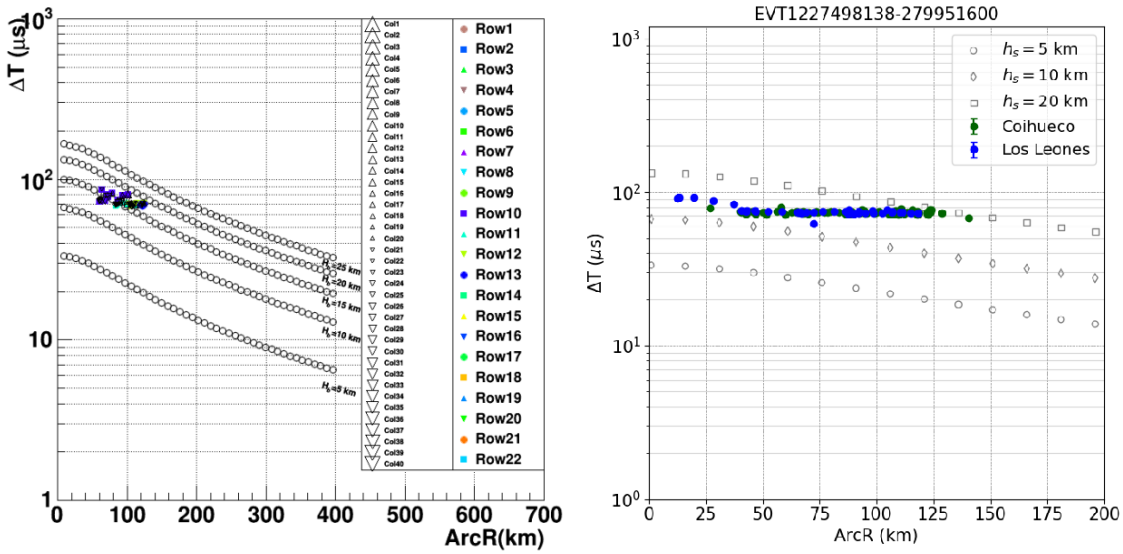

Figure 5.9: Comparison of the ΔT values of the event occurred on November 29, 2018, 03:42:00 UTC, obtained with the pre-processing code (left) and the new Python code (right). With the new code, we obtain more ΔT values, and what looked like a candidate of the bouncing mechanism on the left panel shows a quasi-constant ΔT from two FD sites (Coihueco and Los Leones) on the right panel. This also happened for the other 15 events we had as candidates of this model in the 2014-20 period.

Gaussian fit. In figure 5.9, the comparison of the ΔT obtained from both codes of the event on November 29, 2018, 03:42:00 UTC. We obtain more ΔT data with the multiple Gaussian fit, allowing us to analyse values and behaviour more accurately.

Note how this event, which with the old code seemed to be a candidate for the EMP bounce model (left panel in the same figure), turned into an event with a constant ΔT (see right panel in figure 5.9) due to the large number values recovered with the new code developed in this work. The same happened with 15 more events tagged as bounce model candidates by the previous code.

Available in: https://gitlab.iap.kit.edu/auger/cosmogeo/elves/-/tree/master/reco

5.5 Other transient luminous events detected in Auger

Through the analysis of ΔT in the elves observed during the selected storms, we identified certain events with high values of around 400 μs, which intrigued us. Figure 5.10 shows an example of this occurring on April 28, 2020 at 03:10:01 UTC. After analyzing all the event traces, we observed that most of them are synchronous with the time when the lightning occurred. As shown in the right panel of the figure, the traces within the red box are identified as "Double ELVES". The other traces in the box labelled as "Halo", are offset by approximately 450 μs.

The aligned traces correspond to a typical double elve detected in Auger, while the others could belong to a halo generated a few kilometres lower in altitude from the elve. Therefore, what initially appeared to be a triple elve with a very high ΔT value could be a double elve (with $\Delta T \approx 10\,\mu$s) occurring very close to a halo.

Moreover, we also have some events where the time gap does not exhibit a clear trend, neither constant nor decreasing, as observed in the example in figure 5.11. The left panel displays the time gap that varies from 8 to 90 μs. These variations are due to the multiple peaks present in the traces of this event occurring on April 28, 2020, at 03:10:01 UTC. For example, in the right panel of the figure, the trace corresponding to pixel R8_C1 contains four prominent peaks, while in pixels R9_C1 and R7_C1, one of these peaks disappears, and the code only identifies three of them. The trace of pixel R6_C1 shows only two peaks, whereas the trace of R5_C1 displays multiple, less prominent peaks.

We cannot definitively assert whether these multiple peaks are due, for example, to a quadruple elve or a "TIGER elve" (a striated elve aligned with convectively generated gravity waves in the atmosphere (Yue and Lyons, 2015)). In the four analysed storms, approximately five events exhibiting these multiple peaks were identified. It is essential to examine these projected emissions in the ionosphere to determine whether "TIGER"

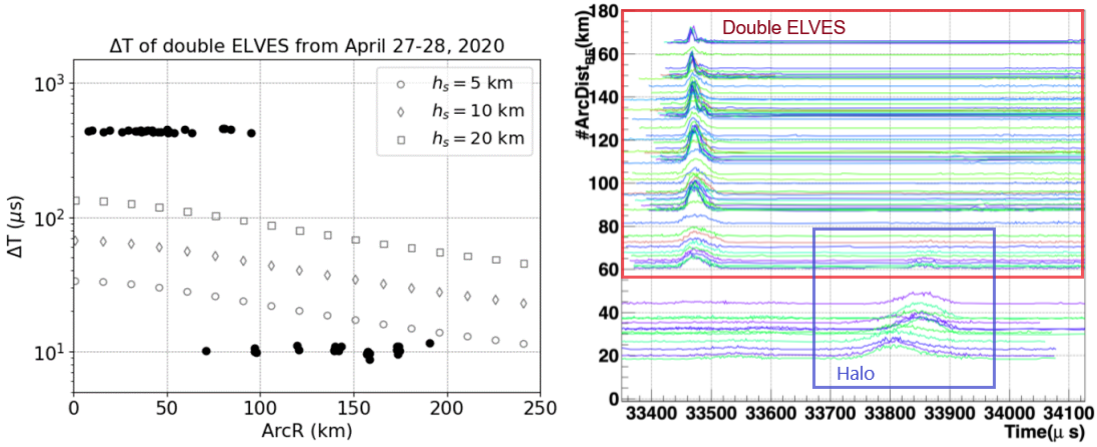

Figure 5.10: Left: very high ΔT of an event detected in the storm on April 28, 2020 at 03:10:01 UTC. Right: upon closer examination, most traces align with the lightning occurrence time (red box), while some exhibit a 450 μs offset (blue box). Aligned traces indicate a double elve, suggesting others may belong to a halo occurring lower in altitude. Thus, what seemed like a triple elve with a high ΔT is a double elve (with $\Delta T \approx 10\,\mu$s) occurring 450 μs before the halo.

lines are observed to be aligned with the gravity waves or if they represent a different luminous phenomenon. While in this study we did not extensively explore this aspect, it would be of significant interest to find if the Auger FD is detecting such phenomena.

Additional information about the transient luminous events we are detecting in the Auger FD is required to perform a more comprehensive study. To facilitate this, a photographic camera was installed at the observatory by the end of 2023. Although we have only recently started detecting sprites, we aim to establish a database of these events soon to gain a new perspective on their analysis.

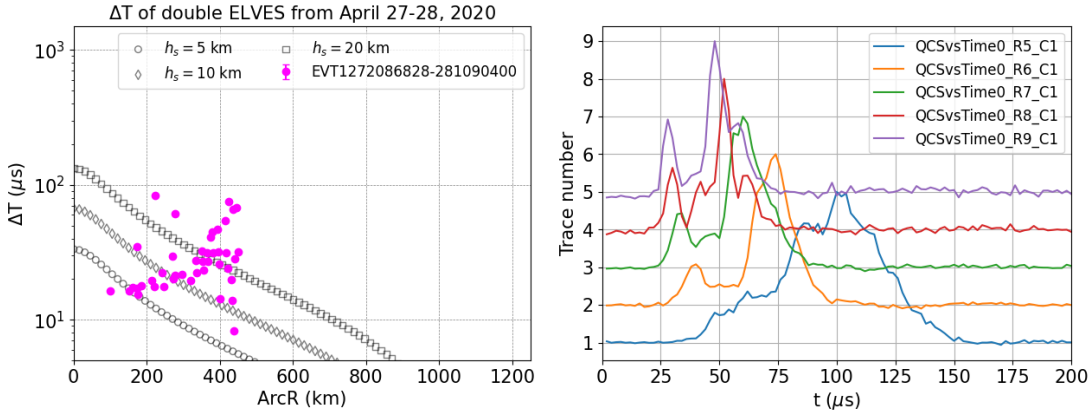

Figure 5.11: Left: Time gap of the event occurring on April 28, 2020, at 05:26:50 UTC without a clear trend. Right: examples of traces from the event showing multiple peaks within a temporal window of 200 μs. The trace of the pixel R8_C1 contains four prominent peaks, while in pixels R9_C1 and R7_C1, one of these peaks disappears. The trace of pixel R6_C1 shows only two peaks, whereas the trace of R5_C1 displays multiple, less prominent peaks.

Chapter 6

Characteristics of storm and lightning producing multi-elves

A preliminary analysis was conducted on correlative measurements from external experiments to understand how the characteristics of elves observed by Auger depend on the physics of lightning and the storms themselves.

As shown by Merenda (2020), the synergetic study of elves with a large body of correlative measurements can significantly contribute to the community's understanding of the return stroke process, the lightning initiation processes, and the charge distribution within clouds at a global level.

Merenda (2020) summarises the overlap in the observational coverage between the Auger FD and experiments, from which valuable information could be recovered (see table 6.1). These experiments include measurements of lightning variables from ground networks and space, such as current, polarity, type, the energy of the electromagnetic pulse, waveforms, channel length and traces; and meteorological observations from geostationary satellites for estimating cloud temperature, cloud top height, and the temporal evolution of storms through real-time lightning mapping.

Table 6.1: Experiments for which Auger has the potential to obtain to measure a correlation with elves. The status of searches is listed in the rightmost column. All experiments provide the time and geodetic location of their events. The variable column lists the specific information that this experiment could provide. Adapted from (Merenda, 2020).

Experiment	Description	Variables	DAQ Overlap	Comment
LMA	1 LMA in AR	Channel length	11/18 – 05/19	5 -20 events
LF	4 sites in AR	Current, traces	11/18 – 12/18	Not Done
CAMMA	Marx Meter Array	Type	11/18 – 12/18	Not Done
LDS	4 sites at Auger	Traces	01/14– Present	Poor Corr.
LIS	Satellite		03/13 – 02/15	No Corr.
WWLLN	4 sites in SA	EMP energy	03/13– Present	72% Corr.
ENTLN	> 10 sites in AR	Current, polarity type, waveform	11/18-Present	> 30% Corr.
GLD-360	> 10 sites in AR	Current, polarity	01/16-Present	> 80% Corr
JEM-GLIMS	Satellite		03/13 – 08/15	No Corr.
ABI	Onboard GOES-16 satellite	Cloud top height	06/17 to Present	100% Corr.
GLM	Onboard GOES-16 satellite	Lightning intensity, temporal evolution	06/17 to Present	Not Studied

In this chapter, we focus on lightning and meteorologic observations obtained from Earth Networks and the Advanced Baseline Imager (ABI) onboard the GOES-16 satellite to further analyse the elves-producing storms previously selected.

Data from ENTLN allow cross-validation of the accuracy of our lightning location algorithm through a comparison with the network-provided locations, and at the same time, it is a test of the accuracy of the network geolocation. Detections from ENTLN allow us to analyse the type of lightning that produced the elves, including their peak current and polarity (see section 6.1). In section 6.2, a preliminary meteorological analysis is performed on GOES-16 data, characterizing the elves population in terms of parent lightning region, temperature and cloud-top height.

6.1 Characteristics of lightning producing multi-elves

Earlier in section 4.1, we have discussed how the ENTLN network functions, and we have utilised the waveforms correlated with our elves to analyse whether there is a

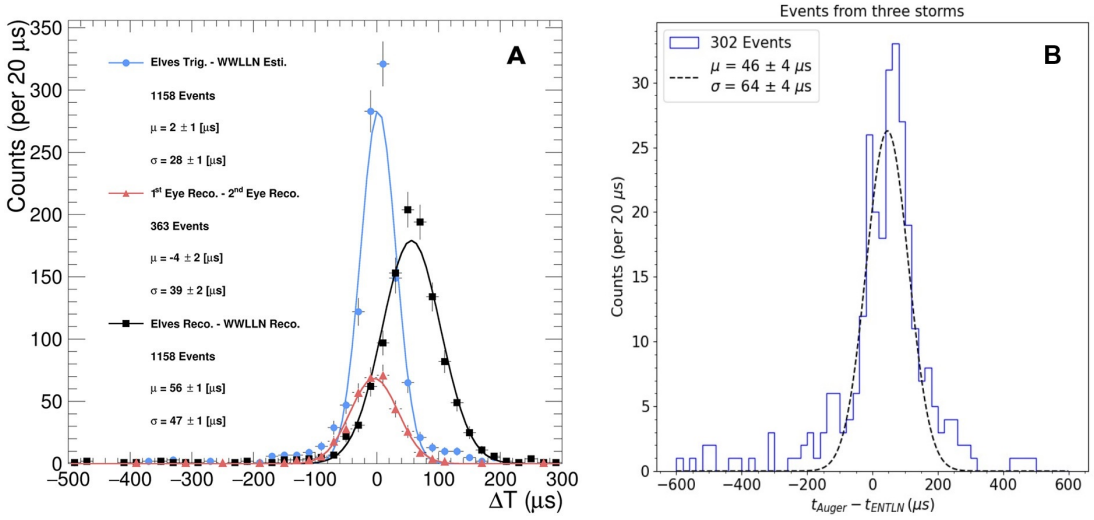

Figure 6.1: Comparison of the lightning strike time reconstructed by Auger, WWLLN and ENTLN. A) The black curve obtained by (Aab et al., 2020) shows a mean difference of 56 μs between the time determined by Auger and that reported by WWLLN in a sample of 1158 events. B) Time difference between Auger and ENTLN, for a total of 285 correlated events in three storms analysed in this work, we obtained a mean value of 46 μs.

relationship between the duration of the lightning current pulse and the production of single, double, and triple elves. In this section, we assess the efficiency of our code in determining the time of occurrence of the lightning that produced the elves, as well as its location. Additionally, we evaluate the peak current and polarity distributions of the storms to discern the properties of lightning that produce multiple elves.

As explained previously in chapter 3, we can reconstruct the location and time of lightning strikes by detecting the elve light in the Auger FD. We refer to this time as t_{Auger} and denote the location in latitude and longitude as Lat_{Auger} and Lon_{Auger}. In panel A of figure 6.1, the black curve represents the distribution of the difference between the t_{Auger} and the lightning strike time provided by the World Wide Lightning Location Network (WWLLN) obtained by Aab et al. (2020). This distribution has a mean value of 56 μs with a standard deviation of 47 μs for a sample of 1158 correlated events.

In panel B of the same figure, we show the time difference between Auger and ENTLN

for the 302 correlated events that occurred during storms on 10th November 2018, 20th December 2019, and between 27th and 28th April 2020. This distribution has a mean value of 46 μs with a standard deviation of 64 μs, which is consistent with the values obtained in the correlation with WWLLN, despite the difference in the number of events correlated with WWLLN and ENTLN. This difference demonstrates the efficiency of our algorithm in locating lightning from observed elves data in the FD.

Figure 6.2 shows the results of the analysis for the storm on November 10, 2018. Figure 6.3 displays the results for the storm on December 20, 2019, and figure 6.4 corresponds to events from April 27-28, 2020. The A panel of each figure shows the location of lightning correlated with single (red circles), double (blue triangles), and triple (green squares) elves compared to other lightning events of the storm reported by ENTLN (cyan dots), which were not associated to elves.

Panel B of these figures show the difference between the lightning latitude obtained in Auger and that reported by ENTLN, whereas panel C illustrates the difference between the longitudes. Overall, it is observed that the variance in longitudes is significantly greater than that in latitudes: the corresponding mean values for each storm are approximately 0.203°, 0.182°, and 0.210° for longitude, whereas the differences in latitude are -0.018°, -0.016°, and 0.054° for the November, December, and April storms, respectively. The enhanced accuracy along latitudes is attributed to the relative positioning of the observatory to the three storms.

The lightning strike time difference between Auger and ENTLN for each storm can be observed as follows: panel D illustrates the distribution of all events along with the mean value and standard deviation, highlighting in red the distribution of events correlated with single elves; panel E and F show the distribution of all events, indicating those correlated with double elves (blue in panel E) and triple elves (green in panel F).

The best temporal correlation is achieved in the storm occurring from April 27 to 28, 2020, with an average temporal difference of 18 μs (see panel D in figure 6.4). Following

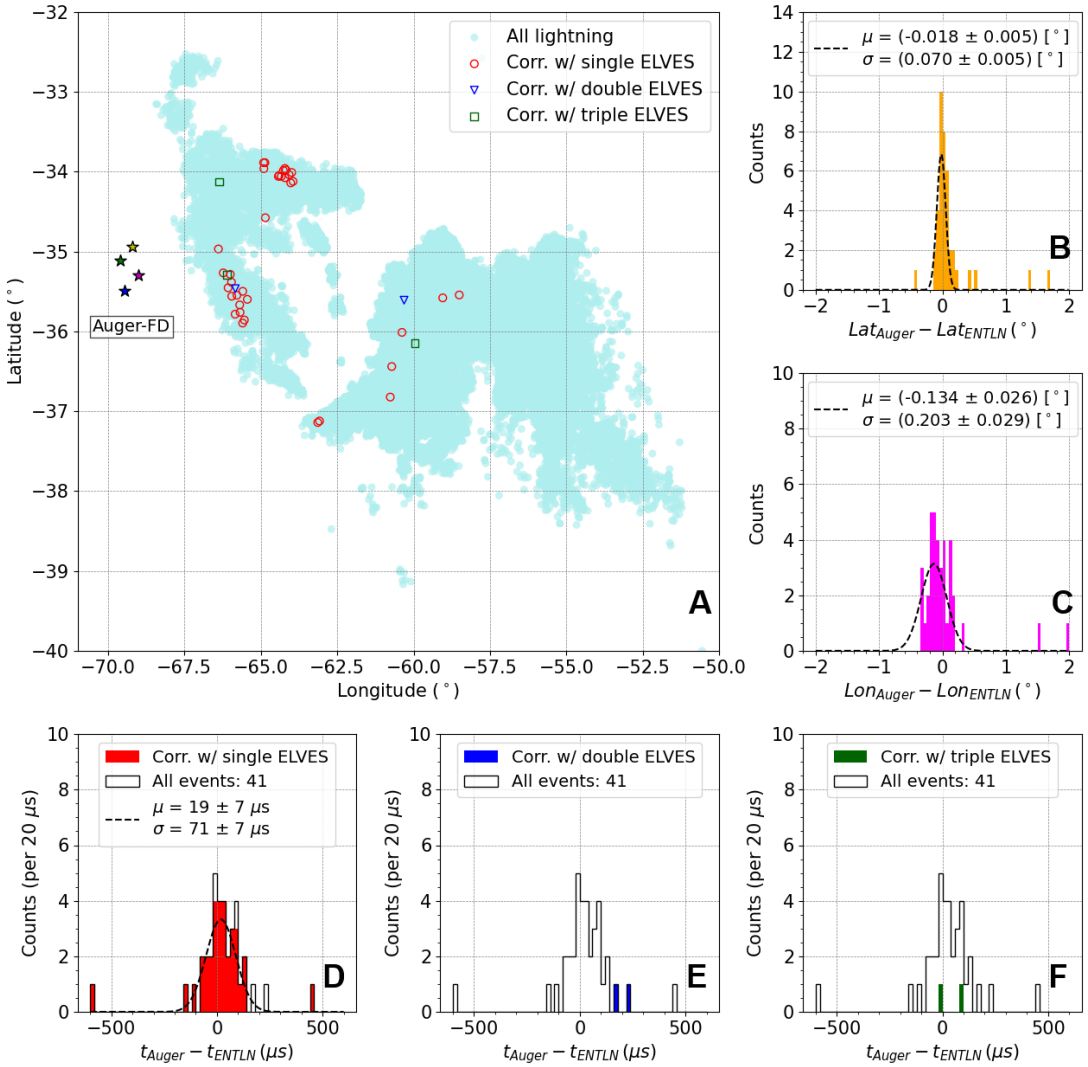

Figure 6.2: Time and location of the lightning strikes from the storm on November 10, 2018, correlated with the elves detected in the Auger Fluorescence Detector during the time window of 01:26:46 - 07:49:03 UTC. A) Location of storm lightning, highlighting those correlated with single elves (red circles), double elves (blue triangles), and triple elves (green squares). B) and C) shows the difference between the location of the lightning reconstructed by Auger (Lat_{Auger}, Lon_{Auger}) and from ENTLN (Lat_{ENTLN}, Lon_{ENTLN}) with a mean value of -0.018 degrees difference in latitude and -0.134 degrees difference in longitude. D) Distribution of the temporal difference between the lightning time reconstructed by Auger (t_{Auger}) and reported by ENTLN (t_{ENTLN}) of the 41 events correlated, with a mean value of 19 μs. Events correlated with single elves are highlighted in red. Events correlated with double and triple elves are shown in E) and F) respectively.

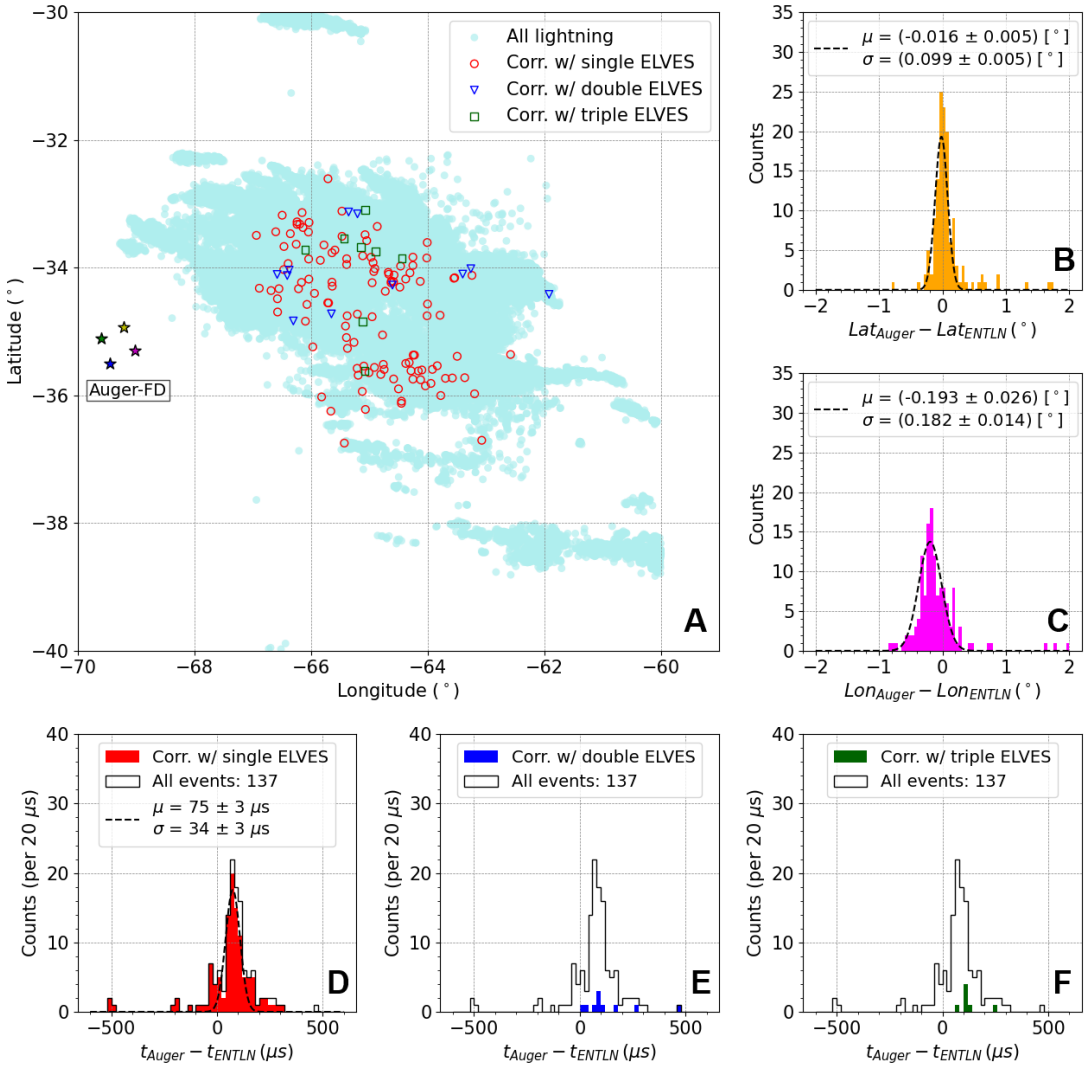

Figure 6.3: Time and location of the lightning strikes from the storm on December 20, 2019, correlated with the elves detected in the Auger Fluorescence Detector during the time window of 01:56:40 - 06:14:18 UTC. A) Location of storm lightning, highlighting those correlated with single elves (red circles), double elves (blue triangles), and triple elves (green squares). B) and C) shows the difference between the location of the lightning reconstructed by Auger (Lat_{Auger}, Lon_{Auger}) and from ENTLN (Lat_{ENTLN}, Lon_{ENTLN}) with a mean value of -0.016 degrees difference in latitude and -0.193 degrees difference in longitude. D) Distribution of the temporal difference between the lightning time reconstructed by Auger (t_{Auger}) and reported by ENTLN (t_{ENTLN}) of the 137 events correlated, with a mean value of 75 μs. Events correlated with single elves are highlighted in red. Events correlated with double and triple elves are shown in E) and F) respectively.

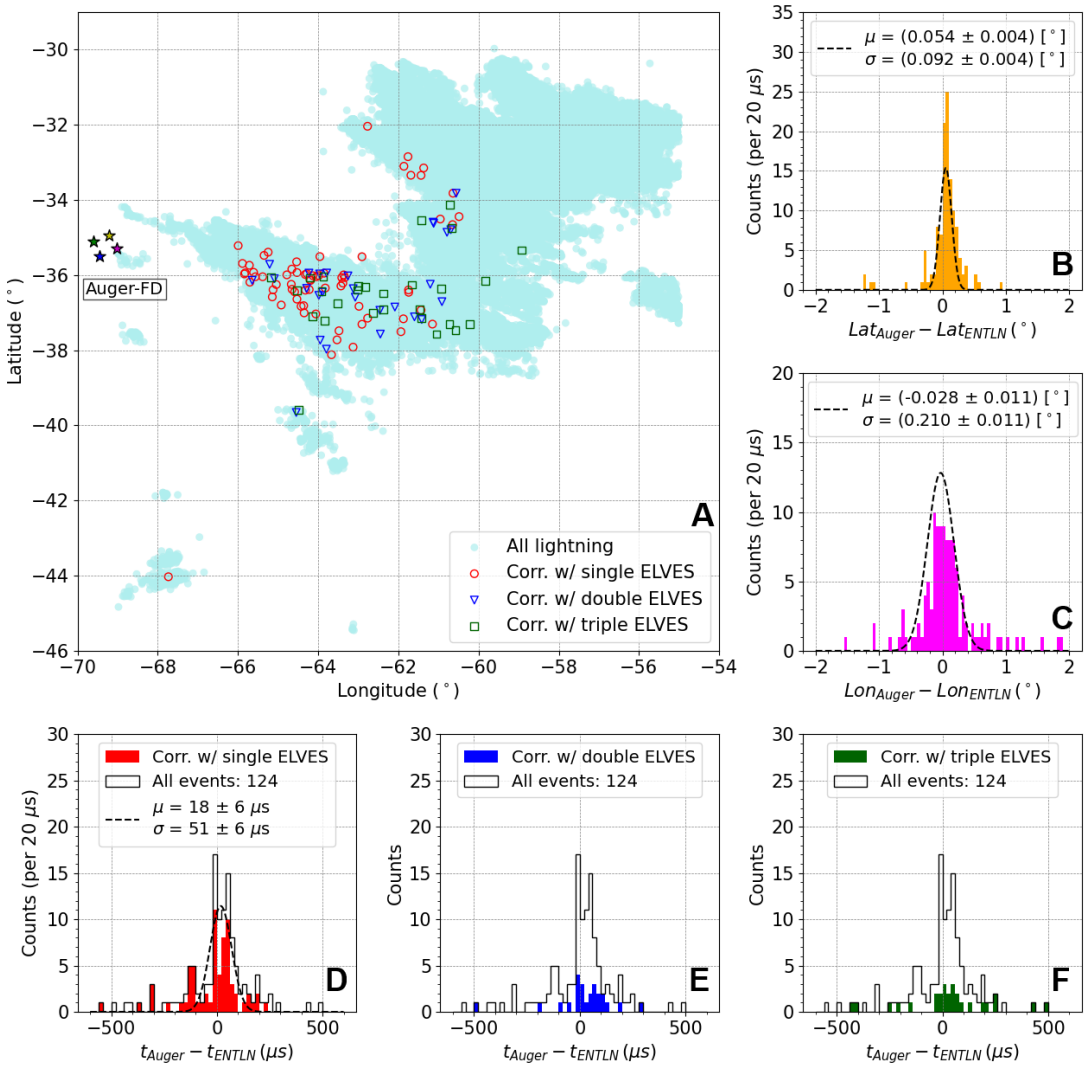

Figure 6.4: Time and location of the lightning strikes from the storm on April 27-28, 2020, correlated with the elves detected in the Auger Fluorescence Detector during the time window of 23:36:58 - 09:36:05 UTC. A) Location of storm lightning, highlighting those correlated with single elves (red circles), double elves (blue triangles), and triple elves (green squares). B) and C) shows the difference between the location of the lightning reconstructed by Auger (Lat_{Auger}, Lon_{Auger}) and from ENTLN (Lat_{ENTLN}, Lon_{ENTLN}) with a mean value of -0.054 degrees difference in latitude and -0.028 degrees difference in longitude. D) Distribution of the temporal difference between the lightning time reconstructed by Auger (t_{Auger}) and reported by ENTLN (t_{ENTLN}) of the 124 events correlated, with a mean value of 18 μs. Events correlated with single elves are highlighted in red. Events correlated with double and triple elves are shown in E) and F) respectively.

this is the November storm with a mean value of 19 μs (panel D in figure 6.2), and the December storm exhibits a mean difference of 75 μs (panel D in Figure 6.3). The December storm has more correlated events (137 lightning strikes), April registers 124, while the November storm shows very few correlated events (41).

From these correlations, we can derive lightning characteristics such as polarity and peak current, as well as lightning type. In Figures 6.5, 6.6, and 6.7, panel A shows the polarity and peak current of all lightning within the storm (black), lightning identified as intra-cloud (IC, depicted in yellow histogram), and those classified as cloud-to-ground (CG, shown in dark cyan). It is noteworthy that a considerable portion of the lightning is categorized as "undefined" because the ENTLN network was unable to classify them as either IC or CG using its algorithm, despite having access to the waveforms of these lightning events.

Unfortunately, most of our elves correlate with these undefined lightning events, as shown in the E panel of these figures. Thus, we cannot establish a clear correlation between the type of elves (single, double, or triple) and the type of lightning that produces them (IC or CG). We observed a lack of "undefined" data in the November storm, which could explain the low number of correlated events we obtained.

According to the EMP bounce model, we would expect multi-elves to be correlated, preferably with IC lightning. However, in the November storm, it can be observed that 4 out of the five multi-elves are correlated with CG lightning and one triple-elve with IC lighting (see panel E in figures 6.5). We have double and triple elves correlations with CG and IC lightning in the December and April storms (panel E in figures 6.6 and 6.7).

In panels B, D, and F, we compare the peak current values and polarity of the lightning strikes correlated with elves, highlighting in red those associated with single elves in panel B, double elves in panel D, and triple elves in panel F. In storms with a higher number of correlated events, such as December and April, a predilection for negative

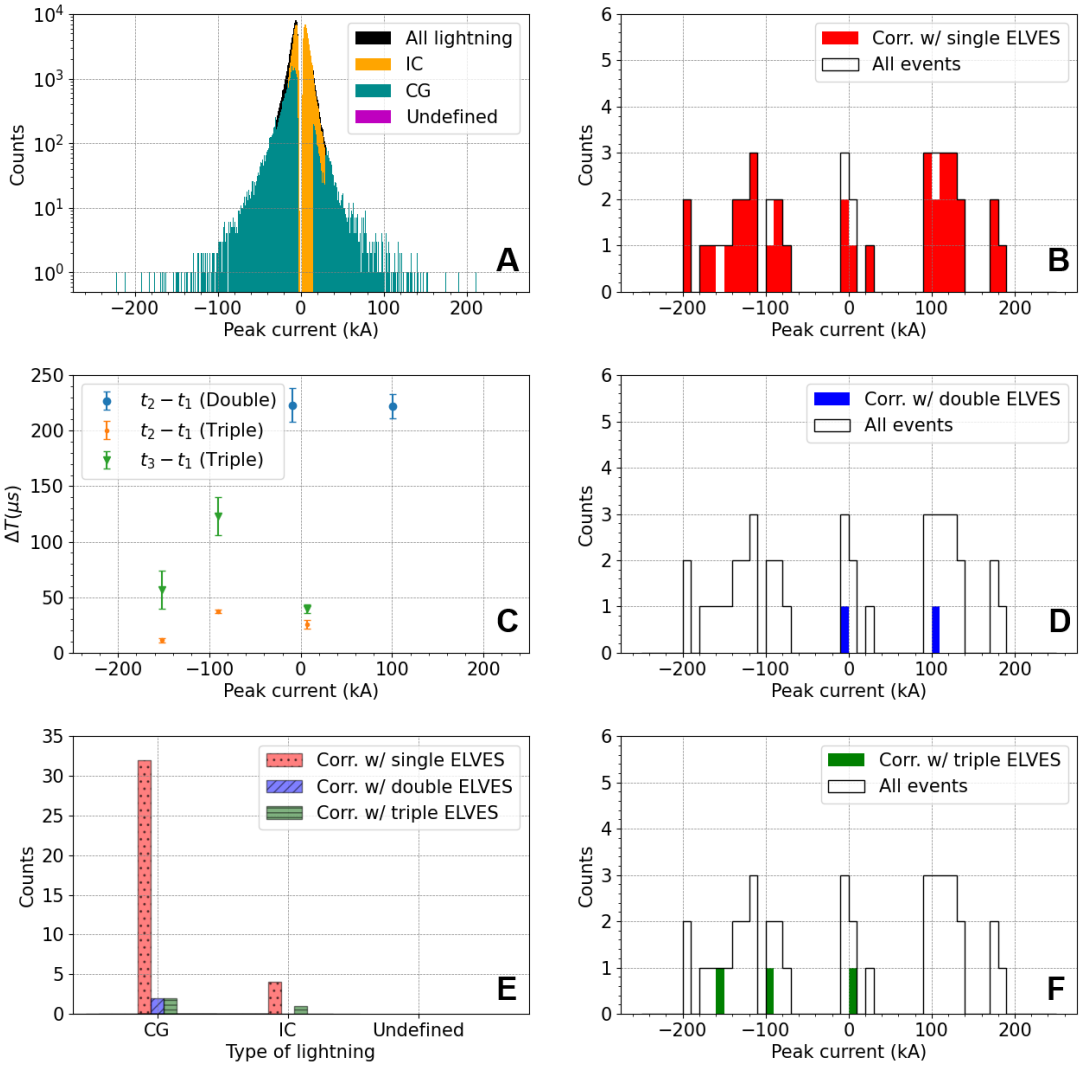

Figure 6.5: Correlation between the characteristics of lightning from the storm on November 10, 2018, and the elves detected in the Auger Fluorescence Detector: A) Lightning peak current distribution of this storm, identifying the types of lightning as IC, CG, and undefined. The distribution of the peak current and polarity of lightning correlated with single (B), double (D), and triple elves (F). C) Relationship between the time gap of the multi-elves and the peak current of the lightning that produced them. E) Comparison between lightning type and type of elves: most of the elves from this storm are correlated with CG lightning.

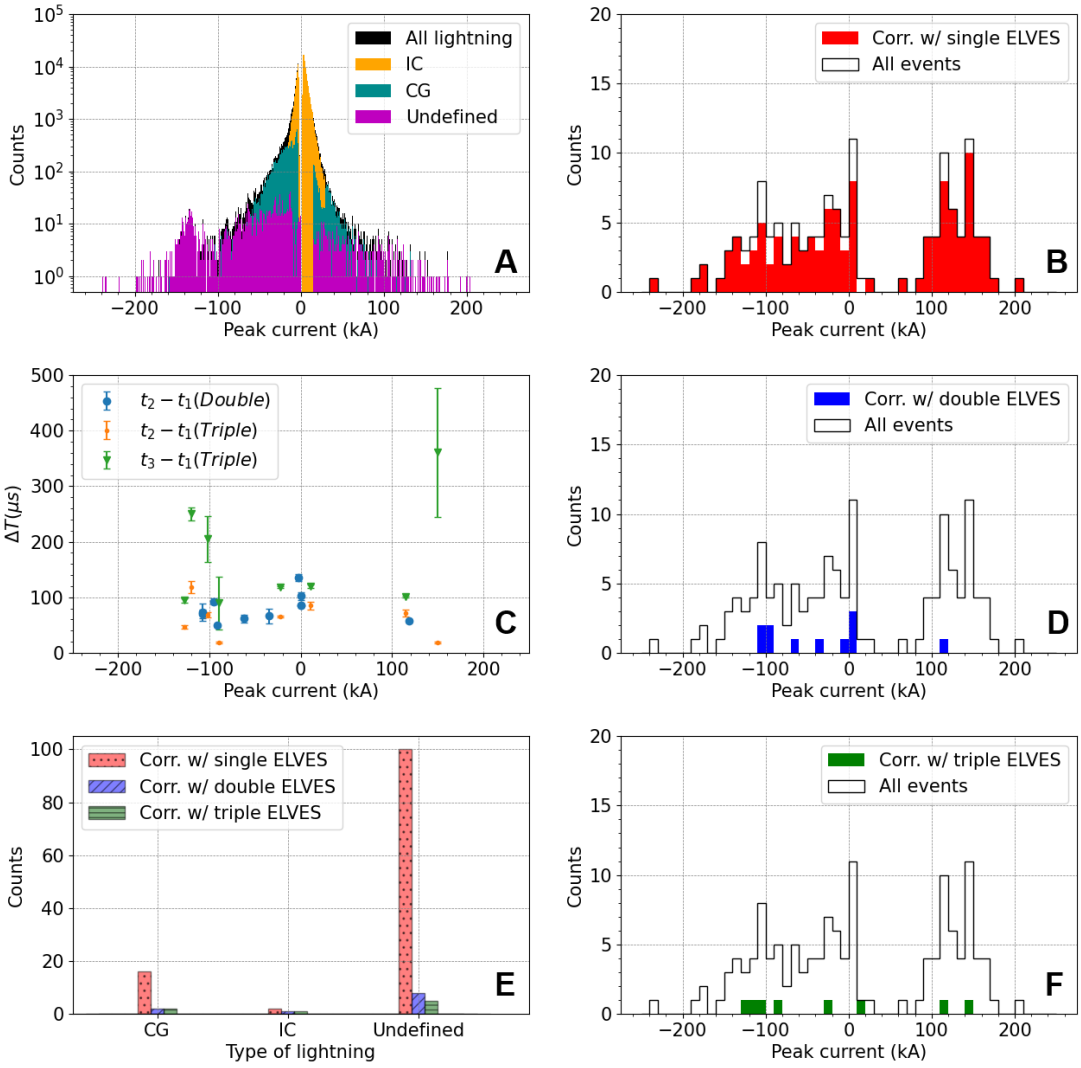

Figure 6.6: Correlation between the characteristics of lightning from the storm on December 20, 2019, and the elves detected in the Auger Fluorescence Detector: A) Lightning peak current distribution of this storm, identifying the types of lightning as IC, CG, and undefined. The distribution of the peak current and polarity of lightning correlated with single (B), double (D), and triple elves (F). C) Relationship between the time gap of the multi-elves and the peak current of the lightning that produced them. E) Comparison between lightning type and type of elves: most of the elves from this storm are correlated with WWLLN lightning, so its type cannot be identified.

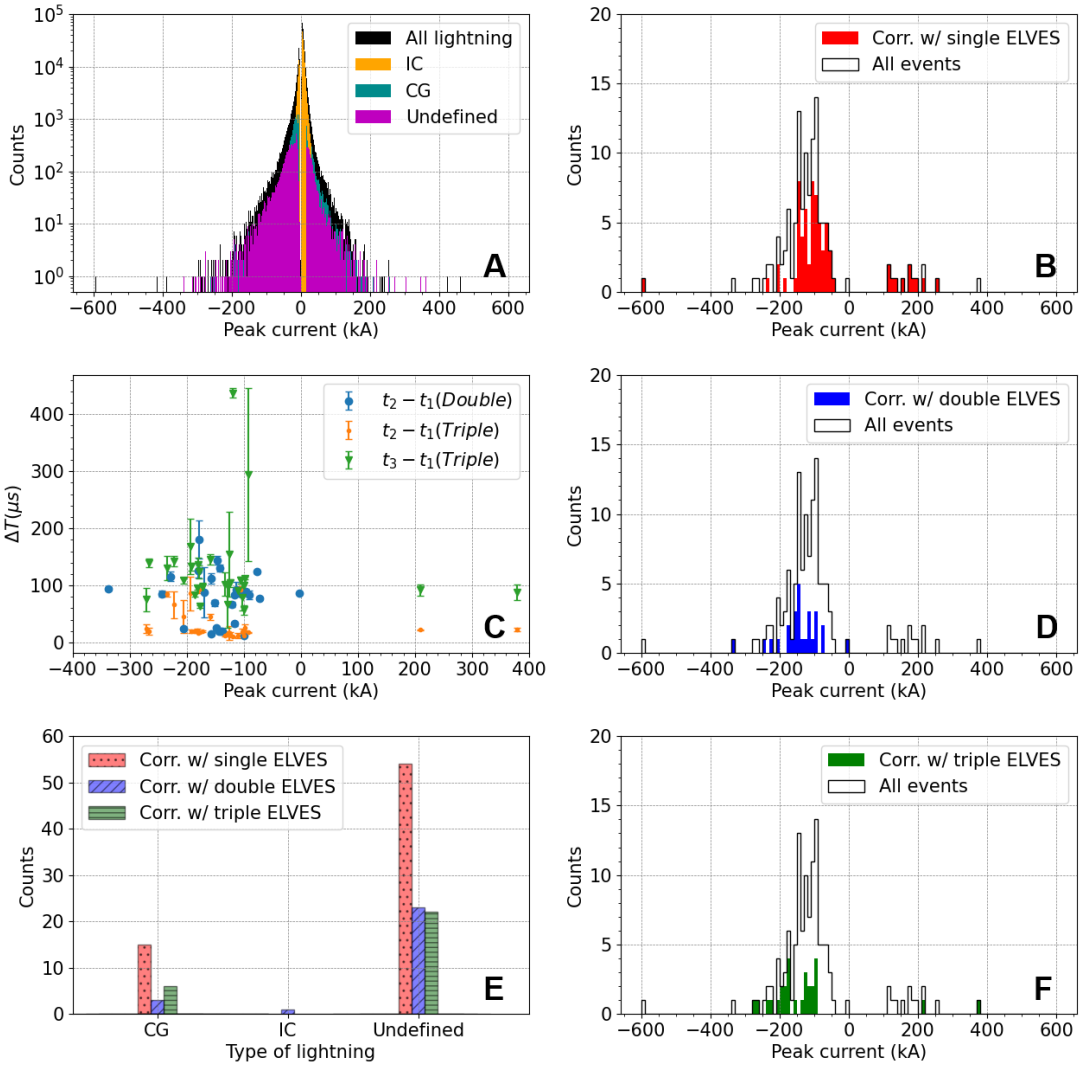

Figure 6.7: Correlation between the characteristics of lightning from the storm on April 27-28, 2020, and the elves detected in the Auger Fluorescence Detector: A) Lightning peak current distribution of this storm, identifying the types of lightning as IC, CG, and undefined. The distribution of the peak current and polarity of lightning correlated with single (B), double (D), and triple elves (F). C) Relationship between the time gap of the multi-elves and the peak current of the lightning that produced them. E) Comparison between lightning type and type of elves: most of the elves from this storm are correlated with WWLLN lightning, so its type cannot be identified.

polarity in lightning-producing elves is observed: 73 negative and 64 positive events in December and 111 negative and 13 positive events in April.

We observe a continuous distribution of peak current values for negative polarities, with a minimum absolute value of 0.9 kA and a maximum of 591 kA, whereas, in the positive polarity of the distribution, a gap is noticeable around 0 and 100 kA in both the April and December storms. Although present in the November storm as well, this gap is less noticeable due to the limited number of correlated events. Elves have predominantly been associated with negative polarity lightning, and in these storms, we not only observe this trend but also note that peak values over 70 kA are requisite for the production of elves in cases of positive polarity currents (as shown in the December storm).

Finally, panel C of these figures presents the analysis of the correlation between the time gap of the peaks of double and triple elves (ΔT) with the peak current and polarity of the lightning. There is no discernible relationship between these variables in any storm.

Thus, based on these observations, we cannot assert a preference for the type of lightning that generates multi-elves. Additionally, there is no evident association between the polarity of lightning-producing multi-elves, unlike those generating single elves; however, the majority of events typically exhibit negative polarity, and the few with positive polarity tend to have peak values exceeding 100 kA. Furthermore, we do not observe a correlation between the time gap of multi-elves and the lightning's peak current that triggers them. As demonstrated earlier, the origin of elves and multi-elves primarily depends on the rise and fall times of the current density pulse rather than the type, peak current, and polarity of the lightning that produces them.

6.2 Multi-elves and cloud top height

The Geostationary Operational Environmental Satellite (GOES-16 or GOES-East) is part of a new generation of meteorological satellites operated by the United States National Oceanic and Atmospheric Administration (NOAA) (Schmit et al., 2017). It was designed for monitoring weather events such as hurricanes, storms, and tornadoes to enhance the forecasting capabilities for these climatic events. Launched on November 19, 2016, GOES-16 is expected to continue its monitoring mission until the mid-2030s. The satellite has instruments, including the Advanced Baseline Imager (ABI), which provides high-resolution images of the Earth and the atmosphere and the Geostationary Lightning Mapper (GLM) for lightning monitoring.

The ABI functions as a 16-band radiometer, capturing spectral bands across the visible, near-infrared, and infrared regions of the electromagnetic spectrum (Schmit et al., 2017). Band 13 of the ABI, sensitive in the thermal infrared range (wavelength 10.3 μm), allows for measuring surface temperature on Earth and cloud tops. Utilising the surface temperature of clouds, the estimated altitude of the cloud top can be calculated, as lower temperatures often correspond to higher cloud altitudes. The conversion of the temperature recorded by the ABI to cloud top height involves using standard atmospheric profiles, taking into account the atmospheric conditions of the specific region.

In this section, we discuss temperature and cloud top height in the context of the three storms selected for this study, along with the spatial distribution of elves detected by the Auger Fluorescence Detector.

Figures 6.8, 6.9 and 6.10, present the evolution of each selected storm in this study. The middle panel shows the cloud top height (CTH) of the storm. For completeness, we show the storm brightness temperature in the left panel and the cloud top temperature in the right panel. For each storm, we chose three 10-minute time windows with more occurrences of elves (the time label in the right panel of each figure). The locations of

the four FD sites are marked as stars with the corresponding colour: Los Leones (blue), Los Morados (magenta), Loma Amarilla (yellow), and Coihueco (green).

In the middle panel of each of these figures, we observe that single elves (red circles), double elves (blue triangles), and triple elves (green squares) tend to be located in areas where the cloud's top height is very high, implying that the elves are associated with the largest vertically region of the storm, and, therefore, with its most active part.

For instance, in the figure corresponding to the December storm (see figure 6.9), the elves are situated in regions where the CTH is between 12 and 16 km, while in the April storm, elves are found around areas with CTH between 10 and 15 km (see Figure 6.10). These heights are close to the expected tropopause height at this latitude, therefore pointing to very intense thunderstorm systems with possible stratospheric intrusion.

Unfortunately, we lack images of cloud top height and temperature for the November storm, and the time windows are 15 minutes long. However, figure 6.8 indicates the presence of elves in areas with extremely low brightness temperatures, which typically range from -75 and -60 °C. These low temperatures are usually associated with cloud top heights of around 15 km or higher if we compare them to the December data.

These observations point to elves being produced by some of the highest and most active regions of the storms, in analogy with previous reports in other regions of the globe for elves and other TLEs (van der Velde and Montanyà, 2016). Interestingly, elves were observed not necessarily in all of the highest regions but often clustered in some compact active areas at the edge of the storm (see e.g., November and the April storms). Such confined and very active regions of the storms are also typically associated with other TLEs and in particular to TGF production.

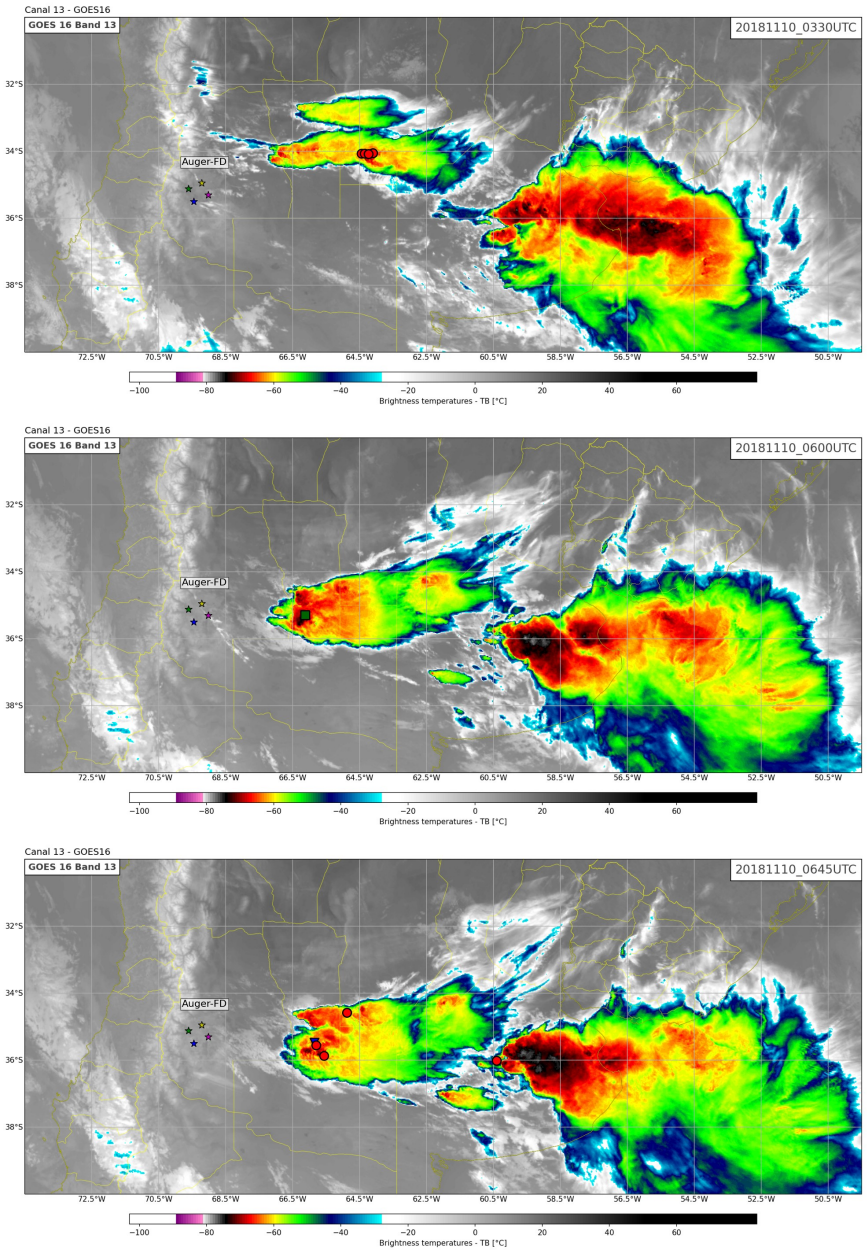

Figure 6.8: Storm brightness temperature for the storm on November 10, 2018. The top plot corresponds to the time window between 3:30 and 3:45 UTC, the centre panel between 5:45 and 6:00 UTC, and the bottom panel corresponds to 6:45-7:00 UTC interval. During the evolution of the storm, we observe that the distribution of single elves (red circles), double elves (blue triangles), and triple elves (green squares) tends to be in areas of lowest brightness temperatures, between -75 and -60 °C. A full video is available in november_clouds_elves.gif.

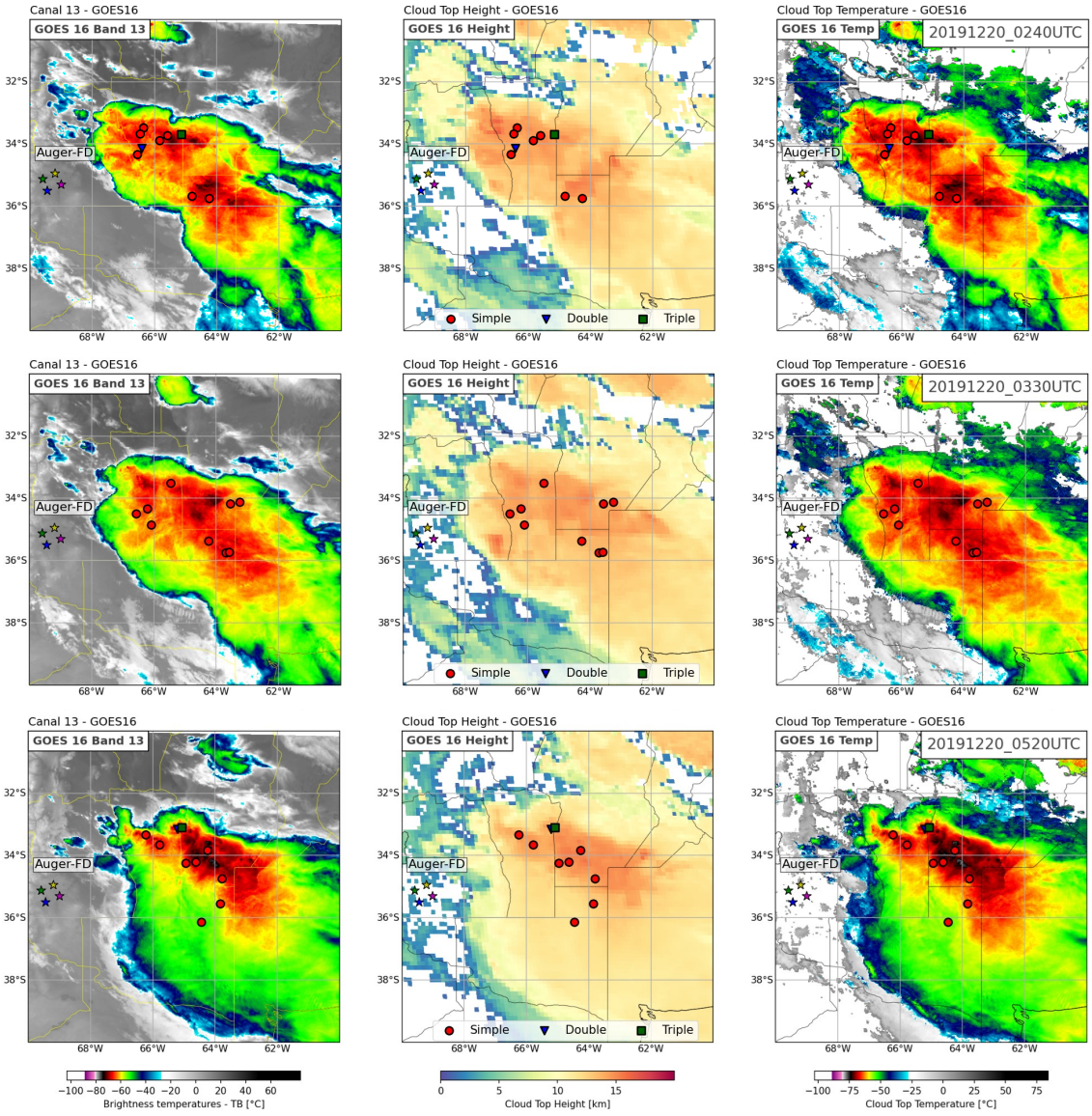

Figure 6.9: Storm brightness temperature (left), cloud top height (middle), and cloud top temperature (right) for the storm on December 20, 2019. The top graphs correspond to the time window between 2:40 and 2:50 UTC, the centre panel between 3:30 and 3:40 UTC, while the bottom panel corresponds 5:20-5:30 UTC interval. During the evolution of the storm, We observe that the distribution of single elves (red circles), double elves (blue triangles), and triple elves (green squares) tends to be in areas of high cloud top height values, between 12 and 16 km. A full video is available in december_clouds_elves.gif.

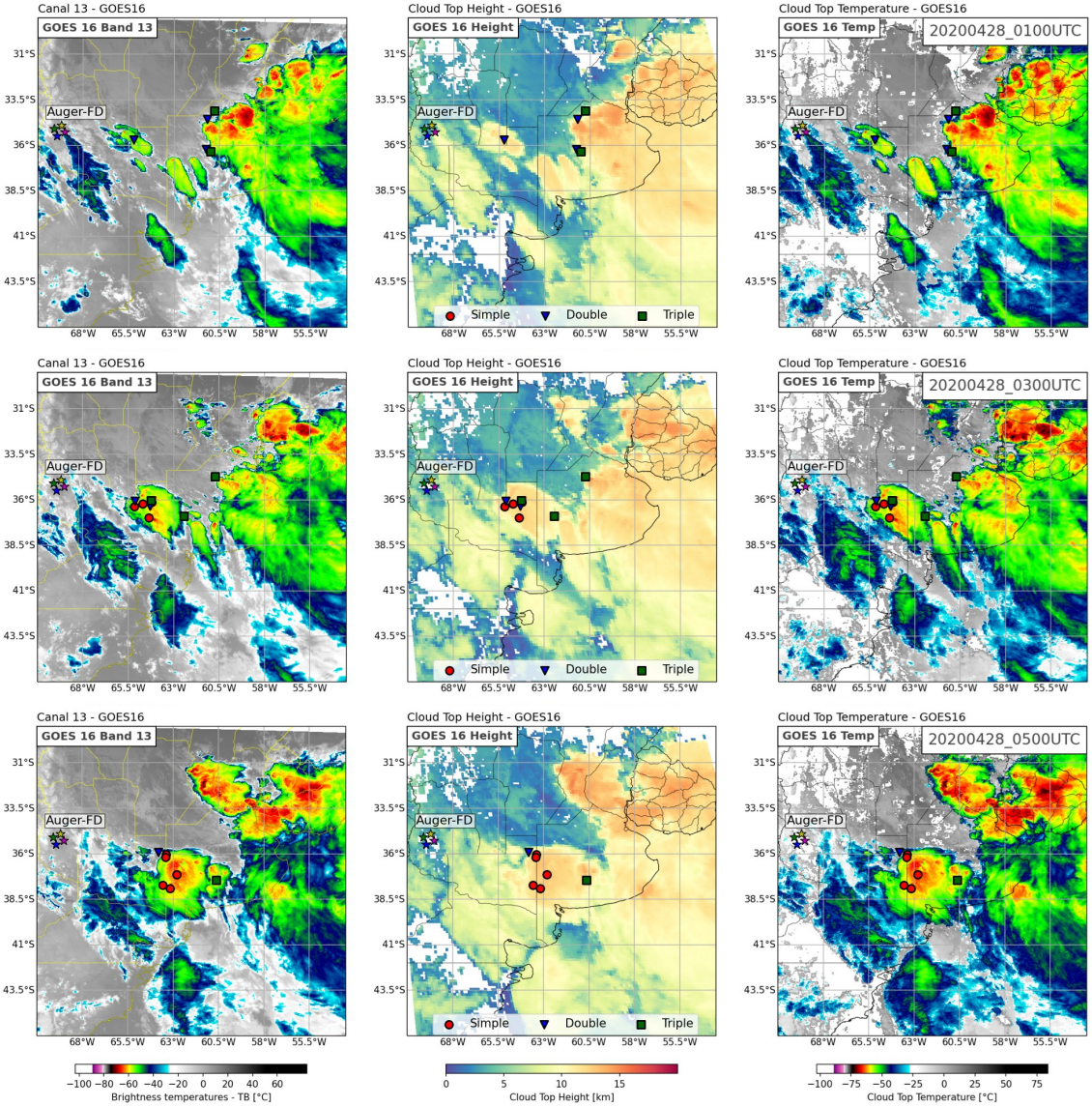

Figure 6.10: Storm brightness temperature (left), cloud top height (middle), and cloud top temperature (right) for the storm on April 27-28, 2020. The top graphs correspond to the time window between 1:00 and 1:10 UTC, the centre panel between 3:00 and 3:10 UTC, while the bottom panel corresponds to the 5:00-5:10 UTC interval. During the evolution of the storm, we observe that the distribution of single elves (red circles), double elves (blue triangles), and triple elves (green squares) tends to be in areas of high cloud top height values, between 10 and 15 km. A full video is available in april_clouds_elves.gif.

Chapter 7

Conclusions

We present an unprecedented number of 63 double and 30 triple elves across four different storms of the Cordoba region, Argentina. These events exhibited multiple rings separated in time ranges from 7 to 280 μs, significantly higher compared to the PIPER events, which have so far reported the most doubles with 40 events in four storms in New Mexico, USA. The time delay of these events ranges from 60 and 180 μs (Newsome and Inan, 2010).

Seventy percent of the multi-elves events exhibit a quasi-constant time gap between the rings, challenging the expectations of the electromagnetic pulse bounce model, which predicts that the time gap should decrease with distance from the lightning. Moreover, we demonstrated that this behaviour is independent of the fluorescence detector site where the elves are detected. The remaining 30% of the events show mixed behaviour, where the trend is generally towards a nearly constant ΔT. Only 1 out of the 93 reported multi-elves events from four storms appears to follow the bounce model.

The multi-elves with a time gap exceeding 50 μs exhibit a linear relationship with the base time of the second component of the lightning waveform, indicating that the origin of the multiple rings depends on the pulse shape of the lightning current density. Events with a time gap below 50 μs do not follow a clear trend, which may be attributed to

the use of the base time rather than the rise and fall times as indicated by the model, due to the saturation of the waveform shapes from Earth Networks. An alternative mechanism may also be involved.

We found halos occurring hundreds of microseconds after the detection of single and double elves. As expected, these halos are brighter than elves.

We observed that lightning correlated with our elves occur in locations where the cloud top is very high, showing that elves are generated in some of the most intense and active regions within storms.

The seasonal distribution of elves detected in Auger is consistent with the monthly lightning activity in the Subtropical region of South America, where the detected event count decreases between May and September and increases between November and April.

Despite having a high correlation percentage between our elves and ENTLN events, this network did not provide information about the type and height of lightning for all events, so we could not establish a relationship between the time of the rings and these lightning characteristics. There is also no clear relationship between the peak current and the time gap of multi-elves reported in these three storms. However, the majority of our observed elves were associated with negative polarity lightning, ranging from -0.9 to -591 kA.

Future work and open questions

In this work we show two main results that contribute to advancing the understanding of the mechanisms and sources responsible for multi-peaked elves occurring in the upper atmosphere. The multiple rings of elves are associated with the lightning pulse waveform but not with the bouncing of the components of the electromagnetic pulse of an IC

lightning strike. In future work, we will require enhancements in lightning data to determine if any other characteristics, such as height, peak current and type of the lightning, influence the generation of elves or multi-elves.

From these results we observed two groups of time gap between the rings ($\Delta T < 50$ μs and $\Delta T \geq 50$ μs) leading to the following open questions:

- Are these two groups due different mechanisms?
- How can we explain the events with $\Delta T < 50$ μs? Is it due to the de-excitation time of the molecules in the fluorescence process?
- Do the multiple peaks originate from multiple sources of EMP? Or from the same source but at different stages of the lightning discharge development?
- Does the radiated EMP of the return stroke exhibits multiple peaks as proposed by Newsome and Inan (2010)? If we find multiple peaks in the waveforms that explain the events with $\Delta T < 50$ μs, we will have a general model to explain the origin of multi-elves.

We report an in-depth study of four storms using the developed code, which is more efficient at identifying multi-elves in the data. Analyzing these events is highly complex, as not all traces of the event exhibit the same quality. This analysis is currently being applied to the whole dataset over 2014-2024 with the new code, which we expect to increase the reported ratio of multi-elves.

We installed a new camera in Coihueco to detect TLEs simultaneously with the Auger FD. Their joint analysis will allow to study into detail the traces of further TLEs such as halos, sprites and jets, and their simultaneous occurrence with elves at unprecedented spatial-temporal resolution.

Bibliography

Aab, A., Abreu, P., Aglietta, M., Albuquerque, I., Albury, J., Allekotte, I., et al. (2020). A three year sample of almost 1600 elves recorded above south america by the pierre auger cosmic-ray observatory. *Earth and Space Science*, page e2019EA000582.

Abdul Halim, A., Abreu, P., Aglietta, M., Allekotte, I., Almeida Cheminant, K., Almela, A., Aloisio, R., Alvarez-Muniz, J., Ammerman Yebra, J., Anastasi, G. A., et al. (2023). Investigating multiple elves and halos above strong lightning with the fluorescence detectors of the pierre auger observatory. In *Proceedings of 38th International Cosmic Ray Conference—PoS (ICRC2023), Nagoya, 26th July-3rd August, 2023*, page 372.

Abraham, J., Abreu, P., Aglietta, M., Aguirre, C., Ahn, E., Allard, D., Allekotte, I., Allen, J., Allison, P., Alvarez-Muñiz, J., et al. (2010). The fluorescence detector of the pierre auger observatory. *Nuclear Instruments and Methods in Physics Research Section A: Accelerators, Spectrometers, Detectors and Associated Equipment*, 620(2-3):227–251.

Albrecht, R. I., Goodman, S. J., Buechler, D. E., Blakeslee, R. J., and Christian, H. J. (2016). Where are the lightning hotspots on earth? *Bulletin of the American Meteorological Society*, 97(11):2051–2068.

Arnone, E., Bór, J., Chanrion, O., Barta, V., Dietrich, S., Enell, C.-F., Farges, T., Füllekrug, M., Kero, A., Labanti, R., et al. (2020). Climatology of transient luminous

events and lightning observed above europe and the mediterranean sea. *Surveys in Geophysics*, 41:167–199.

Barrington-Leigh, C. P. and Inan, U. S. (1999). Elves triggered by positive and negative lightning discharges. *Geophysical Research Letters*, 26(6):683–686.

Barrington-Leigh, C. P., Inan, U. S., Stanley, M., and Cummer, S. A. (1999). Sprites triggered by negative lightning discharges. *Geophysical Research Letters*, 26(24):3605–3608.

Bjørge-Engeland, I., Østgaard, N., Mezentsev, A., Skeie, C. A., Sarria, D., Lapierre, J., Lindanger, A., Neubert, T., Marisaldi, M., Lehtinen, N., et al. (2022). Terrestrial gamma-ray flashes with accompanying elves detected by asim. *Journal of Geophysical Research: Atmospheres*, 127(11):e2021JD036368.

Blakeslee, R. J., Christian, H. J., Stewart, M., Mach, D., Bateman, M., Walker, T. D., Buechler, D., Koshak, W., OBrien, S., Wilson, T., et al. (2014). Lightning imaging sensor (lis) for the international space station (iss): mission description and science goals. In *International conference on atmospheric electricity (ICAE 2014)*, number M14-3658.

Boeck, W., Vaughan Jr, O., Blakeslee, R., Vonnegut, B., and Brook, M. (1992). Lightning induced brightening in the airglow layer. *Geophysical research letters*, 19(2):99–102.

Chanrion, O., Neubert, T., Lundgaard Rasmussen, I., Stoltze, C., Tcherniak, D., Jessen, N. C., Polny, J., Brauer, P., Balling, J. E., Savstrup Kristensen, S., et al. (2019). The modular multispectral imaging array (mmia) of the asim payload on the international space station. *Space Science Reviews*, 215:1–25.

Chen, A. B., Kuo, C.-L., Lee, Y.-J., Su, H.-T., Hsu, R.-R., Chern, J.-L., Frey, H. U., Mende, S. B., Takahashi, Y., Fukunishi, H., et al. (2008). Global distributions and occurrence rates of transient luminous events. *Journal of Geophysical Research: Space Physics*, 113(A8).

Christian, H. J. (1992). *Lightning imaging sensor (LIS) for the earth observing system*, volume 4350. NASA.

Christian, H. J., Blakeslee, R. J., Boccippio, D. J., Boeck, W. L., Buechler, D. E., Driscoll, K. T., Goodman, S. J., Hall, J. M., Koshak, W. J., Mach, D. M., et al. (2003). Global frequency and distribution of lightning as observed from space by the optical transient detector. *Journal of Geophysical Research: Atmospheres*, 108(D1):ACL–4.

Dwyer, J. R. (2008). Source mechanisms of terrestrial gamma-ray flashes. *Journal of Geophysical Research: Atmospheres*, 113(D10).

Dwyer, J. R. (2012). The relativistic feedback discharge model of terrestrial gamma ray flashes. *Journal of Geophysical Research: Space Physics*, 117(A2).

Dwyer, J. R., Smith, D. M., and Cummer, S. A. (2012). High-energy atmospheric physics: Terrestrial gamma-ray flashes and related phenomena. *Space Science Reviews*, 173(1-4):133–196.

Dwyer, J. R. and Uman, M. A. (2014). The physics of lightning. *Physics Reports*, 534(4):147 – 241. The Physics of Lightning.

Fishman, G. J., Bhat, P., Mallozzi, R., Horack, J., Koshut, T., Kouveliotou, C., Pendleton, G., Meegan, C., Wilson, R., Paciesas, W., et al. (1994). Discovery of intense gamma-ray flashes of atmospheric origin. *Science*, 264(5163):1313–1316.

Franz, R., Nemzek, R., and Winckler, J. (1990). Television image of a large upward electrical discharge above a thunderstorm system. *Science*, 249(4964):48–51.

Fukunishi, H., Takahashi, Y., Kubota, M., Sakanoi, K., Inan, U., and Lyons, W. (1996). Elves: Lightning-induced transient luminous events in the lower ionosphere. *Geophysical Research Letters*, 23(16):2157–2160.

Füllekrug, M., Mareev, E. A., and Rycroft, M. J. (2006). *Sprites, elves and intense lightning discharges*, volume 225. Springer Science & Business Media.

Gaskill, M. (2018). Once upon a time in a thunderstorm. https://phys.org/news/2018-04-thunderstorm.html.

Giles, R. S., Greathouse, T. K., Bonfond, B., Gladstone, G. R., Kammer, J. A., Hue, V., Grodent, D. C., Gérard, J.-C., Versteeg, M. H., Wong, M. H., et al. (2020). Possible transient luminous events observed in jupiter's upper atmosphere. *Journal of Geophysical Research: Planets*, 125(11):e2020JE006659.

Harrison, R. G. (2013). The carnegie curve. *Surveys in Geophysics*, 34(2):209–232.

Holzworth, R., McCarthy, M., Brundell, J., Jacobson, A., and Rodger, C. (2019). Global distribution of superbolts. *Journal of Geophysical Research: Atmospheres*, 124(17-18):9996–10005.

Inan, U., Barrington-Leigh, C., Hansen, S., Glukhov, V., Bell, T., and Rairden, R. (1997). Rapid lateral expansion of optical luminosity in lightning-induced ionospheric flashes referred to as 'elves'. *Geophysical Research Letters*, 24(5):583–586.

Inan, U. S. (1990). Vlf heating of the lower ionosphere. *Geophysical Research Letters*, 17(6):729–732.

Klimov, P., Khrenov, B., Kaznacheeva, M., Garipov, G., Panasyuk, M., Petrov, V., Sharakin, S., Shirokov, A., Yashin, I., Zotov, M., et al. (2019). Remote sensing of the atmosphere by the ultraviolet detector tus onboard the lomonosov satellite. *Remote Sensing*, 11(20):2449.

Kumar, S., Siingh, D., Singh, R. P., Singh, A. K., and Kamra, A. K. (2018). Lightning discharges, cosmic rays and climate. *Surveys in Geophysics*, 39(5):861–899.

Lang, T. J., Ávila, E. E., Blakeslee, R. J., Burchfield, J., Wingo, M., Bitzer, P. M., Carey, L. D., Deierling, W., Goodman, S. J., Medina, B. L., et al. (2020). The relampago lightning mapping array: Overview and initial comparison with the geostationary lightning mapper. *Journal of Atmospheric and Oceanic Technology*, 37(8):1457–1475.

Lapierre, J., Hoekzema, M., Stock, M., Merrill, C., and Thangaraj, S. C. (2019). Earth networks lightning network and dangerous thunderstorm alerts. In *2019 11th Asia-Pacific International Conference on Lightning (APL)*, pages 1–5. IEEE.

Le Vine, D. M. (1980). Sources of the strongest rf radiation from lightning. *Journal of Geophysical Research: Oceans*, 85(C7):4091–4095.

Liu, N. and Dwyer, J. R. (2013). Modeling terrestrial gamma ray flashes produced by relativistic feedback discharges. *Journal of Geophysical Research: Space Physics*, 118(5):2359–2376.

Liu, N., Dwyer, J. R., and Cummer, S. A. (2017). Elves accompanying terrestrial gamma ray flashes. *Journal of Geophysical Research: Space Physics*, 122(10):10–563.

Liu, N., Dwyer, J. R., Tilles, J. N., Stanley, M. A., Krehbiel, P. R., Rison, W., Brown, R. G., and Wilson, J. G. (2019). Understanding the radio spectrum of thunderstorm narrow bipolar events. *Journal of Geophysical Research: Atmospheres*, 124(17-18):10134–10153.

Lyons, W. A. (1994a). Characteristics of luminous structures in the stratosphere above thunderstorms as imaged by low-light video. *Geophysical Research Letters*, 21(10):875–878.

Lyons, W. A. (1994b). Low-light video observations of frequent luminous structures in the stratosphere above thunderstorms. *Monthly Weather Review*, 122(8):1940–1946.

Lyu, F., Cummer, S. A., and McTague, L. (2015). Insights into high peak current in-cloud lightning events during thunderstorms. *Geophysical Research Letters*, 42(16):6836–6843.

MacKenzie, T. (1886). Meteorological phenomena. *Nature*, 33(846):245–245.

Marisaldi, M., Fuschino, F., Labanti, C., Galli, M., Longo, F., Del Monte, E., Barbiellini, G., Tavani, M., Giuliani, A., Moretti, E., et al. (2010). Detection of terrestrial

gamma ray flashes up to 40 mev by the agile satellite. *Journal of Geophysical Research: Space Physics*, 115(A3).

Marshall, R., Da Silva, C., and Pasko, V. P. (2015). Elve doublets and compact intracloud discharges. *Geophysical Research Letters*, 42(14):6112–6119.

Marshall, R., Newsome, R., and Inan, U. (2008). Fast photometric imaging using orthogonal linear arrays. *IEEE transactions on geoscience and remote sensing*, 46(11):3885–3893.

Marshall, R. A. (2012). An improved model of the lightning electromagnetic field interaction with the d-region ionosphere. *Journal of Geophysical Research: Space Physics*, 117(A3).

Merenda, K.-D. (2020). *Studies of ELVES and their connection to lightning with the Pierre Auger Observatory*. PhD thesis, Colorado School of Mines.

Mussa, R. (2019). Analysis of elves at the pierre auger observatory. In *EPJ Web Conf.*, volume 197, page 03004.

Mussa, R., Ciaccio, G., Collaboration, P. A., et al. (2012). Observation of elves at the pierre auger observatory. *The European Physical Journal Plus*, 127(8):94.

Nesbitt, S. W., Salio, P. V., Ávila, E., Bitzer, P., Carey, L., Chandrasekar, V., Deierling, W., Dominguez, F., Dillon, M. E., Garcia, C. M., et al. (2021). A storm safari in subtropical south america: Proyecto relampago. *Bulletin of the American Meteorological Society*, 102(8):E1621–E1644.

Neubert, T. (2003). On sprites and their exotic kin. *Science*, 300(5620):747–749.

Neubert, T., Allin, T. H., Blanc, E., Farges, T., Haldoupis, C., Mika, A., Soula, S., Knutsson, L., van Der Velde, O., Marshall, R. A., et al. (2005). Co-ordinated observations of transient luminous events during the eurosprite2003 campaign. *Journal of Atmospheric and Solar-Terrestrial Physics*, 67(8-9):807–820.

Neubert, T., Østgaard, N., Reglero, V., Blanc, E., Chanrion, O., Oxborrow, C. A., Orr, A., Tacconi, M., Hartnack, O., and Bhanderi, D. D. (2019). The asim mission on the international space station. *Space Science Reviews*, 215(2):26.

Newsome, R. and Inan, U. (2010). Free-running ground-based photometric array imaging of transient luminous events. *Journal of Geophysical Research: Space Physics*, 115(A7).

Orville, R. E. (2008). Development of the national lightning detection network. *Bulletin of the American Meteorological Society*, 89(2):180–190.

Palacios, A., Todd, C., Barbagallo, E., Birtwhistle, A., Van Den Braembussche, P., Girard, A.-F., Langlois, S., Pirson, L., Marracci, R., Ferraguto, M., et al. (2023). Meteosat third generation: Data handling architecture of a state-of-the-art geo meteorological satellite. In *2023 European Data Handling & Data Processing Conference (EDHPC)*, pages 1–6. IEEE.

Pasko, V. P., Yair, Y., and Kuo, C.-L. (2012). Lightning related transient luminous events at high altitude in the earth's atmosphere: Phenomenology, mechanisms and effects. *Space science reviews*, 168:475–516.

Peterson, M. J., Lang, T. J., Logan, T., Wee Kiong, C., Gijben, M., Holle, R., Kolmasova, I., Marisaldi, M., Montanya, J., Pawar, S. D., et al. (2022). New wmo certified megaflash lightning extremes for flash distance and duration recorded from space. *Bulletin of the American Meteorological Society*, 103(4):257–261.

Rakov, V. A. and Uman, M. A. (2003). *Lightning: physics and effects*. Cambridge university press.

Rasmussen, K. L., Zuluaga, M. D., and Houze Jr., R. A. (2014). Severe convection and lightning in subtropical south america. *Geophysical Research Letters*, 41(20):7359–7366.

Rison, W., Krehbiel, P. R., Stock, M. G., Edens, H. E., Shao, X.-M., Thomas, R. J., Stanley, M. A., and Zhang, Y. (2016). Observations of narrow bipolar events reveal how lightning is initiated in thunderstorms. *Nature communications*, 7(1):1–12.

Roberts, O., Fitzpatrick, G., Stanbro, M., McBreen, S., Briggs, M., Holzworth, R., Grove, J., Chekhtman, A., Cramer, E., and Mailyan, B. (2018). The first fermi-gbm terrestrial gamma ray flash catalog. *Journal of Geophysical Research: Space Physics*, 123(5):4381–4401.

Rodger, C., Brundell, J., Dowden, R., and Thomson, N. (2004). Location accuracy of long distance vlf lightning locationnetwork. *European Geosciences Union*, 22(3):747–758.

Rodger, C. J. (1999). Red sprites, upward lightning, and vlf perturbations. *Reviews of Geophysics*, 37(3):317–336.

Romoli, G. (2023). Study of multiple ring elves with the mini-euso telescope on-board the international space station. *arXiv preprint arXiv:2310.02617*.

Rudlosky, S. D., Goodman, S. J., Virts, K. S., and Bruning, E. C. (2019). Initial geostationary lightning mapper observations. *Geophysical Research Letters*, 46(2):1097–1104.

Sato, M. and Fukunishi, H. (2003). Global sprite occurrence locations and rates derived from triangulation of transient schumann resonance events. *Geophysical Research Letters*, 30(16).

Schmit, T. J., Griffith, P., Gunshor, M. M., Daniels, J. M., Goodman, S. J., and Lebair, W. J. (2017). A closer look at the abi on the goes-r series. *Bulletin of the American Meteorological Society*, 98(4):681–698.

Schulz, W., Diendorfer, G., Pedeboy, S., and Poelman, D. R. (2016). The european lightning location system euclid–part 1: Performance analysis and validation. *Nat. Hazards Earth Syst. Sci*, 16(2):595–605.

Sentman, D. D. and Wescott, E. M. (1993). Observations of upper atmospheric optical flashes recorded from an aircraft. *Geophysical Research Letters*, 20(24):2857–2860.

Sentman, D. D., Wescott, E. M., Osborne, D., Hampton, D., and Heavner, M. (1995). Preliminary results from the sprites94 aircraft campaign: 1. red sprites. *Geophysical Research Letters*, 22(10):1205–1208.

Smith, D., Shao, X., Holden, D., Rhodes, C., Brook, M., Krehbiel, P., Stanley, M., Rison, W., and Thomas, R. (1999). A distinct class of isolated intracloud lightning discharges and their associated radio emissions. *Journal of Geophysical Research: Atmospheres*, 104(D4):4189–4212.

Smith, D. M., Lopez, L. I., Lin, R. P., and Barrington-Leigh, C. P. (2005). Terrestrial gamma-ray flashes observed up to 20 mev. *Science*, 307(5712):1085–1088.

Soler, S., Gordillo-Vázquez, F. J., Pérez-Invernón, F. J., Luque, A., Li, D., Neubert, T., Chanrion, O., Reglero, V., Navarro-González, J., and Østgaard, N. (2021). Global frequency and geographical distribution of nighttime streamer corona discharges (blues) in thunderclouds. *Geophysical Research Letters*, 48(18):e2021GL094657.

Taranenko, Y., Inan, U., and Bell, T. (1993). Interaction with the lower ionosphere of electromagnetic pulses from lightning: heating, attachment, and ionization. *Geophysical Research Letters*, 20(15):1539–1542.

Thomas, R. J., Krehbiel, P. R., Rison, W., Hunyady, S. J., Winn, W. P., Hamlin, T., and Harlin, J. (2004). Accuracy of the lightning mapping array. *Journal of Geophysical Research: Atmospheres*, 109(D14).

Tilles, J. N., Liu, N., Stanley, M. A., Krehbiel, P. R., Rison, W., Stock, M. G., Dwyer, J. R., Brown, R., and Wilson, J. (2019). Fast negative breakdown in thunderstorms. *Nature communications*, 10(1):1–12.

van der Velde, O. A. and Montanyà, J. (2016). Statistics and variability of the altitude of elves. *Geophysical Research Letters*, 43(10):5467–5474.

Vásquez Ramírez, A., Abreu, P., Aglietta, M., Albury, J., Allekotte, I., Almela, A., Alvarez-Muniz, J., Alves Batista, R., Anastasi, G., Anchordoqui, L., et al. (2022). Study on multi-elves in the pierre auger observatory. In *37th International Cosmic Ray Conference. 12-23 July 2021. Berlin*, page 327.

Wilson, C. T. (1925). The acceleration of β-particles in strong electric fields such as those of thunderclouds. In *Mathematical Proceedings of the Cambridge Philosophical Society*, volume 22, pages 534–538. Cambridge University Press.

Witze, A. (2018). Inside argentina's mega-storms. *Nature*, 563(166).

Yue, J. and Lyons, W. A. (2015). Structured elves: Modulation by convectively generated gravity waves. *Geophysical Research Letters*, 42(4):1004–1011.

Zhu, Y., Stock, M., Lapierre, J., and DiGangi, E. (2022). Upgrades of the earth networks total lightning network in 2021. *Remote sensing*, 14(9):2209.

Appendix A

Coding and repositories

In this appendix, we show the different codes developed for analysing multi-elves data detected at the Pierre Auger Observatory and the Earth Networks codes for studying lightning data correlated with elves. Each section contains the respective repositories to reproduce the results reported in this thesis.

A.1 Reconstruction of the location of lightning strikes

The 24 FD telescopes are ideal for the observation of elves. Still, for the online selection of these events with reasonable efficiency, studies based on auxiliary sub-triggers have been carried out that allowed the third level of the triggering system to be modified (Mussa, 2019). The FD trigger is structured on three levels:

1. The first level trigger (FLT) operates at the pixel level, with an adjustable threshold that maintains the PMT activation rate at 100 Hz.

2. The second level trigger (SLT) searches for segments with at least five adjacent pixel paths that have passed the first stage.

3. The third level trigger (TLT) is designed to exclude nearby lightning strikes ef-

ficiently. Lightning events have a high multiplicity of triggered pixels randomly distributed temporarily throughout the camera within a time window of 100 μs.

The multiplicity-based TLT, installed at the end of 2007 as a replacement for a less efficient previous version, allowed the unexpected finding of elves in the first data from the Pierre Auger Observatory (Mussa et al., 2012). After a four-year study of FLT events, the TLT was modified and yielded 58 new elves candidates (Mussa, 2019).

The new TLT verifies the angular evolution of the light front around the first triggered pixel. For a set of pixels from the same column as this, the algorithm requires that at least two pixels before and two after the central one have a pulse. Besides, 80% of these pulses must show an increase in time. Compared to CRs, elves deposit a lot of light, so at least one pixel with a pulse amplitude greater than 50 ADC counts is required (Mussa, 2019).

To locate the source lightning that produced the elves detected in the FD, we employed the scheme shown in figure A.1 and followed the steps outlined in (Mussa, 2019):

1. We first fitted the ADC trace for each pixel to one or more asymmetric Gaussian.

2. We perform a set of polynomial fits on the pulse times T_i of each row and column to obtain a first rough estimate of the lightning longitude and latitude. The results are inputs to the second fit.

3. We perform a second fit to minimise the $\chi^2 = \sum_N^{i=1}(T_i - \Delta T_0 - \overline{OPS}_i/c)^2$, where ΔT_0 is the time lag between the emission of the EMP from the source and the observation of the first light at the FD camera. The first triggered pixel indicates the shortest light propagation path towards the lightning strike. $\overline{OPS}_i$ is the sum of the distances $\overline{SP}$ (from the source to the emission layer in the scheme) and $\overline{PO}$ (from the emission layer, assumed to have zero thickness and altitude $H_{EM} = 92$ km, to the FD). The lightning is assumed to be at sea level.

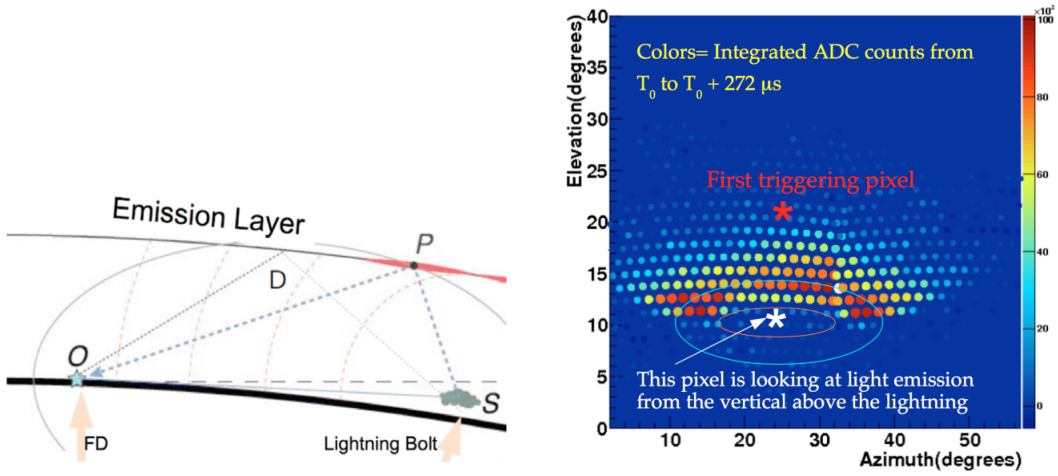

Figure A.1: Right: Scheme of the path taken by light from the lightning source (S) bouncing at a point P in the emission layer, to the observer in the FD (O). Left: Example of the light distribution from an event integrated in the first 272 μs after the trigger. The vertical above the lightning is represented by a white star. In contrast, the red star indicates the first triggered pixel, and the red ellipse indicates the region where the light emission dies down (Mussa, 2019).

4. The third fit is done, releasing the emission altitude H_{EM}.

5. The fourth fit also allows the lightning altitude H_B to vary above sea level.

From this algorithm, latitude, longitude, and the time of the lightning strike that produced the elve are obtained. Figure A.2 displays the map of lightning strike locations for elves produced between 2014 and 2016. This study by Aab et al. (2020) demonstrates a 72% correlation (1158 events) between WWLLN events and lightning strikes reconstructed using the Auger algorithm.

When projected to the ionosphere's base, the figure's large and small blue circles represent the pixel array's lower and upper boundaries. (a) Reconstructed lightning strike locations from Auger elves, with the number of contributing FD sites. Shaded regions indicate FoV overlap. (b) WWLLN events correlated with the ELVE dataset, presented by energy. (c) Density map of WWLLN events with overlaid elve-inducing lightning. (d) Coverage regions (one-site to four-site) overlaid on a density map of reconstructed

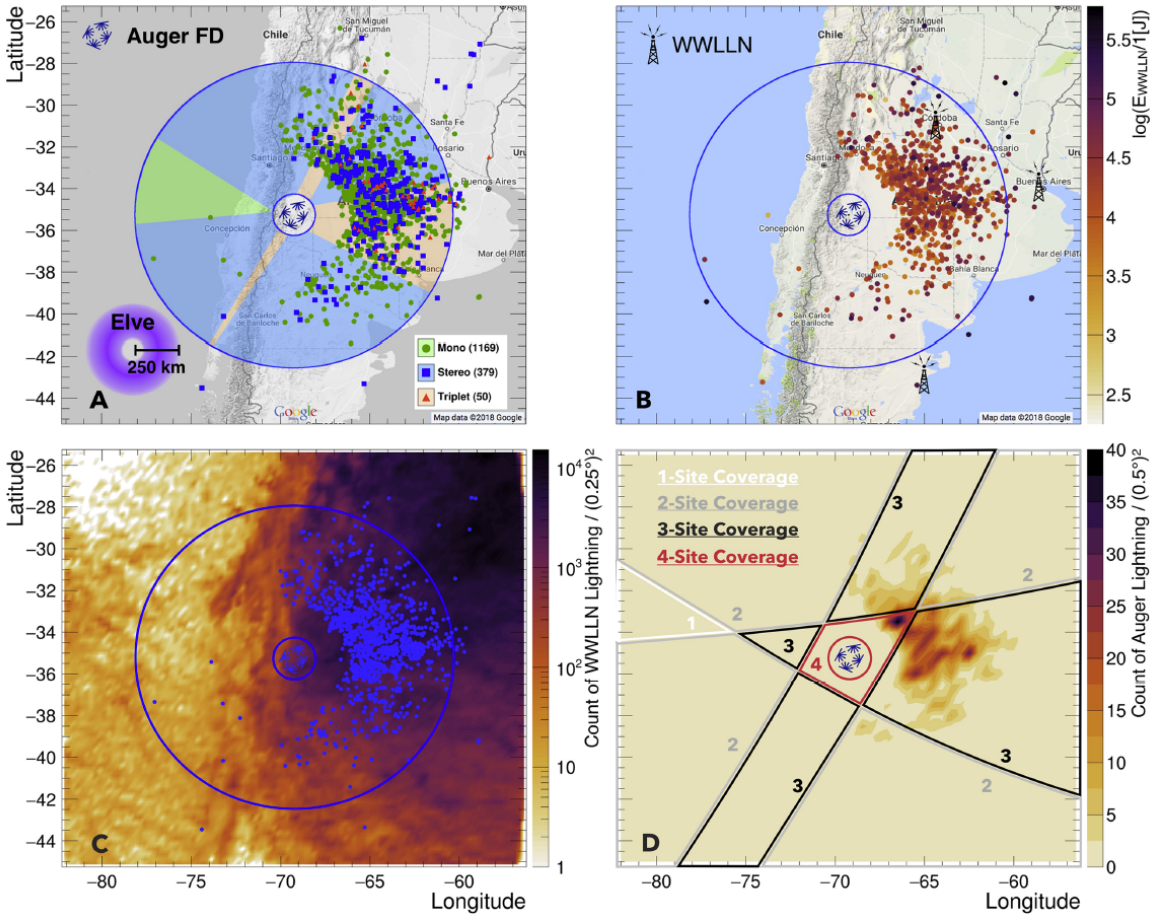

Figure A.2: These maps denote the location of the reconstructed lightning strikes causing elves seen by the observatory in geodetic coordinates. The large and small circles outline the lower and upper boundaries of the pixel array when projected to the base of the ionosphere, approximately with 860 and 110-km radius, respectively. (a) The reconstructed lightning strike location from Auger elves and the number of FD sites contributed to each observation. The overlap of the FoV of each FD site is shown in the shaded regions. (b) The WWLLN events correlated with our elves data set against a log-color scale representing their energy in Joule. (c) A density map of WWLLN events with an overlay of elves-inducing lightning in coincidence. (d) The one-site, two-site, three-site, and four-site coverage regions as an overlay on a density map of reconstructed locations of lightning strikes obtained from Auger elves (Aab et al., 2020).

lightning strike locations from Auger elves.

A.2 Seasonal distribution of elves

Histograms of the number of elves per day for each year between 2014-2020 (figures 3.8 and 3.9) as well as the seasonal distribution of elves (figure 3.7), can be reproduced with the Python notebooks available in this repository: https://github.com/adrianacvr/multi-elves-repository/tree/master/seasonal_distribution.

Inputs

The data is organised by year. Individual csv files for each year are available:

- **elves_$year$_toplot.csv** contains the list of events with the header: **GPS, Nanosec, site, count**. The time tag of the events is given by "GPS" and "Nanosec" columns, "site" indicates the FD site where the events were detected and "counts" shows the number of FD sites that have detected the event: 1 is for mono, 2 for stereo, 3 for triple and 4 for quadruple. Check the indicative "site" in the **tmp_$year$.csv** files to look for the same GPS event from different FD sites.

- **elves_$year$_toplot_d.csv** is a subset of the above file but contains only multi-elves. Also, to analyze the events from different sites, please check the **tmp_$year$_d.csv** files.

- **elves_$year$_toplot_dt80.csv** contains a subset of multi-elves with a time difference greater than 80 microseconds.

Outputs

- Histograms of elves per day:
  - **elves_2014.png**
  - **elves_2015.png**
  - **elves_2016.png**
  - **elves_2017.png**
  - **elves_2018.png**
  - **elves_2019.png**
  - **elves_2020.png**
- **elves_month.csv** is the number of events per month (1-12). Each row corresponds to the events/month from a year.
- The file **multi_month.csv** is a subset of the above file with only the multi-elves per month.
- **seasonal_distribution.png** displays the seasonal distribution of elves and multi-elves, along with the ratio of ME to the total count.

Methods

1. Execute the **distribution_years.ipynb** notebook.
   (a) Print the table containing the following header: **Trace Length (μs), Year, Total Events, Total ME, Ratio**.
   (b) For each year, identify the day with the highest occurrence of multi-elves.
   (c) For each year, generate a histogram illustrating the counts of both elves and multi-elves per day. Highlight the day with the maximum multi-elves count.

(d) For each year, compute and record the counts of elves and multi-elves per month.

(e) Save the results in the **elves_month.csv** and **multi_month.csv** files.

2. Execute the **seasonal_distribution.ipynb** notebook and obtain the plot depicting the seasonal distribution along with the ratio of multi-elves to the total count.

A.3 Lightning waveforms analysis correlated with elves

In this appendix is the analysis of the lightning waveforms correlated with single, double and triple elves (figure 4.3) and the plot of the time gap of multi-elves related to the base time of the second component of the waveforms (figure 4.5). The data from ENTLN and the codes developed are available in this repository: https://github.com/adrianacvr/multi-elves-repository/tree/master/waveforms_analysis.

Some events may exhibit a signal at only one sensor, as depicted in the top panel of figure A.3. Others may show signals where it is not possible to identify waveform components, as illustrated by the event in the middle panel. Additionally, there are events where the Python function '`find_peaks()`' incorrectly computes the pulse base, resulting in very high values, as observed in the bottom panel of the figure.

Inputs

- The **data/** directory contains the base time waveform data for each event correlated with our elves. The name of the file indicates the GPS, nanosecond, millisecond and type of elves (ss for singles, dd for doubles and tt for triples). The header of **Trace_EVTGPS.$nanosec$_$msec$_$type$.csv** files is:

stationID, distance, type_elves, tb1, tb2, tb180, tb280

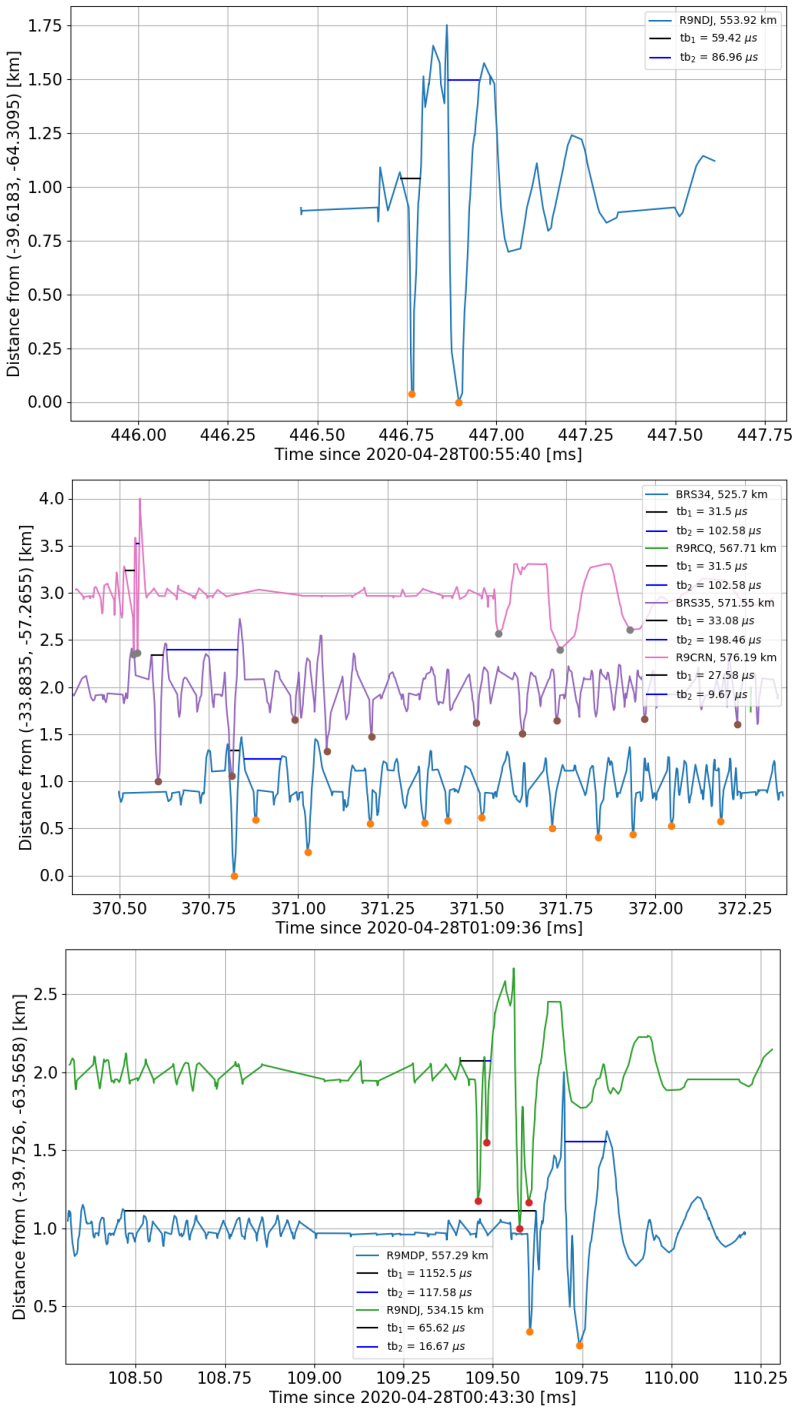

Figure A.3: Example of events with waveforms from a single sensor (top), signals where the main waveform components cannot be identified (middle), and signals where the pulse base time is incorrectly calculated (bottom).

- **stationID:** is the ID of the ENTLN sensor that detected the lightning.
- **distance:** distance from the lightning location to the ENTLN sensor (in this analysis is between 500 and 600 km).
- **type_elves:** single (ss), double (dd) or triple (tt) elves correlated with the lightning.
- **tb1 and tb2:** base time of the first and second pulse at 95% of the corresponding amplitude (we choose this one for the analysis).
- **tb180 and tb280:** base time of the first and second pulse at 90% of the corresponding amplitude.

  Each file has the values from at least one sensor. For multiple sensors, we compute the mean values of **distance**, **tb1** and **tb2** in the **base_time.ipynb** notebook.

- The correlation file called **t_base_vs_dt_april.csv**. The header is:

  gps,nanosec_x,msec,type_elves_x,antena_distance,std_distance,
  tb1_component,std_tb1,tb2_component,std_tb2,nanosec_y,
  lat_auger,lon_auger,t0_auger,type_elves_y,dt1_mean,std_dt1,
  dt2_mean,std_dt2

  - **gps, nanosec_x, msec and type_elves_x**: indicates the time of the lightning from ENTLN and type of the elves.
  - **antena_distance and std_distance:** is the mean distance between the lightning and the ENTLN sensors, and the standard deviation of the value.
  - **tb1_component and std_tb1:** is the mean base time of the first component (95%) and its standard deviation.
  - **tb2_component and std_tb2:** is the mean base time of the second component (95%) and its standard deviation.
  - **nanosec_y,lat_auger,lon_auger,t0_auger,type_elves_y:** indicates the time of the elve and type of elve.

- **dt1_mean and std_dt1:** mean time gap $(t_2 - t_1)$ of multi-elves and its standard deviation.
- **dt2_mean and std_dt2:** mean time gap $(t_3 - t_1)$ of multi-elves and its standard deviation.

Outputs

- Running the notebook **base_time.ipynb** outputs the plot **waveforms_april.png**
- Running the notebook **basetime_vs_DT.ipynb** outputs the plot **tbase_dt.png**

Methods

1. Run the **base_time.ipynb** notebook
   - Read the single elves files
     - Calculate the mean values of the variables of the same lightning waveforms from different ENTLN sensors.
     - Calculate the mean base time of the first and second pulse from all lightning correlated with single elves.
     - Mean distance from lightning location correlated with single elves and the ENTLN sensors.
   - Repeat this method for double elves files and triple elves files.
   - Read examples of lightning waveforms correlated with single, double and triple elves. Normalize the amplitude.
   - Plot the definition of the second component of the waveform at 100% and 95% of the altitude.

- Plot the examples of the second component of waveforms correlated with single, double and triple elves.
- Plot the histogram of the mean base time of the first pulse waveforms (95%) correlated with single, double and triple elves.
- Plot the histogram of the mean base time of the second pulse waveforms (95%) correlated with single, double and triple elves.
- Save the figure as **waveforms_april.png**

2. Run the **basetime_vs_DT.ipynb** notebook

- Read the file **t_base_vs_dt_april.csv**
- Sort ΔT_2 and ΔT_1 so that $\Delta T_1 < \Delta T_2$.
- Remove outliers and split ΔT into two groups ($\Delta T \geq 40\mu$s and $\Delta T < 40\mu$s).
- Plot base time t_b vs time gap ΔT of double elves.
- Plot the linear fit of ΔT vs t_b of the two groups.
- Plot base time vs time gap of triple elves.
- Plot the linear fit of ΔT vs t_b of the two groups.

A.4 Time gap Python code for multi-elves

The calculation of the time gap between multiple pulses of elves is available in the repository:
https://gitlab.iap.kit.edu/auger/cosmogeo/elves/-/tree/master/analysis/pysrc.

We produced with this code the figures 5.1, 5.5, 5.6, 5.9, 5.11 and 5.10.

Inputs

The inputs for this code are:

- Root file containing the traces labelled as **QCVvsTime** i.e., the amount of light vs the pulse time in each pixel. The file's name provides the UTC tag of the event in the format **GPSsecond-nanosecond.root**.
- The **number of the eye** (from 1 to 5, including HEAT-up) and the **number of the bays** where the event was detected. The bays takes values from 1 to 6 for eye 1 (LL), from 7-12 for eye 2 (LM), from 13 to 18 for eye 3 (LA), from 19-24 for eye 4 (CO) and from 25 to 27 for eye 5 (HEAT-up).
- Location of the lightning reconstructed from the pre-processing code: latitude (**latBolt**), longitude (**lonBolt**) and time (**t0Bolt**).
- From the above values, we build an input file "**events.txt**", containing the list of events to be analysed, where the data for each event is organised as follows:

  GPS nsec bay1 bay2 eye latBolt lonBolt t0Bolt height width prominence sigma

  Where height, width, prominence and sigma are the minimum necessary elements of the python function **find_peaks()**, that can be customised for a finer analysis of each event, and by default their values are 500, 4, 2.5 and 1 respectively.
- In **/auxiliary/fdPixelMap_5sites.csv** file, there is the elevation and azimuth of each of the bay pixels for the five sites, taken from Auger's outreach data and modified to enter the HEAT-up values.
- The latitude, longitude, altitude and backwall of the five sites, in the **/auxiliary/latlonsite.csv** file.

Outputs

Output files in the form EVTgps-nanosec.csv contain the following header:

pixID, row, col, t1, dt1, t2, dt2, t3, dt3, dT1, ddT1, dT2, ddT2, q1, dq1, q2, dq2, q3, dq3, arcR

- pixID, row and col refer to the pixel ID of a given row and column of the camera.
- t1, t2 and t3 are the times of the peaks found in the signal and the respective Gaussian fit error dt1, dt2 and dt3.
- dT1 and dT2 are the time differences between the first and second peaks and the first and third peaks, respectively. The errors of these values are ddT1 and ddT2.
- q1, q2 and q3 are the amount of light of each pulse given by its amplitude $\times$ sigma and the respective error dq1, dq2 and dq3.
- arcR is the arc distance between the latitude and longitude of the emission point in the ionosphere and the latitude and longitude of the lightning that produced the elve.

Methods

- Read input file: **events.txt**
- For each event in the input file:
    1. Extract event parameters (GPS nsec bay1 bay2 eye latBolt lonBolt t0Bolt height width prominence sigma).
    2. Open the Root file for each event.

3. For each pixel of the bay1 and bay2:
   (a) Get site, bay and pixel location to calculate arcR.
   (b) Read the "QCSvsTime" histogram from the Root file to get the pulse data (pulsex, pulsey, errory).
   (c) Find peaks in the pulse data using the find_peaks() function.
   (d) Determine the number of peaks found (1, 2, or 3).
   (e) If one peak is found:
      – Fit a single Gaussian function to the data.
      – Output the results (amplitude, centre, sigma, alpha, chi-square).
   (f) If two peaks are found:
      – Fit a single and double Gaussian function to the data.
      – Compare the chi-square values of single and double Gaussian fits.
      – Choose the best fit and output the results accordingly.
   (g) If three peaks are found:
      – Fit a single, a double and a triple Gaussian function to the data.
      – Compare the chi-square values of single, double, and triple Gaussian fits.
      – Choose the best fit and output the results accordingly.
4. Save the results to a CSV file.

A.5 Lightning properties from Earth Networks

The properties of the lightning correlated with elves in figures 6.2, 6.3, 6.4, 6.5, 6.6 and 6.7, can be reproduced by the data and code available in this repository: https://github.com/adrianacvr/multi-elves-repository/tree/master/entln_correlation.

Inputs

- The files of type **auger_$month$_stamp.csv**, contain data from the elves detected at the Auger FD with the header: **gps, nanosec, lat_auger, lon_auger, t0_auger, type_elves, dt1_mean, std_dt1, dt2_mean, std_dt2, time_stamp**.
  - **gps, nanosec**: the second and nanosecond of the elve detected.
  - **lat_auger, lon_auger and t0_auger** are the latitude, longitude and time of the lightning reconstructed from the elve detected in the FD. The nanosecond time of the lightning is nanosec-1000 t0_auger.
  - **type_elves** is 1 for single, 2 for double and 3 for triple elves.
  - **dt1_mean** is the mean value of the time delay between the first and the second peak of multi-elves and its standard deviation (**std_dt1**).
  - **dt2_mean and std_dt2** is the mean value of time delay between the first and the third peak of multi-elves and its standard deviation.
  - The **time_stamp** indicates the reconstructed time of the lightning in **year-mm-ddThh:mm:ss.nanosecond** format. This is the time we compare with ENTLN time stamp to correlate the events.
- The files of type **correlation_$month$.csv**, contain the data from elves in Auger and the data from the lightning correlated with the event. The header is **stamp_auger, lat_auger, lon_auger, type_elves, dt1_mean, std_dt1, dt2_mean, std_dt2, type_lightning, stamp_entln, lat_entln, lon_entln, peakcurrent, icheight, numbersensors, majoraxis, minoraxis, bearing**.
  - **type_lightning** that is 0 for CG, 1 for IC and 40 for Undefined lightning (from WWLLNN data).
  - **stamp_entln** is the time stamp from ENTLN.
  - **lat_entln, lon_entln** are the latitude and longitude of the lightning from ENTLN.

  - The peak current of the lightning (A) is indicated by **peakcurrent**.
  - **icheight** is the height of the IC lightning (m).
  - **numbersensors** is the number of sensors that detected the lightning.
  - **majoraxis, minoraxis and bearing** of the ellipse.

- The ENTLN files of type **lxarchive_pulse$year$mmdd.csv** contain the data from the lightning as detailed above but for all events of the storm. With this data, the plot of the map of all lightning strikes and the distribution of the type of lightning and its polarity is created.

Outputs

- **entln_nov.png**, from the November 10, 2018 storm.
- **entln_dec.png**, for the December 20, 2019 storm.
- **entln_apr.png**, from the April 27-28, 2020 storm.

Methods

1. Execute the **correlation_plots.ipynb** notebook.
   (a) Use nanosecond time from Auger and ENTLN to calculate time differences for each storm.
   (b) Categorize lightning types for each storm: IC, CG or Undefined.
   (c) Categorize elves types for each storm: single, double or triple.
   (d) Categorize lightning types according to the type of elves correlated for each storm:
      - CG correlated with single, double or triple elves.

- IC correlated with single, double or triple elves.
- Undefined correlated with single, double or triple elves.

(e) Plot the lightning location highlighting those correlated with single, double and triple elves.

(f) Plot the time difference of lightning time from Auger and ENTLN.

(g) Plot the distribution of the lightning peak current of the storm.

(h) Plot the distribution of type of lightning correlated with single, double and triple elves.

(i) Plot the distribution of peak current of lightning correlated with the three types of elves.

(j) Plot the peak current of the lightning-inducing multi-elves and the time gap between its pulses.

A.6 Cloud top height from GOES-16

The correlation between the cloud top height of storms and the elves detected in Auger from the figures 6.8, 6.9, and 6.10 can be reproduced using the images and Python notebooks available in this repository: https://github.com/adrianacvr/multi-elves-repository/tree/master/cloud_top_height.

Inputs

- GOES-16 satellite images in the **/Auger/** folder.
  Each file of the form **Auger_$year$mmdd_hhmm$UTC.png** shows the brightness temperature, the cloud top height and cloud top temperature over 10 minutes (except for the November storm which is shown every 15 minutes).

- The location of the lightning correlated with elves (**lat_entln**, **lon_entln**), that can be found in the **correlation_$month$.csv** files in appendix A.5.

Outputs

The videos of the development of the storms, showing the ENTLN location of the lightning correlated with the elves detected in the Auger FD:

- November 10, 2018: november2018/november_clouds_elves.gif
- December 20, 2019: december2019/december_clouds_elves.gif
- April 27-28, 2020: april2020/april_clouds_elves.gif

Each directory also contains the images with 10-minute intervals of each video.

Methods

1. Execute the **november_clouds.ipynb** notebook.
    - Read the input file **correlation_november.csv** and get the location of the lightning (lat, lon).
    - Define the function **loc(lat, lon)** to convert latitude and longitude coordinates to pixel coordinates on the image.
    - For each time stamp, read the corresponding satellite image file.
    - Plot the lightning events on the satellite image and the location of the FD sites as stars on the image.
    - Save each resulting plot as a PNG file.
    - Creates a GIF animation from the PNG files.

2. Execute the **december_clouds.ipynb** notebook.

3. Execute the **april_clouds.ipynb** notebook.

Appendix B

Scientific production and academic contributions

During the development of this research, I was part of the *Grupo de Investigación en Relatividad y Gravitación* at the Industrial University of Santander, where I continued working in Particle Physics. In this area, I published papers, supervised undergraduate students, designed and delivered masterclasses, and engaged in scientific outreach activities.

Additionally, I was part of the Pierre Auger Collaboration and co-author since April 2019. I regularly reported my research progress in Multi-elves in the Task Cosmogeophysics meetings bi-weekly. I presented reports in the Collaboration's General Meetings in March 2020, November 2020, March 2021, June 2021, November 2021, November 2022, March 2023, and November 2023.

The results obtained during this work were disseminated in various spaces, leading to my recognition as a Junior Researcher under the Call 894 of 2021 by *Minciencias*, Colombia. The following are the outcomes of this research.

Publications:

1. Paper in preparation: Quasi-constant time gap in multiple rings of ELVES: a disconnect from IC lightning electromagnetic pulse mechanism.

2. Vásquez-Ramírez, A., on behalf of The Pierre Auger Collaboration (2022). Study on multi-elves in the Pierre Auger Observatory. POS PROCEEDINGS OF SCIENCE, 395, 1-12.
   DOI: https://doi.org/10.22323/1.395.0327

3. Mussa, R., Vásquez, A., & Pierre Auger Collaboration. (2022, December). Classification and Reconstruction of single and multiple elves in AUGER. In Journal of Physics: Conference Series (Vol. 2398, No. 1, p. 012006). IOP Publishing.
   DOI: https://doi.org/10.1088/1742-6596/2398/1/012006

4. Mussa, R., Abdul Halim, A., Abreu, H. et al (2023). Investigating multiple elves and halos above strong lightning with the fluorescence detectors of the Pierre Auger Observatory. POS PROCEEDINGS OF SCIENCE, 444, 327.
   DOI: https://doi.org/10.22323/1.444.0372

5. Sarmiento-Cano, C., Suárez-Durán, M., Calderón-Ardila, R. et al. The ARTI framework: cosmic rays atmospheric background simulations. Eur. Phys. J. C 82, 1019 (2022).
   DOI: https://doi.org/10.1140/epjc/s10052-022-10883-z

6. Peña-Rodríguez, J., Vesga-Ramírez, A., Vásquez-Ramírez, A., Suárez-Durán, M., de León-Barrios, R., Sierra-Porta, D., Calderón-Ardila, R., Pisco-Guavabe, J., Asorey, H., Sanabria-Gómez, J., & Núñez, L. (2022). Muography in Colombia: Simulation Framework, Instrumentation, and Data Analysis. Journal of Advanced Instrumentation in Science, 2022.
   DOI: https://doi.org/10.31526/jais.2022.271

7. de Leon-Barrios, R., Peña-Rodríguez, J., Sanabria-Gómez, J., Vásquez-Ramírez, A., Calderón-Ardila, R., Sarmiento-Cano, C., ... & Nunez, L. A. (2022, March). Muography for the Colombian Volcanoes. In 37th International Cosmic Ray Conference (p. 280).
   DOI: https://doi.org/10.22323/1.395.0280

8. A. Vásquez Ramírez, M. Ariza Gómez, M. Carrillo Moreno, V. Baldovino Medrano, H. Asorey and L.A. Núñez (2022). Improvised Explosive Devices and cosmic rays. POS PROCEEDINGS OF SCIENCE, 395, 1-4.
   DOI: https://doi.org/10.22323/1.395.0480

Schools and congresses:

- **School:** International School on Astroparticle Physics. March 1-9, 2019. Pierre Auger Observatory, Malargüe, Argentina. Poster: "Simulation of the hybrid detector MuTe for volcano tomography". BEST POSTER PRIZE AT THE ISAPP 2019. Poster in: https://indico.nucleares.unam.mx/event/1396/contribution/48

- **Talk:** "Study on multi-elves in the Pierre Auger Observatory", in 37th International Cosmic Ray Conference (ICRC), July 12-23, 2021. Berlin, Germany & Online. Abstract: https://indico.desy.de/event/27991/contributions/102301/

- **Poster:** "Parametrization and Characterization of multi-elves Events at the Pierre Auger Observatory", in American Geophysical Union (AGU) Fall Meeting, December 13-17, 2021. New Orleans, LA & Online. Virtual poster in: https://agu2021fallmeeting-agu.ipostersessions.com/default.aspx?s=24-49-6A-35-69-9E-E0-86-88-CC-CD-AF-C2-87-8C-14&guestview=true

- **Talk:** "Study of multiple elves at the Pierre Auger Observatory", in European Geosciences Union (EGU) General Assembly, April 23-28, 2023. Vienna, Austria. Abstract: https://meetingorganizer.copernicus.org/EGU23/EGU23-7176.html

Visits:

- Internship: "Study on the time correlation between the TLEs observed at Pierre Auger Observatory and the lightning". Istituto Nazionale di Fisica Nucleare. September - November 2018. Torino, Italy.
- Fluorescence Detector Shift of The Pierre Auger Observatory, March 2019. Malargüe, Argentina.
- Visit to the University of Torino (UniTo), Italy, between April 8 and 22, 2023, to advance the study of the time delay behaviour between the rings of multi-elves with Prof. Enrico Arnone, Department of Physics, UniTo, and Prof. Roberto Mussa, INFN, Sezione di Torino.

Seminars:

- **Seminar:** "Analysis of Multiple elves at the Pierre Auger Observatory" April 20, 2023. Università degli Studi di Torino, Dipartimento di Fisica, Italy.

  Abstract: Elves are transient ring-shaped emissions occurring at the base of the ionosphere above thunderstorms. multi-elves are events consisting of two and up to four rings of light separated temporally by tens of microseconds. The Fluorescence Detector (FD) at the Pierre Auger Observatory has been detecting elves with a dedicated trigger since 2013. The high temporal resolution of 100 ns of the FD allows us to record the traces of the events in great detail. From the improved processing of the traces, we have observed elves with double and triple peaks. Such a feature has been proposed as a signature for the emission of Terrestrial Gamma Flashes in thunderstorms. In fact, during 2014-20, about a third of the events detected at Auger were identified as multi-elves. The origin of multi-elves is still not fully understood; therefore, in this report, we test competing

models for double and triple elves emission and show how different emissions, such as halos, can be misinterpreted as multiple elves. For this analysis, we compare the elves parameters measured in Auger with the lightning properties detected by Earth Networks, i.e. the location, waveform, and height of these sources.

- **Colloquium:** "Particle acceleration in thunderstorms", April 14, 2023. Università degli Studi di Torino, Dipartimento di Fisica, Italy.

  Abstract: Did you know that large particle accelerators form in thunderstorms? The electricity in thunderstorms can be powerful enough to produce energy similar to that of a nuclear power plant. One evidence for this is the Terrestrial Gamma-ray Flashes (TGFs), bursts of gamma rays with energies up to 40 MeV, observed by satellites at the top of thunderstorm clouds. But how is it possible to find high-energy particles in such clouds? TGFs are suspected to be produced by the intense electric fields in the vicinity of the tops of thunderstorms. If conditions are right, the field becomes strong enough to produce an upward avalanche of electrons. These high-energy electrons, traveling at relativistic speed, emit gamma rays when they are deflected by air molecules. Transient Luminous Events (TLEs), such as sprites, elves, and blue jets, are detected at different heights in the atmosphere, providing evidence of particle acceleration in thunderstorms. TLEs are observed in correlation with the occurrence of in-cloud or cloud-to-ground lightning strokes. While there are still many open questions about particle acceleration mechanisms in the cosmos, thunderstorms provide a unique opportunity to study some of these processes up close. In this talk we will discuss some key ideas and recent discoveries about the amazing power of lightning.

- **Seminario GIRG:** "Estudio de elves de múltiples anillos en el Observatorio Pierre Auger", 2 de Junio, 2023. Universidad Industrial de Santander, Bucaramanga, Colombia.

  Resumen: Los elves son emisiones transitorias en forma de anillo que se producen en la ionosfera, por encima de las tormentas eléctricas. Los rayos de las tormen-

tas generan pulsos electromagnéticos que excitan las moléculas de la ionosfera y luego emiten luz en forma de anillos. Los multi-elves son eventos que consisten en dos o hasta cuatro anillos de luz, separados temporalmente por decenas de microsegundos. Desde 2013, el Detector de Fluorescencia (FD) del Observatorio Pierre Auger ha estado detectando elves utilizando un sistema de detección especializado. La alta resolución temporal de 100 ns del FD, nos permite registrar con detalle las fototrazas de los eventos y hemos observado elves con dobles y triples anillos. De hecho, durante el período de 2014 a 2020, aproximadamente el 27% de los eventos detectados en Auger fueron multi-elves. El origen de los múltiples anillos en los elves aún no se comprende completamente, sin embargo, hemos probado dos modelos que buscan explicar estos fenómenos: el primero relaciona la altura del rayo fuente dentro de la nube con la diferencia temporal entre los anillos (ΔT), mientras que el segundo relaciona ΔT con los tiempos de subida y de bajada del pulso de la densidad de corriente del rayo. Para este análisis, se compararon los parámetros de los elves medidos en Auger con las propiedades de los rayos detectados por la red Earth Networks, como la ubicación, la forma de onda y la altura de estas fuentes.

- **Ciencia en casa, Grupo Halley UIS:** "Fenómenos luminosos transitorios". 10 de Agosto, 2020.

  Resumen: ¿Medusas en los cielos?, ¿Rayos azules?, ¿Sabías que encima de las tormentas eléctricas se forman estos y otros gigantes luminosos?. Algunos de ellos se pueden ver a simple vista, otros necesitan ser capturados con cámaras especiales.

  Disponible en: https://www.youtube.com/watch?v=B3E5b5pD9a4&t=843s

Theses supervised:

- *Simulación de las respuestas de la interacción de la radiación cósmica con las minas antipersonales en Colombia*. Universidad Industrial de Santander. Tesis en Ingeniería Química, 2019. Coturora de Michael Leonardo Ariza Gómez y Marcos Fernando Carrillo Moreno.

- *Método de calibración basado en simulaciones para los sensores de neutrones cosmogénicos empleados en el monitoreo de la humedad del suelo*. Universidad EAFIT. Tesis en Ingeniería Física, 2023. Tutora de Luigui Joel Miranda Leuro.

Masterclass:

- **Masterclass Astropartículas Halley UIS**, 21 de Abril al 12 de Mayo de 2021. Sesiones virtuales sobre la definición, espectro de energía, fuentes y propagación de rayos cósmicos, así como el uso de softwares para simular detectores de partículas, como CORSIKA y GEANT4.
  Disponible en: https://www.youtube.com/watch?v=OqM2xNojrXI&t=1s

- **Semillero de Astropartículas y Ciencia de Datos**, Grupo Halley UIS Abril-Agosto, 2022. Sesiones teóricas y prácticas presenciales sobre astropartículas, para explorar eventos desde grandes instrumentos alrededor del mundo. Sesiones intensivas del manejo de GEANT4 en un contenedor, para la simulación de una barra centelladora y un detector cherenkov de agua empleados para la detección de muones.
  Repositorio: https://github.com/adrianacvr/geant4-class

Outreach:

- Participation and planning of activities commemorating International Day of Women and Girls in Science (February 2020, 2023 and 2024). Talks, courses and activities aimed mainly at girls and young women in schools to generate curiosity and an approach to science through my personal experiences and those of other female scientists in the country and worldwide.

- Planning and participation of talks and outreach activities for all publics in the framework of "Vecinos y Amigos" (September 2022-March 2023), a space where the Universidad Industrial de Santander opens its doors to the community to enjoy and learn about science. I coordinate the implementation of the activities focused on the following topics: Astrobiology, Astrophysics, Cosmic Rays, Climate change, Solar System.